UNIVERSITÀ
DEGLI STUDI
FIRENZE

DOCTOR OF PHILOSOPHY IN

Energy Engineering and Innovative Industrial Technologies

XXVIII Cycle

PhD COURSE COORDINATOR Prof. Maurizio De Lucia

"Development of innovative waveguide probes with improved measurement capabilities"

Scientific Sector ING-IND/09

PhD Student

Dott. Andrea Fioravanti

Tutor

Prof. Giovanni Ferrara

Co-tutor

Ing. Lorenzo Ferrari

Phd Course Coordinator

Prof. Maurizio De Lucia

2012/2015

Ai miei genitori Rodolfo e Sara,

a mio nonno Alessandro e a Danila

Declaration

I hereby declare that this submission is my own work and, to the best of my knowledge and belief, it contains no material previously published or written by another person, nor material which to a substantial extent has been accepted for the award of any other degree or diploma at University of Florence or any other educational institution, except where due references are provided in the thesis itself.

Any contribution made to the research by others I have been working with is explicitly acknowledged in the thesis.

30 November 2015

Acknowledgments

I would like to thank Prof. Giovanni Ferrara, Ph. D. Lorenzo Ferrari and Prof. Ennio A. Carnevale of the University of Florence for their invaluable contribution and support to this study.

I would like to thank Ph. D. Giulio Lenzi for have shared our researches and works in these years, allowing me to reach this goal.

I would like to thank all members of the REASE GROUP, old and new: Luca Romani, Alfonso Figini, Isacco Stiaccini, Giovanni Vichi, Fabio Esposito, Giovanni Galoppi, Riccardo Maleci, Alessandro Bianchini, Francesco Balduzzi, Davide Biliotti, Michele Becciani, Andrea Tanganelli, Niccolò Fiorni.

Contents

List of figure

List of tables

List of symbols and acronyms

Nomenclature

a	sound velocity	[m/s]
c_p	heat specific at constant pressure	[J kg-1K-1]
C_P	normalized pressure coefficient	
d	diameter of duct	[m]
d_N	diameter of the resonator neck	(m)
d_S	diameter of sensor head	(m)
$D_{(jj)}$	generic element of duct transfer matrix	
$[D_j]$	transfer matrix of a duct	
E_a	absolute error on pressure measurement	[Pa]
E_r	relative error on pressure measurement	
f	frequency	[Hz]
g(f)	transfer function of waveguide probe	
He	Helmholtz number	
i	imaginary unit	
L_H	length of resonator housing	[m]

L_1	length of transmitting duct	[m]
L_C	length of resonator chamber	[m]
L_N	length of resonator neck	[m]
Loss	Attenuation factor of probe	[dB]
Ma	Mach number	
N_B	Number of blades	
N_V	Number of vanes	
J_n	Bessel function of first kind of order n	
J	T-junction	
K_j	transfer function in a multisensor waveguide probe	
k_j	Polynomial coefficient	
K_γ	yaw coefficient	
K_S	static pressure coefficient	
K_T	total pressure coefficient	
n	polytrophic constants in ducts	
p_S	static pressure	[Pa]
p_T	total pressure	[Pa]
p(x,t)	pressure oscillations	[Pa]
p^+	amplitude of forward moving wave	[Pa]
p^-	amplitude of backward moving wave	[Pa]
p_1	pressure at sensor section	[Pa]
p_0	pressure at measurement section	[Pa]

p_0*	estimated pressure	[Pa]
R	duct radius	[m]
R^2	coefficient of determination	
s	shear wave number	[m-1]
t	Time	[s]
u(x,t)	volume flow rate oscillations	[ms-1]
V_C	volume of sensor housing	[m^3]
V_{d1}	volume of transmitting duct	[m^3]
V_{d2}	volume of damping duct	[m^3]
V_{v1}	volume of sensor housing	[m^3]
x	axial position for acoustic wave	[m]
Z_C	characteristic acoustic impedance	[kg $s^{-1}m^{-2}$]
Z_{Dj}	lumped impedance of duct	[kg $s^{-1}m^{-2}$]
Z_p	acoustic impedance of sensor housing	[kg $s^{-1}m^{-2}$]
Z_{Sj}	lumped impedance of sensor housing	[kg $s^{-1}m^{-2}$]
Z_t	acoustic impedance of damping termination	[kg $s^{-1}m^{-2}$]

Greek symbols

Γ	complex propagation constant	[m-1]
γ	yaw angle	[deg]
δp_i	absolute error on sensor section	[Pa]
δp_0	absolute error on measurement section	[Pa]
λ	thermal conductivity	[Wm-1K-1]

μ	dynamic viscosity	[Pa s]
ρ	mean density	[kg m-3]
σ	square root of Prandtl number	
ω	rotational frequency	[s-1]

Subscripts

j	subscript of numbering
m	tangential mode index
n	radial mode index

Abbreviation

FFT	Fast Fourier Transform
FRAPP	Fast Response Aerodynamic Pressure Probe
FRF	Frequency Response Function
MMT	Multi Microphone Method
TMT	Two Microphone Technique
WGP-S	Waveguide Probe Simplified
WGP-M	Waveguide Probe Modified

1 Introduction

1.1 Overview

The unsteady pressure measurements are a fundamental part of all experimental investigation carried out to evaluate the performances of a turbomachinery. These measurements have a crucial role in turbine or compressor development as showed by Fischer in Ref. [1], they are necessary in the study of noise generated by an aeronautical engine (Wegner et al. [2]) and for detecting thermos-acoustic instabilities in the combustor chambers as explained by Johnson et al. in Ref. [3]. This is truer now that the lean combustion engines, designed to respect the pollutions emissions, are affected by acoustic instabilities in this case is often useful identify the acoustic source field in terms of modes and intensity. Another most intruding challenge in the turbomachinery field is the 3D experimental reconstruction of unsteady flows during a machine revolution. Not only this measurement would allow an in-depth understanding of operating conditions of the machine (flow unsteadiness, secondary flow etc. [4]) but also could be a useful reference for the CFD analyses.

The key requirement is to ensure that the measurement instrumentations can operate reliably even in harsh environments (high temperature or corrosive atmosphere) and does not have to affect with its shape and dimensions the phenomena under investigation. The first devices that can respond to these requirements are the optic techniques PIV [5] and LDV [6] by which is possible to measure the acoustic velocity of flow and the pressure distribution is then indirectly estimated. Unfortunately, these techniques are the most expensive and require a window access for the acquisition optic systems.

The other existing measurements techniques are the intrusive types. These methods adopt probes of different shapes, equipped with one or more sensors, which are inserted in the flow. Depending on the type, these probes can measure only the static pressure or all flow characteristics (total and static pressure, flow vector).

In this overview the waveguide probes have found a wide range of applications. These devices are largely used in the turbomachinery field to measure the pressure oscillations when a local installation of a sensor is not possible due to high temperature or scarcely accessible measurement point. In brevity, a waveguide probe allows to measure the pressure oscillations far from the transducer using a transmitting duct which connects the measurement section to the sensor section and a damping duct that attenuates the waves reflected from the duct ends. An early example of the use of a waveguide probe is the study of combustion chamber screeches by Blackshear et al. in Ref. [7]. More recently, Zinn and Habermann [8] used a waveguide probe to measure the pressure oscillations in a combustion chamber. In these two cases, a direct exposition of the sensor was not possible due to the high local temperature exceeding the sensor temperature limit. By using a waveguide probe, it was possible to position the sensor far from the hot temperature zone and keep its temperature low. Examples of the use of waveguide probes where a direct measurement would have affected the results by modifying the pressure field are the applications reported by White et al.[9] and Tijdeman [10]. The first measured the pressure variations over the tip of a centrifugal compressor rotor, highlighting the ability of a waveguide probe to capture the unsteady pressure variations over the tip of the rotor. In Tijdeman's study, waveguide probes were used to investigate the pressure variations on the surface of a supercritical airfoil. More in detail the waveguide systems were employed for the determination of unsteady pressure distributions on harmonically oscillating wind-tunnel models, by means this method it was possible to measure the steady pressure and the sinusoidal varying pressure.

As drawback, in a waveguide probe the amplitude of signal is attenuated and its phase is modified along the path across the transmitting duct. The frequency transfer function of probe express this attenuation in the frequency domain, the higher is the frequency and the higher is the attenuation of signal. Become essential evaluate if the

phenomena of interest in the turbomachinery under study occur at a high frequency such that the probe has an attenuation too high.

As already said a 3D experimental reconstruction of the unsteady flows during a machine revolution is another one of the most intriguing challenge in the turbomachinery field. Unfortunately, due to several phenomena involved, the expected bandwidth for such an investigation is generally very high (over 50 kHz) and this makes the experimental investigation very hard to perform [11]. This is even truer if a measurement technique is requested which does not need a strong machine modifications (such optical access or seeding) and is compatible with an industrial environment.

Among the techniques that were adopted for this purpose, fast aerodynamic pressure probes (FRAPPs) are those with the greatest diffusion [12]. These probes resemble a traditional actual (or virtual) 3, 4 or 5 holes probe but host one or more dynamic pressure sensors at the probe tip. This set up allows a time-resolved measurement of the instantaneous flow quantities but requires a frequency response of the probe capable of detecting the blade passing frequency and its first three to five harmonics. Several authors tried to extend the capabilities of these probes in terms of bandwidth and operating conditions. Even though differences exist between the solutions in the literature, all the designs involve the positioning of a dynamic pressure sensor close to the measurement point. In general terms, the higher is the frequency response, the more exposed to the flow is the sensor. This physical constrain puts a limit to the probe applicability since the measurement conditions have to comply with the maximum allowed operating conditions of the sensor.

Otherwise, the incontrovertible advances in sensor technology have led to improved high-temperature capabilities of a pressure transducer. However this gain is diminished by increased compression ratio and higher turbine inlet temperatures. The measurement of unsteady pressure in a high temperature environment or without an accessible measurement point remains a challenging problem.

In summary, as highlighted by White et al. in Ref. [9] the solutions to high-temperature unsteady pressure measurement (total and static) can be classified into at least three distinct categories:

- direct sensor with integrated active cooling system
- design and develop sensors that can sustain even higher temperatures
- employ a waveguide to move the sensor away from the high-temperature environment, furthermore this solution makes possible to reduce the sensor obstruction in the measurement point

In the first case an existing sensor is equipped with an active cooling system, which uses air or water, this allows to use the sensor for high-temperature but introduce a considerable mechanical complexity and can negatively affect the measurement reliability. Many efforts have been made to realize pressure sensors that can resist at higher temperature, the piezo-resistivity sensors with an opportunity packaging by means of a particular film protector can reach the 150°C in continually operating conditions. There are some promising technologies currently at various stages of development that have the potential to yield sensors with significantly higher temperature capabilities. As an example, Palmer et al. in Ref. [13], fiber-optic pressure sensors have been demonstrated to operate at temperatures as high as 1050°C. Another example is a plasma-based approach capable of operating at temperatures as high as 1335°C, Matlis et al. in Ref. [14]. However, in addition to their complexity the system uses a high voltage alternating current and the resulting electromagnetic radiation could interfere with surrounding equipment.

The advantages of placing the sensor in a remote position respect to the measurement point are then clear, once the drawbacks in the signal transmission along a waveguide are notes and balance out these type of probes could represent an excellent choice in term of poor intrusiveness and cost of the sensor.

1.2 Introduction to waveguide probe

A waveguide probe is made up of a long and narrow duct called transmitting duct, which connects the measurement point with a flush mounted sensor housing. The rest of the duct downstream to the sensor housing is a damping duct that attenuates the pressure oscillations reflected by the duct end. Several theoretical models to describe the behavior of a waveguide probe have been developed over the years.

Iberall in Ref. [15] was among the first to analyze the problem of the attenuation of pressure oscillations in measurement lines. According to the theory of Bergh and Tijdeman [16] and Tijdeman [17], the waveguide can be described as a single narrow duct where the pressure fluctuations propagate with an attenuation depending on both the local temperature and duct geometry. The pressure measurement is considered as a virtual sensor placed near the pressure tap with no junction with the transmitting duct. If the duct is long enough (at least 20m) and the temperature variations cannot be taken into consideration, the measured pressure has an attenuation that increases with a monotone trend as the frequency and the distance between the pressure tap and the sensor increase. If the damping duct is not long enough, the reflected wave from the duct end interacts with the incoming wave leading to a non-monotone attenuation function.

This theory, slightly adjusted, was experimentally assessed by Nyland et al. [18] and Richards [19]. In particular, Richards in his study showed a practical theoretical approach to evaluate the propagation of pressure oscillations along a transmission line composed of different duct geometries and discontinuities. The influence of the probe geometry on its response was investigated by Englund and Richards [20] and White et al. [9] by applying the theoretical model of Bergh and Tijdeman [16]. In particular, these authors showed the dependence of the attenuation trend on the transmitting duct length, diameter, and the sensor housing volume. The effects of temperature on the probe behavior were investigated by Van de Wyer et al. [21], White et al. [9], and Parrott and Zorumski [22].

They demonstrated that the probe response function is only weakly dependent on the average fluid temperature, whereas it is strongly sensitive to intense thermal gradients along the ducts. The above mentioned theories did not take into account the real sensor housing geometry and the manufacturing of the waveguide. Unfortunately, the real geometry and the connections between the components have a strong influence on the behavior of the system. Each discontinuity in the duct connections can affect the pressure oscillations and introduce great distortions on the probe frequency response. The geometry of the sensor housing itself is another element that contributes to increase the differences between the expected and the real frequency responses as was investigated by Ferrara et al.[23]. If not properly manufactured, the frequency response function (FRF)

of the system decays faster than in theoretical models and its trend is strongly frequency dependent. This problem is amplified if one considers that the diameter of the transmitting duct should be as small as possible to reduce the influence on the flow, while the higher the diameter of the sensor, the higher its sensitivity. Therefore, a good measurement setup could lead to a discontinuity between the ducts and the sensor housing. This discontinuity interacts with the pressure fluctuations and modifies the frequency response of the waveguide. In Ref. [24], the authors tested four types of interfaces between the sensor housing and the ducts. They demonstrated that the configuration that shows the best FRF is a junction with a round hole with the same diameter of the transmitting duct, independent of the sensor diameter.

From a theoretical point of view, the sensor housing can be described as a side branch resonator on the transmitting duct, as evidenced in Ref.[9]. During the probe design, in order to take into account the presence of this resonator, Ferrara et al. [24] and Van de Wyer et al. [21] proposed the integration of the standard waveguide model by Bergh and Tijdeman [16] with the electroacoustic approach largely used in acoustic problems (see also Munjal in Ref. [25]) and already applied in this field by Richards in Ref. [19]. In particular, Ferrara et al. [24] proposed a probe model where the sensor housing and the damping duct (considered as a damping device) were described by acoustic impedances while the transmitting duct remained as proposed by Bergh and Tijdeman. [16]. The theoretical model presented by Ferrara et al. [24] shows the dependence of the FRF both on the sensor housing and on the damping device geometries. In order to optimize the probe response, the authors suggested the use of miniaturized mufflers as damping devices. When properly designed, the muffler allows a partial compensation of the negative effects of the sensor housing and other discontinuities. This leads to a FRF that is locally flat and near to the null attenuation. In addition, the use of a muffler instead of a long reel as an infinite duct allows the reduction of the probe dimensions. By using a customized set of mufflers, it is possible to center the waveguide operating range on the measurement range. Unfortunately, this solution is hard to use in an on-field experimental campaign.

1.3 Introduction to fast response aerodynamic pressure probe

One of the most intriguing challenge in the turbomachinery field is the 3D experimental reconstruction of the unsteady flows during a machine revolution. Not only this measurement would allow an in-depth understanding of the operating conditions of the machine (flow unsteadiness, secondary flows, etc.) but also it could be a useful reference for the CFD analyses. Unfortunately, due to the several phenomena involved, the expected bandwidth for such an investigation is generally very high (over 50 kHz) and this makes the experimental investigation very hard to perform [11]. This is even truer if a measurement technique is requested which does not need strong machine modifications (such as optical accesses or seeding) and is compatible with an industrial environment.

Among the techniques that were adopted for this purpose, fast aerodynamic pressure probes (FRAPPs) are those with the greatest diffusion [12]. These probes resemble a traditional actual (or virtual) 3, 4 or 5 hole probe but host one or more dynamic pressure sensors at the probe tip. This set up allows a time-resolved measurement of the instantaneous flow quantities but requires a frequency response of the probe capable of detecting the blade passing frequency and its first three to five harmonics. In more detail, the pressures measured by the sensors are converted in flow quantities (total and static pressure, velocity and flow angles) by using a set of coefficients estimated in a previous calibration performed under known flow conditions. Since the signals are generally treated only from the aerodynamic point of view, a frequency response as flat as possible in the field of interest is generally requested. In addition, to avoid any phase delay, the sensor has to be as close as possible to the measurement point. This has a strong relapse on the sensor housing design since even a small cavity before the sensor might have an eigen-frequency that distorts the frequency response of the probe. Typically, the housing cavity should have a volume small enough to have its resonating frequency over 40 kHz. To improve this aspect and have a higher bandwidth, the sensor has to be moved at the front of the probe tip and any cavities should be avoided.

This basic principle is in contrast to the necessity to have a probe of small dimensions with a reduced interaction with the flow. A significant study on FRAPP has been presented by Brouckaert et al. [26] who developed a probe equipped with three piezo-resistive sensors with a diameter of 3 mm only. The probe had a cylindrical shape since this was the best compromise between the sensitivity to flow angle variations and small dynamic errors in unsteady flow (Humm et al.[27]). Apart from this example, many researchers focused their interest to the so called virtual 3 hole probe to further reduce the stem diameter. With this setup, only one sensor is placed in the probe tip instead of three. To reproduce the data of an actual 3 hole probe, the measurement is performed by repeating the measure three times at different yaw positions. Thanks to its reduced size, a virtual 3-sensor probe allows a greater spatial resolution and a faster adaptation to changing flow conditions [11]. In fact, as demonstrated by Humm et al. [28] the measurements errors in unsteady flow are strictly proportional to the probe size. Some examples of probes featuring this solution are those proposed by Mersinligil et al. [29] and Persico et al.[30]. In Mansour et al. [31] the head of a virtual 3 hole probe with a dimeter of 1.8 mm was equipped with a temperature measurement device (thin-film gauge) to measure the unsteady total temperature and then estimate the flow entropy.

By using an opportunely shaped probe head and adding an additional dynamic pressure sensor it is possible to measure also the pitch angle of the flow as proposed by Pfau et al. in Ref. [32] and Lenherr et al. in [33]. The measurements with this probe, also called virtual 4 hole probe, is performed by acquiring the pressure signal in three different yaw position form both the dynamic pressure sensors. This kind of probe was extensively tested with good results as reported in Pfau et al. in Ref. [34] and [35]. A further development was proposed by Schlienger et al. in Ref. [36] where they presented a virtual 5 hole probe with only one sensor placed in the probe head. The shape of probe head and the position of the hole was studied in detail to have a proper sensitivity to pitch angle. An innovative aerodynamic calibration procedure based on the pressure measurement when the probe is turned around its axis in five different positions was adopted. This probe was able to measure the 3D characteristics of the flow by using only one sensor and provide results comparable with that of a virtual 4-sensor probe.

As a general trend the research on FRAPPs is mainly focused on the packaging of the sensor in the probe head. Different sensor arrangements lead to different resonance frequency of the sensor cavity that could limit the applicability range of probe. For this reason the sensor is generally placed as close as possible to the flow. This arrangement leads to one of the main limits of this kind of probes which is the maximum operating temperature. This limits is strongly related to the sensor operability which is generally very strict. As the temperature increases the dynamic pressure sensor can lose in linearity and reliability and eventually be damaged. Unfortunately, a cooling system would lead to an increase of the complexity and dimension of the probe that could hamper its use.

1.4 Research objective

In the present work are presented three new concepts of waveguide probe, which have been conceived, designed, developed and tested during the research carried out. The aims have been those to extend the measurement capabilities of the waveguide probes and use the know-how acquired applying it in the design of a fast response aerodynamic pressure probe with remote sensor.

1.4.1 Concept of a new single sensor waveguide probe

The first concept of waveguide probe presented is based on the use of a pressure transducer which is no flush mounted on the transmitting duct and where the long damping duct is replaced by an *ad-hoc* damping termination. The transmitting duct diameter has to be small to reduce its influence on the acoustic field. According to one of the working principles of waveguide, the transducer sensing element should not imply strong modifications of the transmitting duct shape [23]. A small size of this component would lead to the adoption of a small size transducer. On the other hand, acoustic pressure transducer sensitivity is directly related to the size of the sensing element so that the reduction of the size leads to a decrease of gain. The use of a large diameter microphone (for gain) and a small diameter transmitting duct (for intrusiveness) makes the theory of waveguides not directly applicable.

The coupling between the transmitting duct and the acoustic pressure transducer becomes the key feature of the developed probe. The size discontinuity makes the behaviour of the probe very dependent on the frequency [10] so that it is not possible to have a single probe for any frequency range. The optimization of the probe geometry according to the frequency range of use is performed both with theoretical models (based on the transfer matrix approach [9], [25] and [37]) and experimental calibrations. Several probe geometries are then investigated in order to identify the configurations that lead to the best performance in terms of frequency response and range of applicability. In addition to the standard probe geometries, an innovative design inspired by a muffler concept is also investigated.

The developed probes are used to measure the 3D acoustic field of two case studies representing typical situations in turbomachinery application: (1) the characteristic acoustic field of a circular duct in the full 3D range of propagation and (2) the acoustic field generated by a rotor-stator interaction in an annular section. The first case study is representative of phenomena taking place in gas turbine combustion chambers where the flame thermoacoustic instabilities are the acoustic source and the global wave field depends on the shape of the combustion chamber [38]. This experimental activity is performed to validate the measurement procedure since the acoustic field propagation in circular duct is well known in the literature [25] and [37]. It is, therefore, possible to compare the experimental results with reliable references. The second experimental campaign is an example of the application of the measurement procedure to a well-known field of interest in turbomachinery: the characterization of the acoustic field generated by a rotor-stator interaction for the reduction of the acoustic emissions of fans and low pressure turbines. In this case, the generated acoustic field is made up of several frequencies and for each one a different acoustic field mode is associated [39]. Experimental mapping campaigns come after a theoretical analysis of the test rig geometries to identify the cut-on and cut-off frequencies and the corresponding acoustic modes [37] [25]. Furthermore, in order to make a first validation of the experimental procedures, a simplified 3D model based on the 3D wave equation is developed. This tool is used to describe the acoustic wave propagation in finite length duct both with annular and cylindrical sections. In this way it is possible to compare the experimental results with the theoretical ones.

1.4.2 Concept of a multisensor waveguide probe

As second step of the present research an innovative approach to design a waveguide probe with an extended operating range and small attenuation factors is proposed. The basic idea is to use several sensors placed on the transmitting duct and a properly designed muffler as damping device. The sensor housings on the transmitting duct are placed at a specific distance from both the measurement point and the termination. Since the sensor housing placement has a strong influence on the behaviour of the probe, a mathematical model was developed to design the probe. As mentioned previously, the theoretical approach was a combination of that proposed by Bergh and Tijdeman [16] and that based on transfer matrix notation by Richards [19]. For the description of the discontinuity within the probe, the models of lumped and distributed impedance by Munjal [25] were used. As a first attempt, the probe was modelled with an infinite duct as termination and the sensor heads were considered as rigid surfaces. The model allowed the determination of the optimal sensor locations. The probe was manufactured and calibrated on a purposely built test rig, in order to estimate the behaviour of each component of the system. In particular, the impedances of each sensor housing and that of the ducts between two sensors were determined. The calibration data allow the definition of the proper miniaturized muffler geometry that can compensate for the real sensor impedance. This muffler was realized and used instead of the infinite duct. It should be noted that in this study an acoustic source was used as calibration device. For this reason, the upper limit of the range of frequencies investigated was 5 kHz. This bandwidth was considered a valid solution, since several phenomena of interest in the turbomachinery field that are commonly investigated with waveguide probes occur within this range of frequencies (e.g., centrifugal compressor stalls, thermoacoustic oscillations in combustion chambers, etc.). The methodology adopted for the development of the probe is valid, however, for any range of frequencies as long as a proper calibration device is used (e.g., a shock tube).

The performance of the multisensor probe was compared with that of a standard single sensor waveguide with particularly promising results. The reason for such interesting results depends on the methodology adopted to estimate the pressure at the pressure tap. In detail, the pressure measurement at the probe tip is calculated as a

combination of the pressures measured by the sensors or as a function of that measured by each single sensor. The use of multiple sensors allows a redundant measurement of the pressure that leads to a reduction in errors. With this approach, not only the error on the signal attenuation but also that on the phase shift is reduced. These important results allow one to overcome some of the major problems of waveguide probes. With this probe, in fact, it is possible to perform a proper reconstruction of a time dependent signal. To assess this capability, the waveguide was used to estimate the pressure oscillations at the outlet of a centrifugal blower and the reconstructed pressure was compared with that obtained with a single sensor probe placed at the same position and that of a flush mounted sensor. In addition, by using a slide, the probe was immersed in the flow and a 2D reconstruction of the static pressure map at a blower outlet was performed. According to the literature, this type of analysis was not possible with a standard single sensor probe without an accurate phase shift analysis as previously shown by White et al. [9] and Van de Wyer et al. [21].

1.4.3 Concept of a fast response aerodynamic pressure probe based on waveguide approach

As last step a probe which combines the concept of a fast response aerodynamic pressure probe with that of a waveguide probe is conceived, developed and tested. Such a device exploits the benefits of having the sensor far from the harsh conditions but still have the capability to perform an accurate flow condition measurement.

By starting from their previous experiences, the authors conceived the possibility to combine the concepts of a fast response aerodynamic pressure probe with that of a waveguide probe with the purpose to reduce the temperature constraints that limits the former's applicability range. By adopting an accurate design, a waveguide probe could be used to have an accurate estimation of the pressure signal at the measurement point. In addition, the probe head could be designed and drilled as to resemble that of a fast response aerodynamic probe. The system would be similar to a virtual 3 holes probe in which the sensing element is far from the harsh environment. This arrangement would be not free from some drawbacks:

1. As the frequency response of the probe is not flat in the range of frequencies of interest, the signal processing need to take into account the transfer function of the probe both in terms of amplitude and phase.
2. Due to the physic behind the operating principle of waveguide probes, the higher the frequency the higher is the attenuation between the measurement point and the sensor housing. This could be a limit to the maximum measurable frequency as the attenuation could be so high to lead the signal to noise ratio below an acceptable threshold. This flaw can be partially compensated with a proper design of the waveguide probe (greater transmitting duct diameter or appropriately designed damping devices).

On the other hand, the advantages of such a devices would be relevant as virtually no temperature limit would exist. The transmitting duct could be realized with high temperature resistant materials and the sensor could be properly cooled without any constrain due to dimensions and interactions with the flow. Up to now the FRAPPs and waveguide probes have been always considered as two separated instrumentations with different field of applications, pros and cons. In this study an effort to combine the two base concepts and exploit the benefits of both was performed. In particular, a waveguide probe featured to act as a virtual 3 holes probe FRAPP was conceived, developed and tested on a centrifugal blower to assess its capability to estimate a complex flow field. As this study was intended as a proof of concept of this solution, the waveguide probe was designed to be as simple as possible (infinite long damping duct and single sensor probe). The dynamic calibration was performed in an acoustic test bench up to 5 kHz, this bandwidth being limited by the calibration facility. Even though the design of the probe is simplified, this study represents the proof of concept of a solution that could open a new perspective on the field of flow reconstruction in turbomachinery applications.

2 Theory of waveguide probes

2.1 Single sensor waveguide theory

In this section the theory of the waveguide probe will be illustrated to understand its critical aspects and how its measurement capabilities were improved by this work.

The waveguide probe (Figure 2.1) is made up of three main elements: a sensor housing, the transmitting duct which connects the sensor to the measurement section, and the damping duct which avoids the interferences with the waves reflected by the duct end.

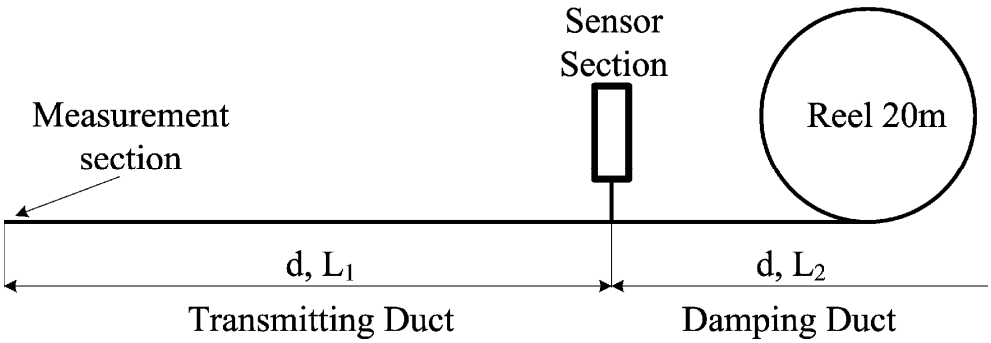

Figure 2.1 Scheme of a waveguide probe, *d* is the diameter of the ducts, L_1 and L_2 are the length of transmitting duct and damping duct respectively

The value of steady pressure at the measurement section can be measured directly with the sensor because the presence of ducts does not affect the results. Whereas more complicated is the measurement of unsteady component of pressure indeed the ducting system leads to a considerable difference between the pressure signal at the measurement section and the signal at the sensor section. Therefore, an essential step in the data-reduction procedure is the translation of unsteady pressure measured with the sensor to

the actual pressure at the measurement section with the use of the complex transfer function of the duct system.

The accurate determination of the probe transfer function, under the use conditions, needs knowing of the dynamic behavior of thin circular ducts connected with small instrument volumes.

2.1.1 Dynamic response of a waveguide probe

Typically, the configuration depicted in Figure 2.1 is analyzed by means of Tijdaman's theoretical model [17] based on the Helmholtz equation derived from Navier-Stokes equations by assuming the following simplifications:

- the pressure oscillations are small in comparison with the steady value
- the fluid properties are constant within each element of the system
- the internal radius of the ducts is small in comparison to their length
- no steady flow

Under these hypotheses and by considering a simplified system made up of a single duct (as in Figure 2.2), the pressure at a generic position x can be estimated by means of the solution of the generic wave equation (Eq. 2.1):

$$p(x,t) = (p^{+} \times e^{\Gamma(\omega x/a_0)} + p^{-} \times e^{-\Gamma(\omega x/a_0)}) \times e^{j\omega t} \qquad 2.1$$

where the first and second terms in the brackets are, respectively the incident and the reflected pressure waves, x is the position where the pressure is estimated, p^{+} and p^{-} are the two constants that depend on the boundary conditions at $x=0$ and $x=L_1+L_2$, and Γ is the propagation constant. Γ consist of a real part representing the attenuation of the waves over a unitary distance and an imaginary part which represents the phase shift over the same distance. This constant assumes several expressions depending on the problem boundary conditions. In the present study, the expression proposed by Zwikker and Kosten in Ref. [40] is used (Eq. 2.2). This equation is valid when the internal tube radius is small in comparison to the wave length and the radial velocity component is small in comparison to the axial velocity.

$$\Gamma = \left[\frac{J_o(i^{3/2}s)}{J_2(i^{3/2}s)}\frac{\gamma}{n}\right]^{1/2} \qquad 2.2$$

where J_0 and J_2 are the Bessel functions of the first kind of zero and second order respectively, γ is the specific heat ratio (c_p/c_v), n is the polytrophic constant for the thermodynamic process inside the tube (Eq. 2.3), s is the shear wave number (Eq. 2.4) and σ is the square root of Prandtl number (Eq. 2.5)

$$n = \left[1 + \frac{\gamma - 1}{\gamma}\frac{J_2(i^{3/2}s\sigma)}{J_o(i^{3/2}s\sigma)}\right]^{-1} \qquad 2.3$$

$$s = \left(\frac{\rho_s\,\omega}{\mu}\right)^{1/2}\frac{d}{2} \qquad 2.4$$

$$\sigma = \left(\frac{\mu\,c_p}{\kappa}\right)^{1/2} \qquad 2.5$$

where d is the duct diameter, ρ_s is the mean density, ω is the rotational frequency, μ is the dynamic viscosity, and κ is the thermal conductivity.

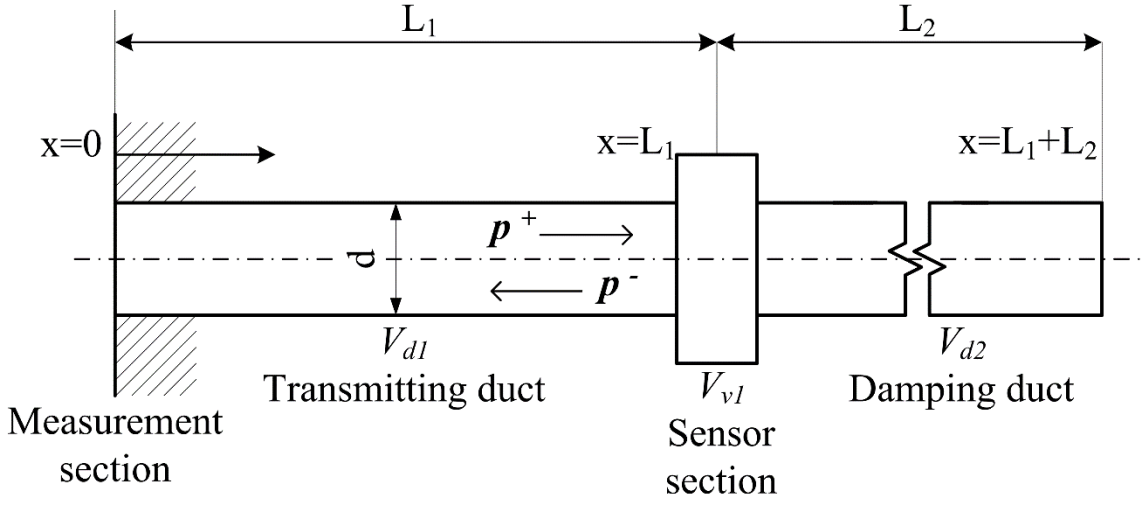

Figure 2.2 Scheme of the analyzed system, V_{d1}, V_{v1} and V_{d2} are the volume of the transmitting duct, sensor housing and damping duct respectively. While R and x are the duct radius and axial coordinate.

$$\begin{cases} p(0,t) = p_0 e^{i\omega t} \\ u(L_1 + L_2, t) = 0 \end{cases} \qquad 2.6$$

By using this mathematical approach and applying the hypothesis of still air (*M=0*) and the boundary conditions at the measurement section and damping duct end (Eq. 2.6), it is possible to express a relation between the pressure at the measurement section p_0 and the pressure at the sensor section p_1.

This function is usually called dynamic response or Frequency Response Function (FRF) of a waveguide probe, defines as depicted in Eq.2.7.

$$\begin{aligned} \frac{p_0}{p_1} = \Bigg[& \cosh\left(\frac{\omega L}{a_0}\right)_1 + \frac{V_{v1}}{V_{d1}} \frac{n_1}{n_{v1}} \left(\frac{\omega L}{a_0}\Gamma\right)_1 \sinh\left(\frac{\omega L}{a_0}\right)_1 \\ & + \frac{V_{d2}}{V_{d1}} \frac{a_{01}^2}{a_{02}^2} \frac{n_1}{n_2} \frac{\left(\frac{\omega L}{a_0}\Gamma\right)_1}{\left(\frac{\omega L}{a_0}\Gamma\right)_2} \frac{\sinh\left(\frac{\omega L}{a_0}\right)_1}{\sinh\left(\frac{\omega L}{a_0}\right)_2} \\ & \times \left(\cosh\left(\frac{\omega L}{a_0}\right)_1 \quad \cosh\left(\frac{\omega L}{a_0}\right)_2 \right) \Bigg]^{-1} \end{aligned} \qquad 2.7$$

Where p_0 is the pressure at measurement section, p_1 is the pressure at the sensor section, a_0 is the sound speed, V_{v1} is the volume of sensor housing, V_{d1} and V_{d2} are the volume of the transmitting and damping duct respectively, and n and n_v are the polytrophic constant for the thermodynamic process inside the duct and the sensor housing volume respectively.

2.1.2 Impact of main geometric dimensions

Considering the implementation of a waveguide probe it is possible to define its geometric dimensions and analyse the influence of each component on the dynamic response of probe itself. First of all it is interesting understand as the length of damping duct can affect the signal transmission.

In Figure 2.3, the FRF in dB calculated by Eq.2.7 for a system with a duct diameter of $d=2mm$, a transmitting duct of $L_1=1,\ 3$, and $5m$, a damping duct of $L_2=20m$ and a negligible sensor housing volume is reported. As evident in Figure 2.3, the longer the transmitting duct, the higher the signal attenuation. In order to obtain a pressure signal attenuation less than $1dB$ in the range $0\text{-}500Hz$ it is necessary define a transmitting duct length less or equal to $300mm$.

The influence of the damping duct is highlighted in Figure 2.4. If the damping duct is not long enough, the pressure waves reflected by the duct end interact with the incident waves leading to distorted attenuation trends. A length of the damping duct less than 20m leads to strong pressure oscillation that can make hard the source signal evaluation, especially for frequency below 200Hz.

Upon examination of 2.7, one can notice that the attenuation is also dependent on the ratio between the transducer housing and transmitting duct volumes (V_{v1}/V_{d1}), the volume define by sensor housing is due to the fact that if the sensor diameter is bigger than duct diameter the sensor cannot be flush mounted on the duct, as consequence a cavity volume result between the sensor head and its pressure tap. The results presented in Figure 2.5 show that, the lower the sensor housing volume V_{v1}, the more monotone the attenuation trends, the effect of housing volume in term of signal, while the average value of attenuation factor has a decay rate equal in each three case.

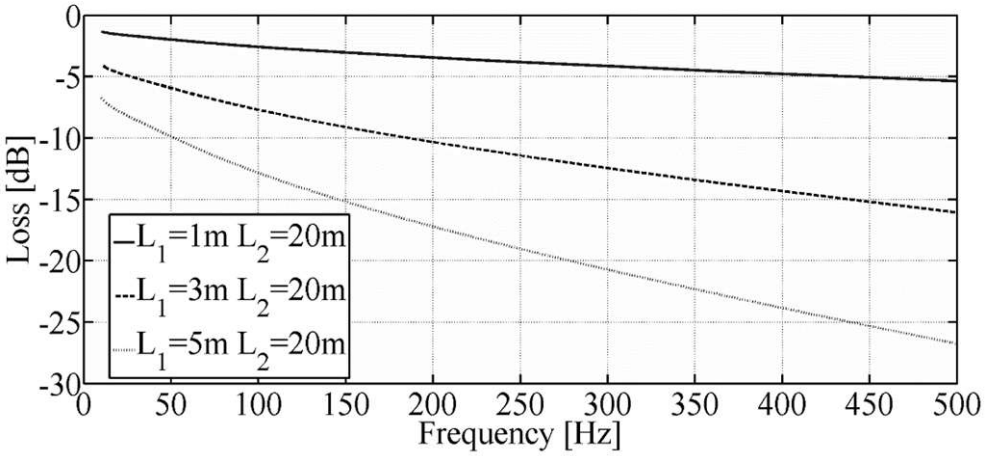

Figure 2.3 Transfer function for a waveguide probe with d=2mm, L_1=1, 3, 5m, and L_2=20 m

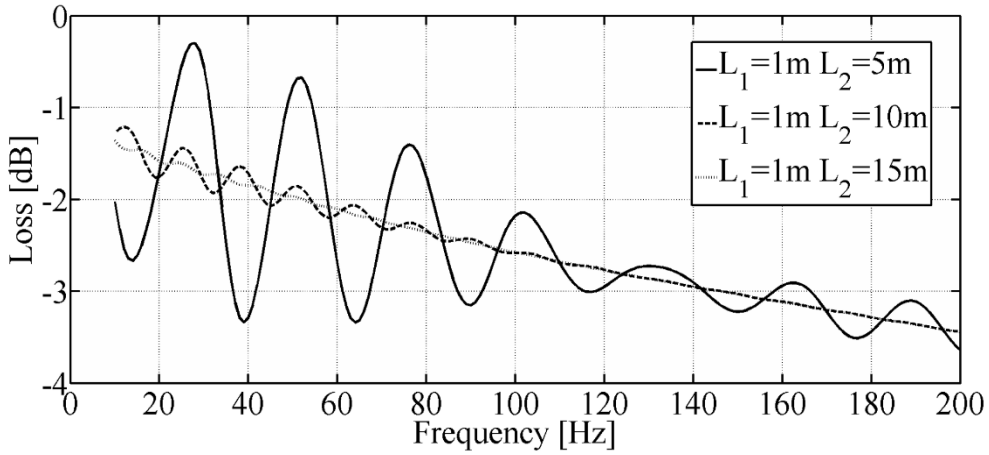

Figure 2.4 Transfer function for a waveguide probe with d = 2 mm, L_1 = 1 m, and L_2 = 5, 10, 15 m.

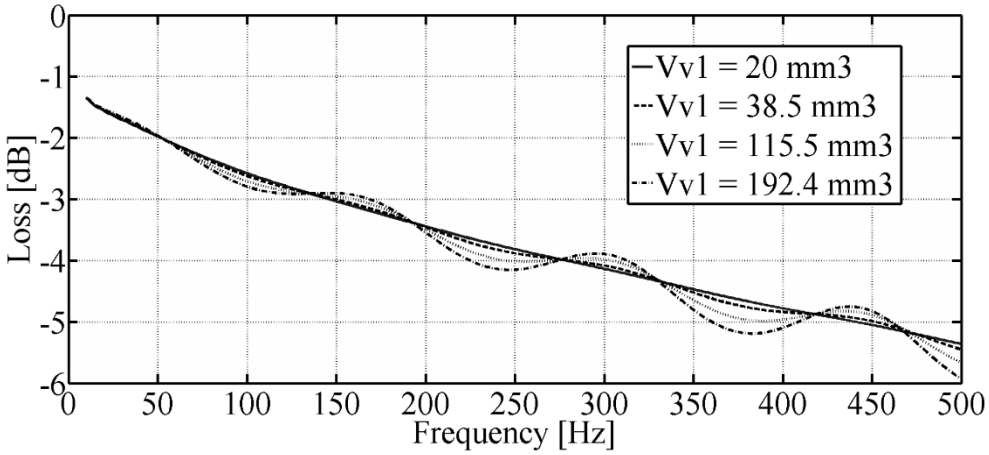

Figure 2.5 Transfer function of waveguide probe with L1 = 1 m, L2 = 20 m, and varying the sensor housing volume V_{v1}

2.1.3 Impact of the mean air temperature

As showed in the above section the dynamic response of the probe strictly depends on the thermodynamic fluid conditions, in particular by the mean steady pressure and the mean temperature. Tijdman in Ref. [10] highlighted that a variation in mean temperature of 30°C does not have much effect, whereas the mean pressure has a considerable influence.

More recently, White et al. in their work [9] found out an analytical expression for the sensitivity of the probe duct system to the variations of mean temperature. Under

simplifying assumptions: that gas properties such as absolute viscosity, the thermal conductivity and the specific heat ratio are independent of temperature. These properties are weak functions of temperature and their variations can be neglected for a low order analysis.

Considering the only wave which moves in positive direction (Figure 2.2), and the expression of propagation constant express in Eq. 2.2 the mean temperature sensitivity is given by Eq. 2.8:

$$\frac{\partial p(x,t)}{\partial T_S} = p^+ \frac{\partial e^{\Gamma x}}{\partial T_S} = \Gamma p^+ e^{\Gamma x} \frac{\partial \Gamma}{\partial T_S} = \quad \frac{\Gamma^2}{2T_S} p^+ e^{\Gamma x} = \quad \frac{C_1}{T_S^2} p^+ e^{\Gamma x} \qquad 2.8$$

where

$$C_1 = \frac{v}{\gamma R} \frac{J_o(i^{3/2}s)}{J_2(i^{3/2}s)} \frac{\gamma}{n} \qquad 2.9$$

Hence, considering the Eq. 2.8, the response of the infinite-line probe is weakly dependent on the mean temperature of fluid medium. Further the sensitivity decreases with increasing temperature. The typical application of a waveguide is for high temperature pressure measurement: rear stages of a high pressure compressor, combustor, or turbine. This means that the waveguide dynamic response obtained using the low temperature rig is indicative of its response under high temperature. Actually the high temperature decreases the decay rate and this requires to design a damping duct of a sufficient length.

3 Design of the innovative waveguide probes

In the present chapter will be presented the theory concepts and design phases of the three innovative waveguide probes conceived which are introduced in the first chapter.

In the first paragraph is showed the design of a single sensor waveguide probe which shows innovative design choices thank to which is possible to use an higher sensitivity sensor coupled with a small probe size and increase the frequency working range of the probe by replacing the damping termination with a miniaturized muffler.

In the second paragraph is showed a further improvement in the waveguide theory. Considering the idea to reduce the error estimation on pressure signal measured by the probe, it has been followed the concept to use two or more sensors. The use of multiple sensors allows a redundant measurement of the pressure signal that leads to a reduction in errors, both in term of signal attenuation that on the phase shift. With this probe it is possible to perform a proper reconstruction of a time dependent signal.

In the last section of this chapter, third paragraph, it is presented a proof of concept that would represents how the advantages of a waveguide probe can be applied and used to design a fast response aerodynamic pressure probe. This mean that the waveguide probes with specific modifications can be used to measure all characteristics of the flow: static and total pressure, velocity and angles. On the other hand, the advantages of such a devices would be relevant as virtually no temperature limit would exist, the remote pressure sensor can be easy saved from high temperatures.

3.1 Design of an innovative single sensor waveguide probe

In this section it will be discussed the development of new concept of single sensor waveguide probe which was employed to measure the 3D acoustic wave field inside a duct and the complex acoustic modes generated by a rotor stator interaction made up by a small blower in a annular duct. This two tests have been conceived to evaluate the measurement capability of the innovative waveguide probe and can be interpreted as a in scale reproductions of some real applications of these measurement devices.

The measurement of the punctual pressure of the acoustic wave field inside a duct requires a probe small enough not to influence the acoustic pressure distribution. Furthermore, the probe has to be able to reach each position inside the measurement section, with an high gain and a nearly smooth frequency response. As described in the chapter 2 a waveguide probe is made up of three main elements, a transmitting duct, a sensor housing and a damping duct.

The transmitting duct gives the possibility to reach the measurement point inside the acoustic field. As consequence, the smaller the duct diameter less modifications are introduced in the wave field under measurement. Unfortunately, reducing the diameter of transmitting duct more complicated is the coupling with the pressure transducer, the size of transducer must be reduced too and its sensitivity is reduced with its size. In this section it will discussed the design of a waveguide probe that tries to solve these drawbacks.

3.1.1 Choice of the sensor

The single sensor waveguide probe designed for measurement the 3D acoustic fields in a circular duct and the acoustic mode produced by rotor stator interaction in an annular duct, was equipped with a pressure microphone. In detail, the microphone chosen for this application is a G.R.A.S ® ¼” pressure field microphone type 46BD, Table 3.1. It is a high-precision condenser microphone with low sensitivity designed for sound measurements at high frequencies and high sound pressure levels. Its small size reduces

the effects of diffraction and reflections of waves around the microphone, resulting in a frequency range extended up to 70 kHz.

This type of microphones are largely used in acoustic tests. It is possible to find many examples where this sensors have been used to carry out acoustic pressure measures in duct where a plane wave field is propagating. In this cases, it is usually useful decompose the acoustic field in incident and reflected waves, indeed are necessary two or more measures in different points to evaluated the two waves. Obviously with this type of sensors it is not possible to measure the steady mean pressure, their use is limited to evaluate the unsteady component of signal.

Table 3.1 Specifications of microphone employed on single sensor waveguide probe

GRAS ¼" pressure field microphone specifications	
Frequency range (±1 dB)	10 – 25kHz
Dynamic range	44 – 170dB (0.003–3169Pa)
Sensitivity	1.6mV/Pa
Outer diameter	7mm

Figure 3.1 GRAS ¼" pressure field microphone

3.1.2 Dimensions of the probe

In the present work the transmitting duct diameter was set to 2.5mm and the length to 140mm in order to have a large flexibility in probe positioning, Figure 3.2. The transducer dimensions made critical its coupling with transmitting duct. The sensor depicted in Figure 3.1 has a diameter of 7mm, it was necessary to design an *ad-hoc* junction between transducer and transmitting duct. Unfortunately, the junction introduced differences between the theoretical response of probe and that real one. [23]

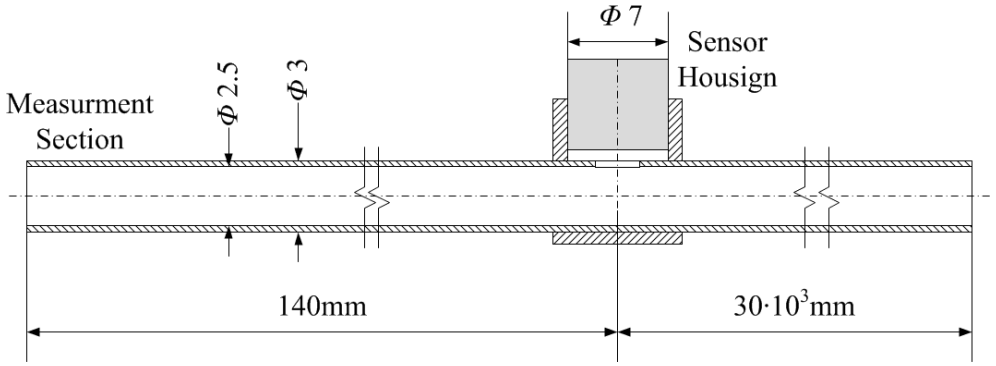

Figure 3.2 Simplify scheme of a waveguide probe, a long damping duct is considered as first step of modelling

The influence of the junction cannot be modelled easily: the transducer head creates a complex acoustic cavity in its connection with the transmitting duct, due to the different diameter between sensor and transmitting duct. For this reason, an experimental campaign was set up to estimate the influence of the junction on the frequency response of the probe. Four kinds of junctions were tested, Figure 3.3:

- Case A, a cylindrical chamber of 1 mm deep and 7 mm of diameter to have the maximum sensing surface of the transducer exposed.
- Case B, a 2 mm hole diameter and the microphone facing the hole to have a side branch configuration.
- Case C, a 1 mm hole diameter and a microphone facing the hole in order to reduce the influence of the side branch on the transmitting duct.
- Case D, a 2 mm eyelet 6 mm long and a microphone facing the eyelet, to have a larger surface preserving the duct shape.

In all four cases, the probes were coupled with a damping duct 30 meters long and with an inner diameter of 2.5mm, this length guaranteed that the reflected waves from rigid termination did not interfere with signal measured by transducer.

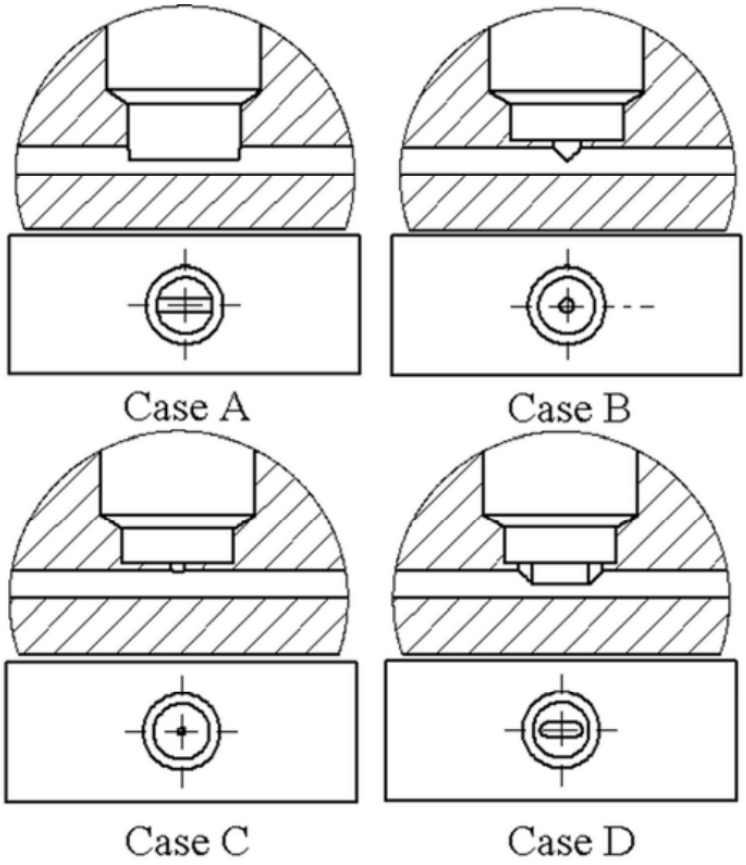

Figure 3.3 Geometries of junctions between transducer and transmitting duct

3.1.3 Calibration test rig

The four different probes described in the previous section were tested in order to evaluate the influence of different junction geometry between transmitting duct and sensor housing, described in previous section. Furthermore, the waveguide prototype needs an experimental characterization to estimate the real frequency response and the acoustic impedances of each component, since the theoretical model could not take into account possible imperfections or the actual geometrical features due to the probe manufacturing.

This experimental calibration procedure was performed on a test rig purposely developed for waveguide probe calibrations, Figure 3.4. The test rig is made up of a

straight duct with a 40mm diameter, a generation section at one end and an acoustic damping termination on the other end. The pressure wave is generated by two compression drivers (Monacor ® KU612T) driven by a waveform generator (Agilent® 33210A). The testing section is placed at 10 diameters from the source (400mm) and 5 from the other end (200mm). This section hosts two flush mounted accesses: one for the reference sensor and the other for the waveguide. The probe was calibrated in the frequency range of 0–5000 Hz with an acoustic planar field of 120 dB (20 Pa). The acoustic damping termination avoids that the resonance of test rig duct can interfere with the measures.

The upper limit of frequency range is defined by the first cut-on frequency of duct, a 3D mode a the measurement section does not guarantee the same pressure signal on the reference sensor and on the tip of probe, affecting the measure of frequency response function of probe.

All signals are acquired by a Compact DAQ 9178 by National Instrument® equipped with NI 9234 acquisition modules: resolution of 24 bit; maximum acquisition frequency: 51.2 kS/s/channel; overall pressure measurement resolution of 0.2 mPa.

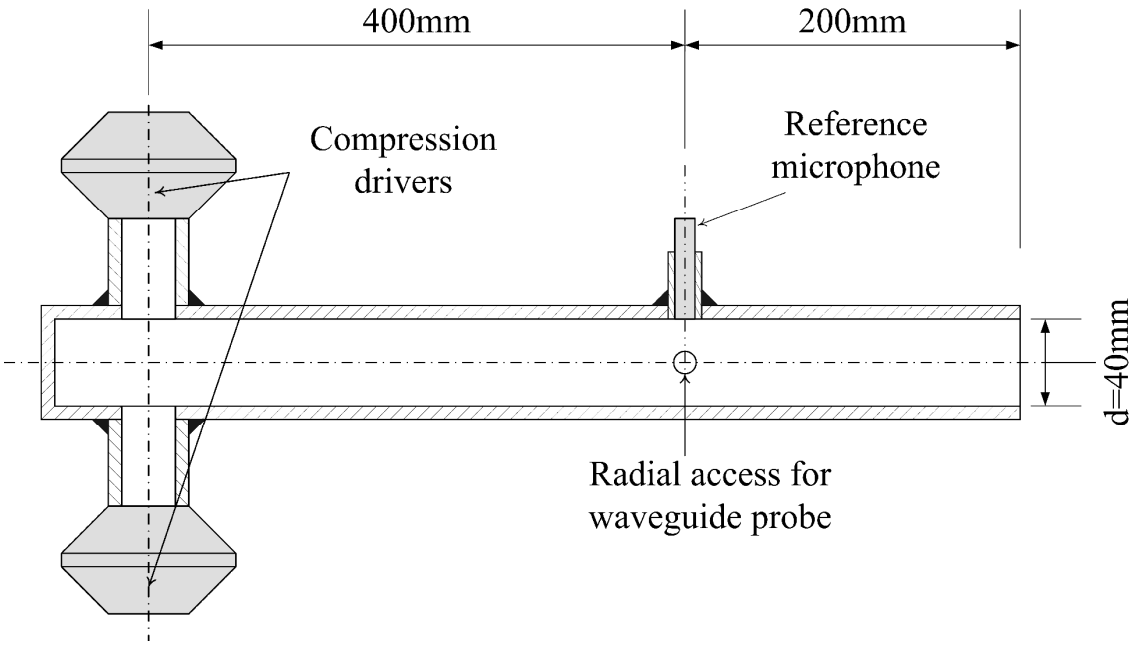

Figure 3.4 Calibration test-rig

3.1.4 Probe junction analysis and design

The optimal probe should have a frequency response which is nearly frequency independent and a low pressure attenuation drop with increasing frequency, as discussed in section 2.1.1. The four probes showed in previous sections have been tested, their attenuation functions are strongly frequency dependent as depicted in Figure 3.5. However, it should be highlighted that in some frequency ranges the probes show a gain close to zero or grater. For example, the probes equipped with housing Case-A and Case-D have frequency responses greater than zero in the range 1.2 to 1.8 kHz.The behaviour of the probe depends on the reflecting and resonance phenomena due to the geometric dimensions of the sensor housing and damping duct and the junction between this components. Furthermore, the manufacturing process can insert geometric imperfection which cannot be avoided but can affect the acoustic phenomena with small wavelength. However, the frequency response could be manipulated by changing the junction geometry, Figure 3.5. Considering the junction Case-B (Figure 3.3), which has every ducts with the same diameter, the signal transmission is function only of the acoustic impedance of side branch sensor housing and of the damping termination, the junction geometry has not influence.

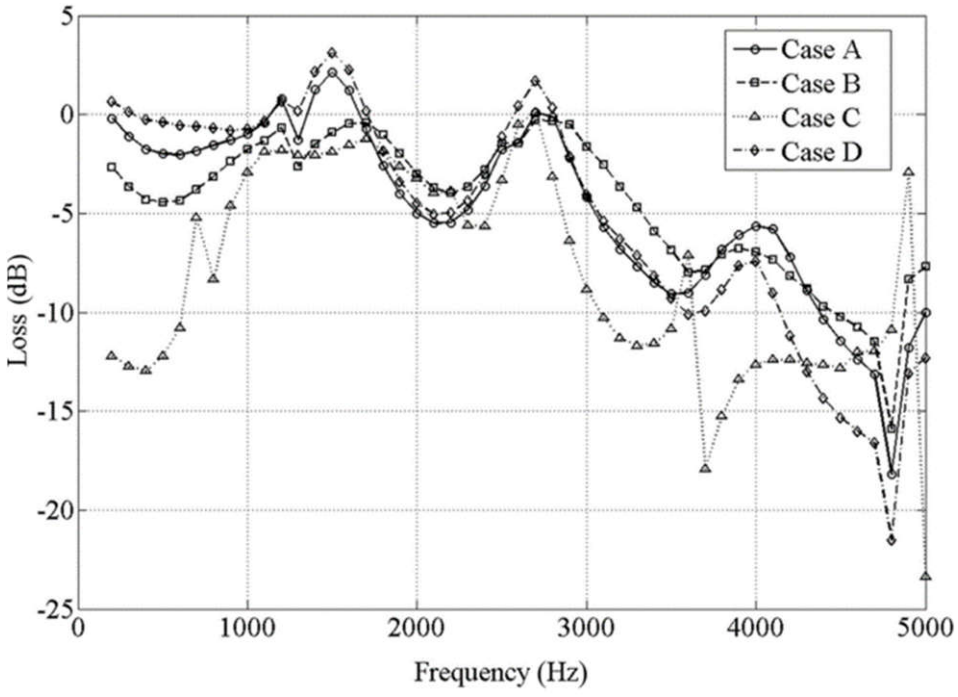

Figure 3.5 Attenuation functions comparison of probe with four different sensor junctions

3.1.5 Probe termination design

A strategy to improve the capabilities of this probes smoothing and decreasing the attenuation coefficient in the range of interest is to modify the probe geometry replacing the damping duct with an *ad-hoc* damping termination. The idea is to use the pressure oscillations reflected by the termination to improve the frequency response of probe.

Referring to Figure 3.6 and to the side branch theory, deeply described by Kinsler et al. in Ref [37] and Munjal in Ref. [25], the frequency response of the probe can be expressed as a function of the acoustic impedances of the transmitting duct, sensor housing and damping duct Eq.3.1.

$$\frac{p_1}{p_0} = \frac{2Z_p \;\; Z_t}{Z_p \;\; Z_t + Z_p + Z_t} \qquad 3.1$$

where Z_p is the impedance of the side branch which is a function of housing geometry and sensor head (Figure 3.6), Z_t is the impedance of the termination, p_1 is the pressure measured by sensor, and p_0 is the pressure on the tip of the waveguide. Since Z_p is fixed, the frequency response of the system can be modified by varying Z_t in order to obtain an attenuation function of probe smaller than possible.

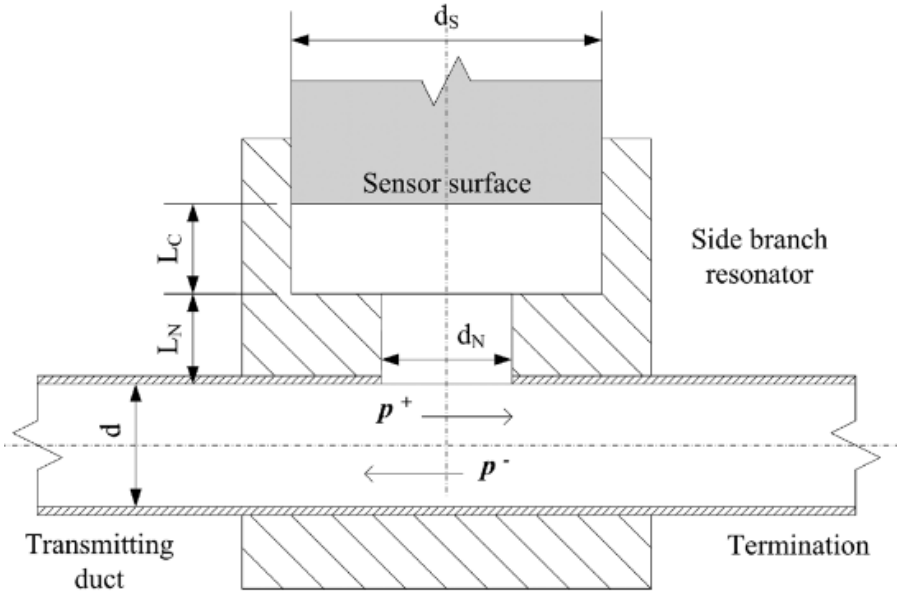

Figure 3.6 Side branch configuration, the sensor surface delimits the resonant cavity of junction, L_c is the cavity length, L_N is the neck length, d_s is the cavity diameter, d_N is the neck diameter, d is the transmitting duct diameter

The impedance of the damping duct depends on its length and the geometry of its end. By adopting a properly designed termination, the acoustic impedance of the damping duct end can be optimized for specific probe application. More in detail, this particular acoustic termination can be made as a miniaturized muffler obviously its acoustic characteristics depend on its geometry and the impedance can be easily estimated with a transfer matrix approach [25] [19]. Once the ideal value Z_t is known, it is possible to design a muffler with an equivalent acoustic impedance.

Unfortunately, due to the typical frequency response of a muffler, an optimization over all of the operating range of the probe is not possible. With a single muffler, an attenuation trend close to 0dB can be achieved only in a limited frequency range. Several mufflers can be adopted to cover different frequency ranges. In order to highlight the advantages provided by an ad-hoc design of the damping termination it is useful show their application on a numerical model of a probe. In Figure 3.7, the attenuation coefficient of a waveguide probe equipped with a muffler optimized in the low frequency range is compared to that obtained with an infinite damping duct. The probe geometry are related to the example that has been showed in the theory section 2.1.2: the transmitting duct is 1m long ($L_1=1m$), the sensor housing has a volume of 20mm^3 ($V_{v1}=30mm^3$) and the damping duct is 15m long ($L_2=15m$). In particular, the muffler is designed to obtain a low attenuation coefficient from 0 to 2250Hz.

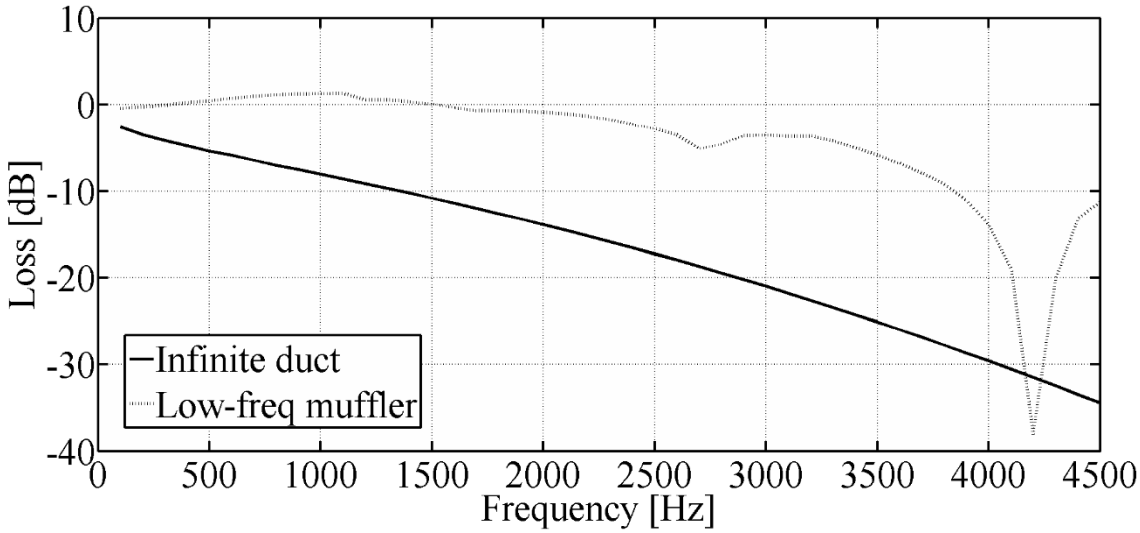

Figure 3.7 Comparison between the response of a single sensor waveguide probe with an infinite long damping duct or with a muffler optimized for low frequencies

Unfortunately, in the real application this design process shows two difficult aspect. First of all requires that sensor housing impedance Z_p is known but this value cannot be accurately estimated with a theoretical models due to the complexity of its geometry. Even if the value of Z_p is known, it will be difficult to design a muffler with a geometry able to provide the ideal value Z_t in all frequency range of probe.

Therefore, the acoustic impedance of the microphone housing is estimated using the calibration test rig. The frequency response of the probe is measured by mounting three different well known acoustic termination: a semi-infinite duct, an open duct and a single chamber muffler. Solving Eq. 3.1 respect to Z_p the microphone impedance is estimated. Once this term is known, the Eq. 3.1 can be used to design a proper termination that optimizes the probe response. By imposing a unity gain in the frequency range from 0.1 to 5 kHz, it is possible to estimate the acoustic impedance Z_t of the ideal muffler for the probe.

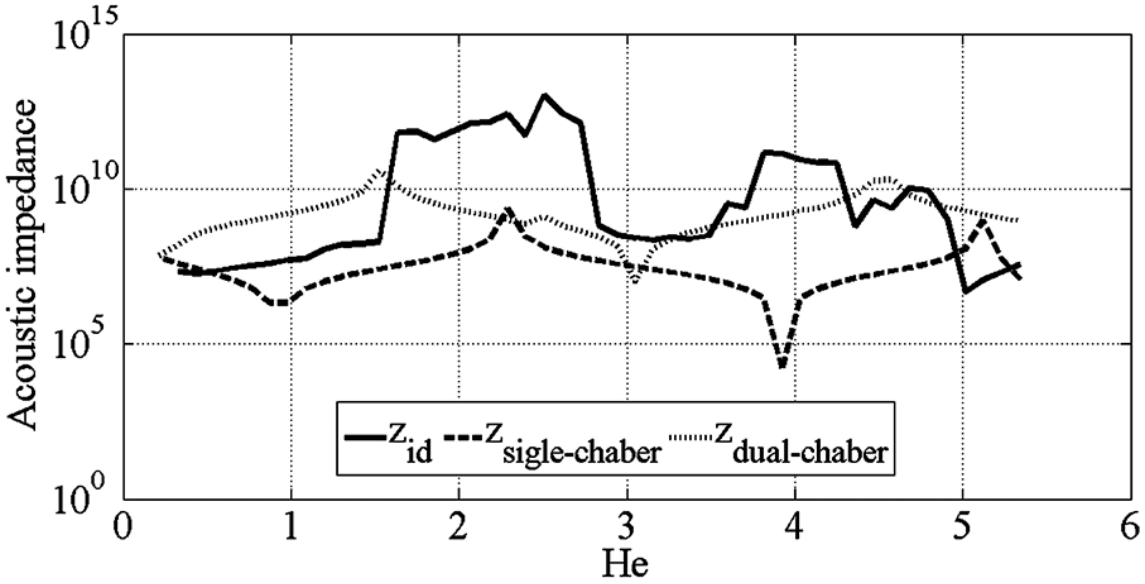

Figure 3.8 Comparison between the ideal impedance of termination with the impedance of a generic single chamber and a dual camber muffler

In Figure 3.8 is shown the global impedance of the ideal muffler Z_{id} in function of the Helmholtz number which is the product of the wave number for the characteristic length of the muffler ($He=2\pi f*D/c$). This dimensionless number takes into account both the thermodynamic condition and the main geometrical characteristics of the acoustic system. The others two plot are the acoustic impedance of a couple of mufflers, $Z_{single-}$

$_{chamber}$ is a simple single chamber muffler while $Z_{dual\text{-}chamber}$ represents a muffler divided in two volume connected by a duct, their geometry are depicted in Figure 3.9.

The analysis of the curve of the ideal muffler highlights a high mean value of impedance and the presence of peaks. The comparison of the ideal muffler curve with those of a single chamber and of a dual chamber muffler (Figure 3.8) shows that the second one better suits this application: it has a higher mean impedance value and higher flexibility to fit the ideal muffler impedance curve.

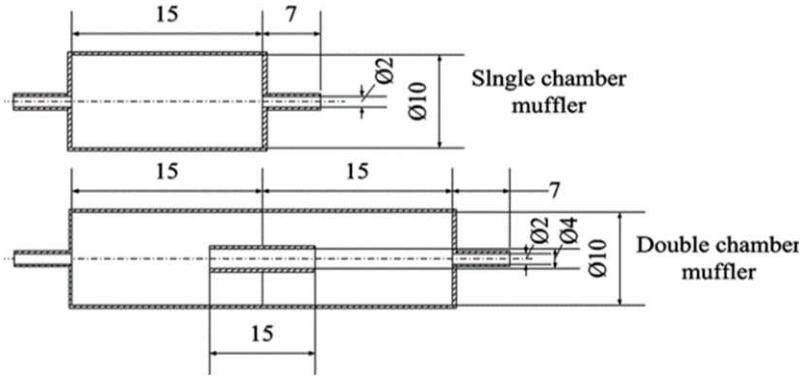

Figure 3.9 Schematic sketch of the reference single and double chamber mufflers

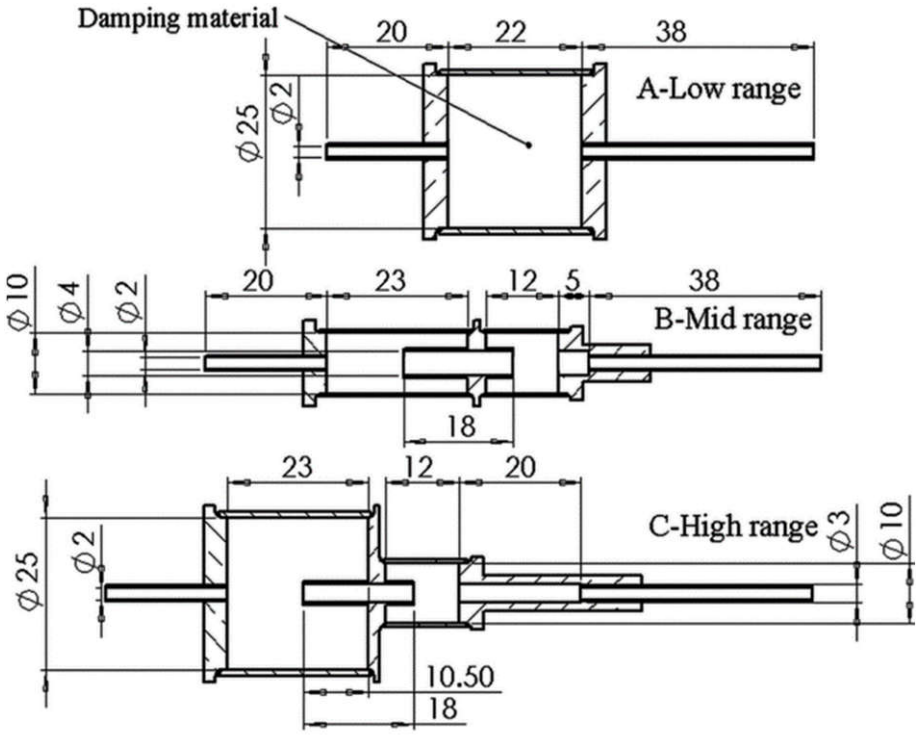

Figure 3.10 Developed mufflers

As already discussed, the reproduction of the ideal muffler impedance in the full frequency range is not possible, but can be satisfied in some ranges by using several properly designed dual chamber mufflers. From the theoretical analysis of the acoustic phenomena which were experimental investigated, section 4, the frequency ranges of interest turn out to be from 4 to 4.5 kHz for the acoustic mode measurement in the cylindrical duct and from 0.05 to 1 kHz for the case study on rotor-stator acoustic interaction. Three different mufflers are designed and realized to cover the whole frequency range of interest (Figure 3.10):

- A for the lower one (0.05 to 1 kHz)
- B for the mid-range (1.5 to 3.2 kHz)
- C for high frequency range (4 to 4.5 kHz)

The designed probes are realized and experimentally calibrated to verify the predicted frequency response Figure 3.11.

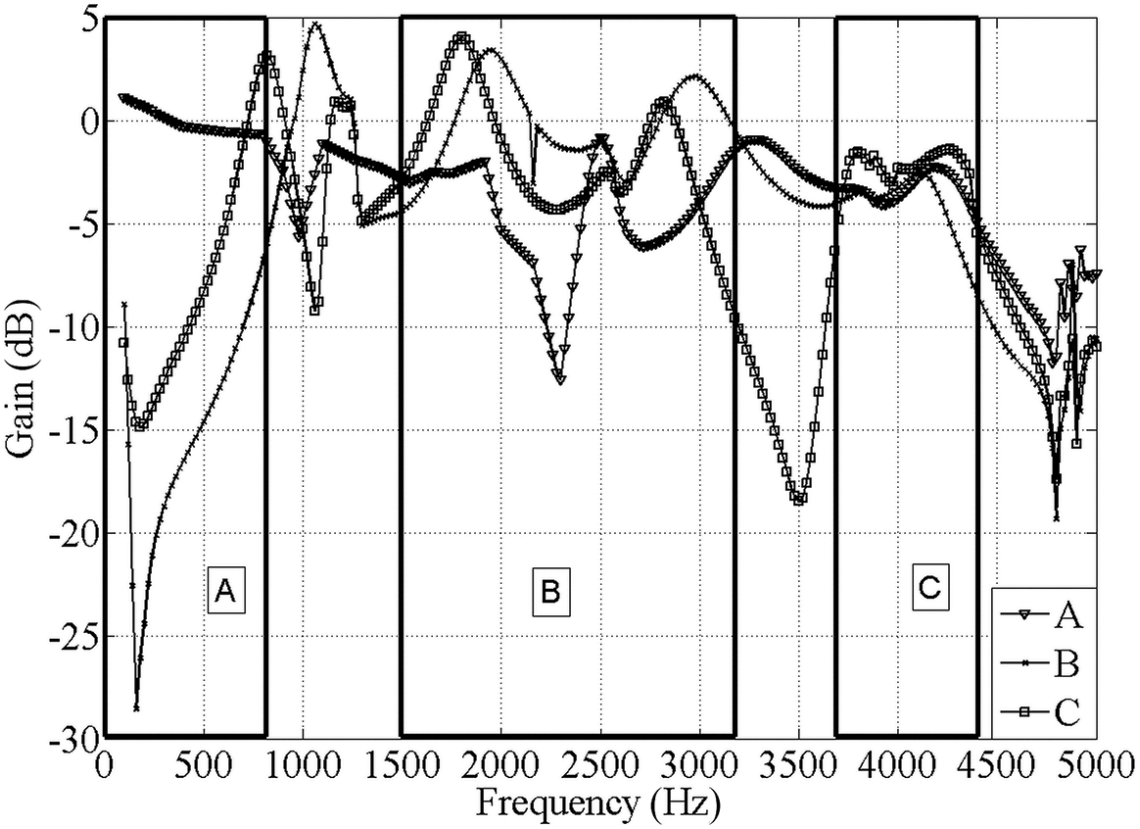

Figure 3.11 Experimental frequency response of probes with three different muffler as damping device

Figure 3.12 shows the definite agreement between the theoretical model prediction and the experimental frequency response of a probe designed to work in a frequency range from 0.8 kHz to 3.8 kHz. The differences between the calculated and experimental FRFs are probably related to the incapacity of the theoretical model to take into account some geometry details due to the probe manufacturing. The thickness of the internal duct, for example, is not negligible in comparison with the muffler dimensions.

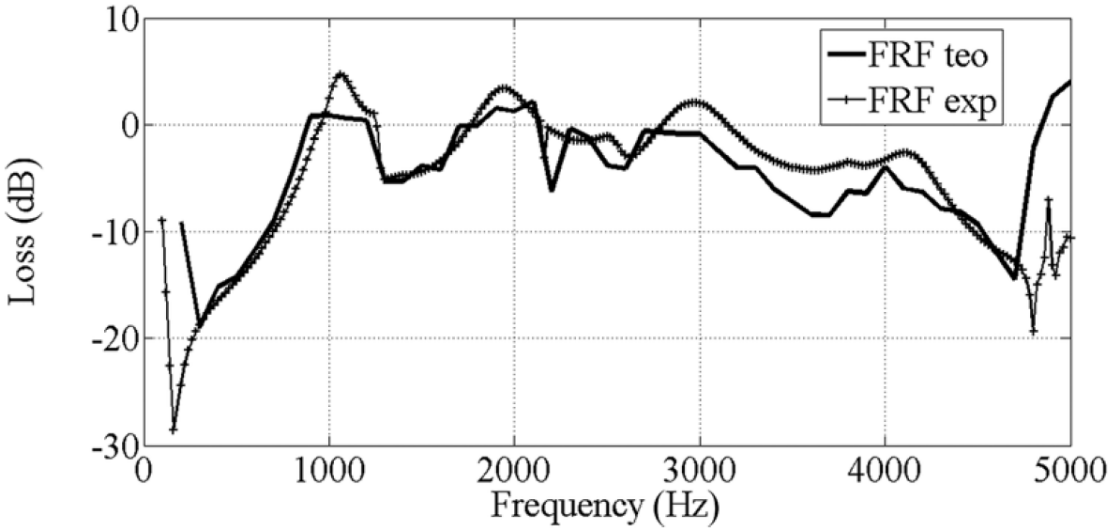

Figure 3.12 Comparison of the predicted FRF of the probe with the experimental calibration

3.3 Design of a multisensor waveguide probe

In this section, a new probe design useful to increase the frequency working range is proposed. The new conception of probe want be a further step to increase the measurement capabilities of this device. It is based on the adoption of a combination of several sensors and the use of an ad hoc designed termination (Figure 3.13). A multisensor waveguide probe is conceived as a transmitting duct, a measurement section with the sensor housings (each one with a well determined position and distance from the others), and a muffler as damping termination (Lenzi et al. in Ref. [41])

As shown in previously sections, the benefits of a muffler as a termination are clear since it allows an adjustment of the probe frequency response function. On the other hand, the use of several sensors instead of only one allows one to exploit additional pressure measurements along the probe and then lower measurement error.

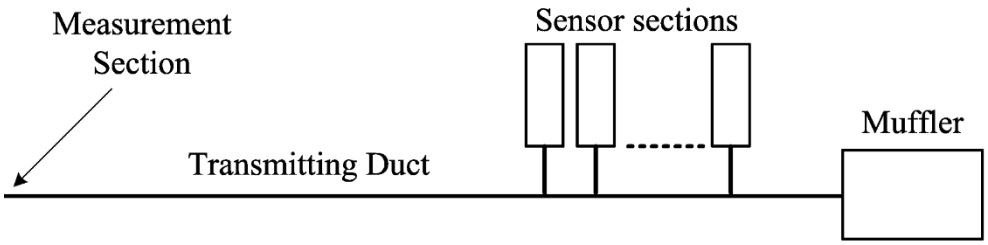

Figure 3.13 Scheme of a multisensor waveguide probe with a muffler as the damping termination

More in detail, in a two sensor probe where the impedances of each component are known, the pressure p_0 can be estimated by using each sensor separately as if they were two one sensor probes. If one considers the pressure read by the two sensors together it is possible to neglect in the reconstruction of the pressure p_0 the impedance of the duct connecting the two sensors or that of the termination. In other words, the use of a two sensor probe is equivalent to the use of four probes with different transfer functions. For each frequency, the configuration with the lowest attenuation value can be adopted. In the present paper, only the impedance between the sensors was neglected in case of a multiple reading since the termination was used to improve the probe response.

3.3.1 Theory of a two-sensor waveguide probe

For the sake of simplicity, in this section, the theoretical analysis of a two-sensor waveguide probe with an infinite duct as damping device will be shown. The probe was supposed as ideal, with no manufacturing imperfections such as unexpected discontinuities. The sensors were considered with rigid sensing elements (no geometry variations due to the pressure applied on them). From a theoretical point of view, each element of the probe can be modelled exploiting the electro-acoustic analogy (see Refs. [19] and [21]) according to which the pressure and volume flow rate oscillations in the connections between two adjacent elements can be described as a two-port matrix,

$$\begin{Bmatrix} p_j \\ u_j \end{Bmatrix} = \begin{bmatrix} M^{(1,1)} & M^{(1,2)} \\ M^{(2,1)} & M^{(2,2)} \end{bmatrix} \begin{Bmatrix} p_{j-1} \\ u_{j-1} \end{Bmatrix} \qquad 3.2$$

where p and u are the state variables, the subscripts j and $j\text{-}1$ refer to the upstream and downstream sections of the element, respectively, and the terms of the matrix depend on the acoustic impedance of the element.

In particular, the probe (transmitting duct, sensor housings, and termination) can be modelled as a combination of three elements: straight ducts, T-junctions, and diameter discontinuities. The sensor housing was modelled as a side branch resonator (Figure 3.6) with a dead volume of 38 mm^3. The probe can be modelled by considering three ducts: (D_j), two T-junctions (J_j) and two side branch resonators (D_{Sj}) (Figure 3.14).

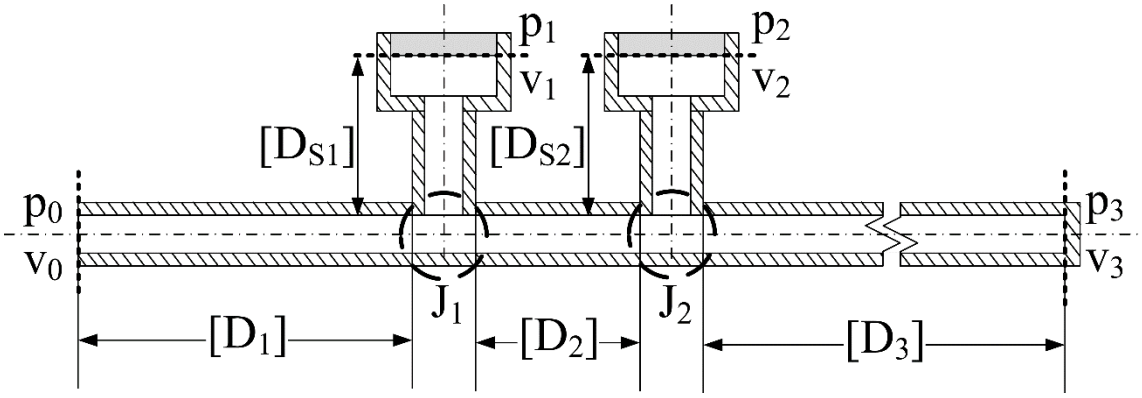

Figure 3.14 Scheme of the two sensors waveguide probe, D_i duct of length L_i, J_i junction, D_{Si} side branch sensors housing, p_i v_i state variables at the considered section. The sections are highlighted as dotted lines.

Starting from the right hand side of the probe, the termination can be described as a pneumatic line whose transfer matrix is depicted in Eq. 3.3

$$\begin{Bmatrix} p_{J23} \\ u_{J23} \end{Bmatrix} = \begin{bmatrix} D_3^{(1,1)} & D_3^{(1,2)} \\ D_3^{(2,1)} & D_3^{(2,2)} \end{bmatrix} \begin{Bmatrix} p_3 \\ u_3 \end{Bmatrix} = \begin{bmatrix} \cosh(\Gamma L_3) & Z_C \sinh(\Gamma L_3) \\ \frac{1}{Z_C}\sinh(\Gamma L_3) & \cosh(\Gamma L_3) \end{bmatrix} \begin{Bmatrix} p_3 \\ u_3 \end{Bmatrix} \quad 3.3$$

Where, L_3 is the duct length and Z_C is the distribuited acoustic impedance of a mono-dimensional line and it is expressed in Eq. 3.4 according to the theory of Tijdman and Bergh [16] and [17]:

$$Z_C = \frac{\Gamma}{i\left(\frac{\omega}{a}\right)\frac{S}{\rho\, a}\,\frac{\gamma}{n}} = i\left(\frac{c}{\omega}\right)\frac{S}{\rho\, a}\,\frac{\gamma}{n\Gamma} = i\left(\frac{c}{\omega}\right)\frac{\pi R^2}{\rho\, a}\,\frac{\gamma}{n\Gamma} \quad 3.4$$

where a is the sound speed, R is the duct radius, ρ is density, n is the polytrophic constant inside the duct and Γ is the complex propagation constant.

The sensor housing is modeled as a side branch resonator whose transfer matrix was obtained as a composition of three different matrix: a duct matrix for the neck, a discontinuity for the abrupt diameter change, and a duct matrix for the cavity. For the sake of brevity, in Eq. 3.5, the resulting matrix is reported and all the mathematical passages can be found in Refs.[19] and [21].

$$\begin{Bmatrix} p_{J22} \\ u_{J22} \end{Bmatrix} = \begin{bmatrix} \cosh(\Gamma L) & Z_C \sinh(\Gamma L) \\ \frac{1}{Z_C}\sinh(\Gamma L) & \cosh(\Gamma L) \end{bmatrix}_N \begin{bmatrix} \cosh(\Gamma L) & Z_C \sinh(\Gamma L) \\ \frac{1}{Z_C}\sinh(\Gamma L) & \cosh(\Gamma L) \end{bmatrix}_C \begin{Bmatrix} p_2 \\ u_2 \end{Bmatrix} \quad 3.5$$

where the subscripts N and C are referenced to the neck and the cavity of the resonator (Figure 3.6). By adopting the hypothesis of operating with signals with wavelengths considerably longer than the dimensions of the duct, $\Gamma^2 L^2 << 1$, Eq. 3.5 can be simplified in the following equation:

$$\begin{Bmatrix} p_{J22} \\ u_{J22} \end{Bmatrix} = \begin{bmatrix} 1 & Z_C \Gamma L \\ \frac{1}{Z_C}\Gamma L & 1 \end{bmatrix}_N \begin{bmatrix} 1 & Z_C \Gamma L \\ \frac{1}{Z_C}\Gamma L & 1 \end{bmatrix}_C \begin{Bmatrix} p_2 \\ u_2 \end{Bmatrix} = \begin{bmatrix} D_H{}^{(1,1)} & D_H{}^{(1,2)} \\ D_H{}^{(2,1)} & D_H{}^{(2,2)} \end{bmatrix} \begin{Bmatrix} p_2 \\ u_2 \end{Bmatrix} \quad 3.6$$

At junction J_2 (Figure 3.15), the equilibrium of pressures and the conservation of volume flow rate can be expressed as in the following equations:

$$\begin{cases} p_{J21} = p_{J22} = p_{J23} \\ u_{J21} = u_{J22} + u_{J23} \end{cases} \quad 3.7$$

By expanding Eq. 3.4 and applying the boundary conditions of rigid wall at the damping duct end and sensor surfaces (u_2=u_3=0), the pressure and volume oscillations at the inlet of section J_{21} of Figure 3.15 can be expressed as:

$$\begin{cases} p_{J21} = p_2 \\ u_{J21} = H_V p_2 \end{cases} \quad 3.8$$

Where

$$H_V = \left[1 + \left(\frac{D_3^{(2,1)}}{D_3^{(1,1)}} + D_{S2}^{(2,1)}\right)\right] \quad 3.9$$

The same approach can be repeated with junction J_1. The pressure p_0 can be expressed in terms of the pressure p_1 and the velocity u_{J13} by means of the transfer matrix of the duct D_1 and the acoustic impedance of first sensor housing (Figure 3.16).

The duct D_2 which connects the two junctions is short. As consequences, the velocity oscillations at the two ends of the duct can be assumed as equal ($u_{J13} = u_{J21}$). Then the state variables at section 0 can be expressed as a complex function of the pressures at the two sensor surfaces,

$$p_0 = Ap_1 + Bp_2 \quad 3.10$$

Where

$$\begin{gathered} A = \left(D_1^{(1,1)} D_{S1}^{(1,1)} + D_1^{(1,2)} D_{S1}^{(2,1)}\right) \\ B = D_1^{(1,2)} H_V \end{gathered} \quad 3.11$$

Equation 3.10 highlights that the state variables at the inlet section can be expressed as a function of the pressure measured by sensor 1 and sensor 2. On the other hand, by means of the transfer matrix of duct D_2, it is possible to correlate the pressures at the sensor sections. This relation depends only on the probe geometry,

$$\alpha = \frac{p_2}{p_1} = \frac{H_P}{D_S^{(1,1)}} \quad 3.12$$

Where,

$$H_P = 1 + Z_{D2}\frac{D_3^{(2,1)}}{D_3^{(1,1)}} \qquad 3.13$$

By considering the relation 3.12 , the Eq. 3.10 can be written as Eq. 3.14 or Eq. 3.15. These two equations show that a two-sensor waveguide can be thought of as two single sensor probes

$$p_0 = (A + B/\alpha)p_1 \qquad 3.14$$

$$p_0 = (A\alpha + B)p_2 \qquad 3.15$$

Equations 3.10, 3.14, and 3.15, are equivalent and can be adopted indiscriminately: each one expresses the pressure p_0 in terms of p_1 and p_2 by means of a proper transfer function. If one considers an absolute error on the sensor pressure measurement, the three equations lead to different absolute errors in term of pressure at the measurement section. In detail, by assuming that the absolute error on each sensor is the same ($\delta p_1=\delta p_2=\delta p$), the error propagation leads to three different expressions for the error at the measurement section (δp_0).

$$\delta p_0 = (A+B)\,\delta p \qquad 3.16$$

$$\delta p_0 = (A+B/\alpha)\,\delta p \qquad 3.17$$

$$\delta p_0 = (A\alpha+B)\,\delta p \qquad 3.18$$

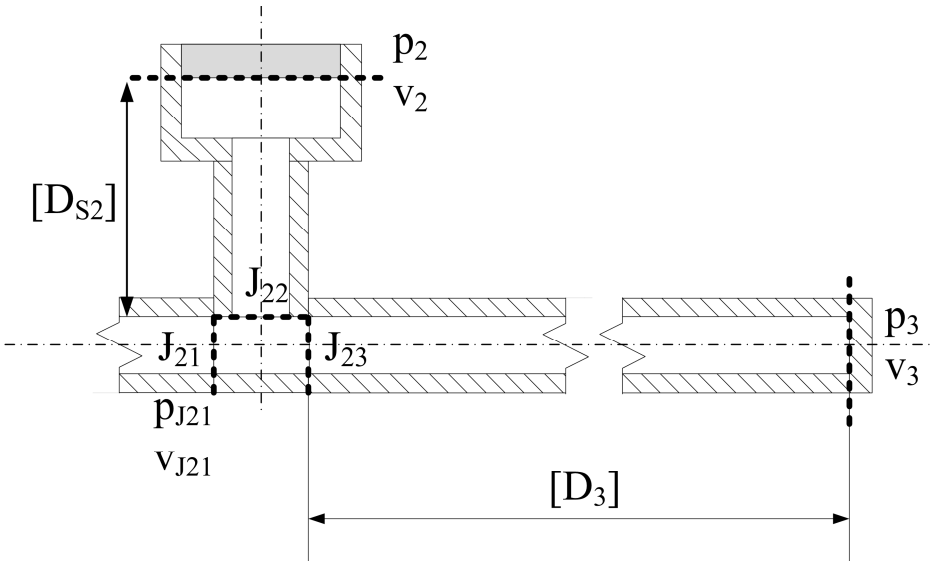

Figure 3.15 Scheme of the junction at second sensor housing J_2, $V_3=0$ and $V_2=0$ as boundary conditions

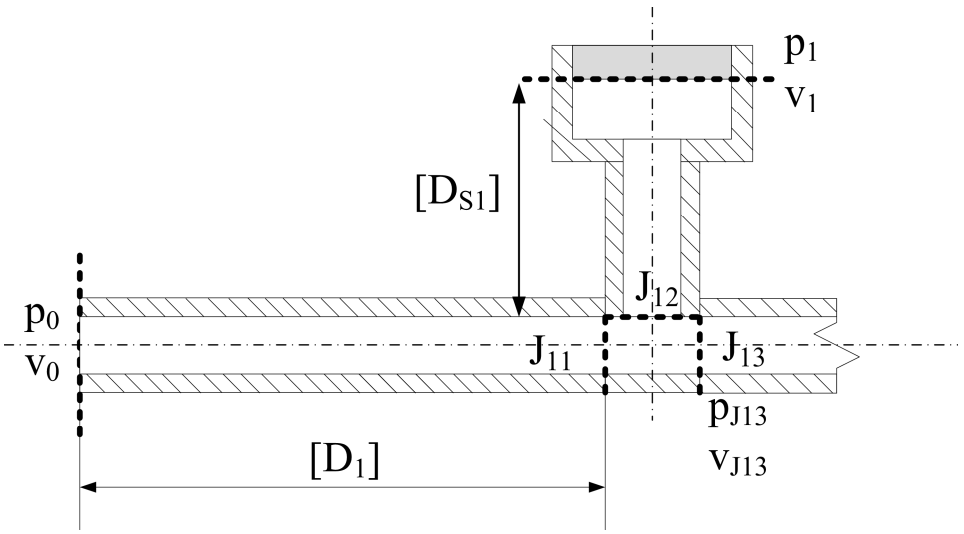

Figure 3.16 Scheme of the junction at first sensor housing J_1, $V_1=0$ as boundary conditions

As mentioned above, A, B, and α are complex coefficients (with a modulus and phase) that were achieved by the combination of the transfer matrix elements. Their combination follows the rules of the operations between complex numbers. Since the equations above are indiscriminately valid it is possible to choose the transfer function that minimizes the error δp_0 in a specific range of frequencies. The previous equations can be expressed as:

$$\delta p_0 = K_j \, \delta p \qquad 3.19$$

where Kj is alternatively $Kj=(A+B/\alpha)$, $Kj=(A\alpha+B)$ and $Kj=(A+B)$. It should be noticed that δp_0 is a complex number expressing an error both in amplitude and phase. For each frequency, the $Kj\delta p$ value that minimizes the error δp_0 is selected for a given δp. Since $Kj\delta p$ is a complex number, it is not possible to define a minimum as with real numbers. As a compromise, the $Kj\delta p$ value that minimizes the modulus of δp_0 was chosen. This choice does not guarantee the minimum error in terms of phase shift, but the smaller the modulus of δp_0, the smaller the phase shift error (E_ϕ) (Figure 3.17).

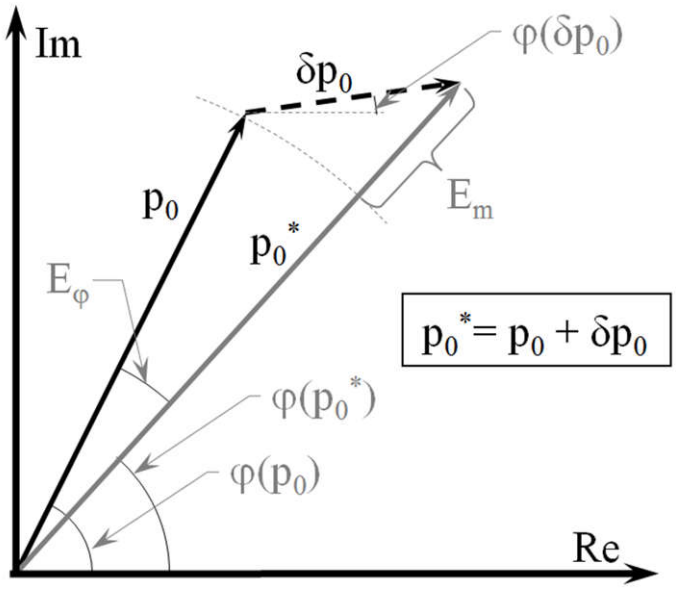

Figure 3.17 Influence of δp_0 modulus and phase on the estimation of p_0. The smaller the modulus δp_0, the smaller the error on the estimation of the modulus (E_m) and phase ($E\phi$) of p_0.

It should be noticed that the K_j parameter is strongly dependent on the α value which, in turn, is only dependent on the probe geometry and, in particular, on the disposition of sensors. For this reason, an accurate investigation to determine the optimal sensor disposition is necessary during the probe design. The advantages of using a multisensor probe instead of a single sensor probe are clear. If one considers the waveguide in Figure 3.18 with two dynamic pressure sensors with a pressure range of 0–5 psi (0 – 35 kPa), an error of 0.1% on full scale output and an error on phase estimation of 2 deg (due to measurement chain uncertainties such as parasitic capacities, lag due to amplification devices, signal noise, low resolution of the frequency spectrum, fluctuations of the turbomachine rotation speed that is usually the reference signal source, etc.), the modulus of K_j in the range of frequency 0 – 5 kHz is that reported in Figure 3.19. This range of frequency was chosen by taking into account the calibration device adopted for the experimental assessment (an acoustic source). By considering the same methodology, the probe can be developed for any range of frequencies as long as a proper calibration device is used.

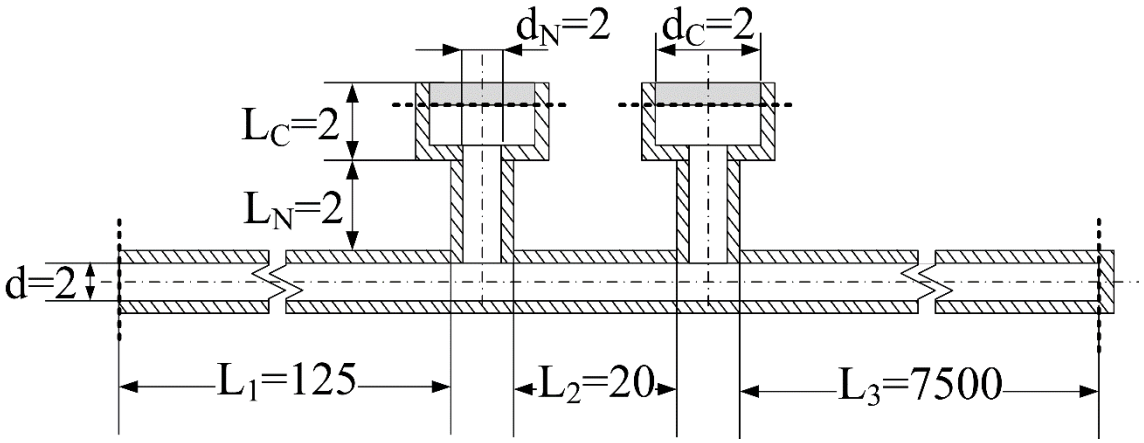

Figure 3.18 Two sensor waveguide geometry (dimensions in mm)

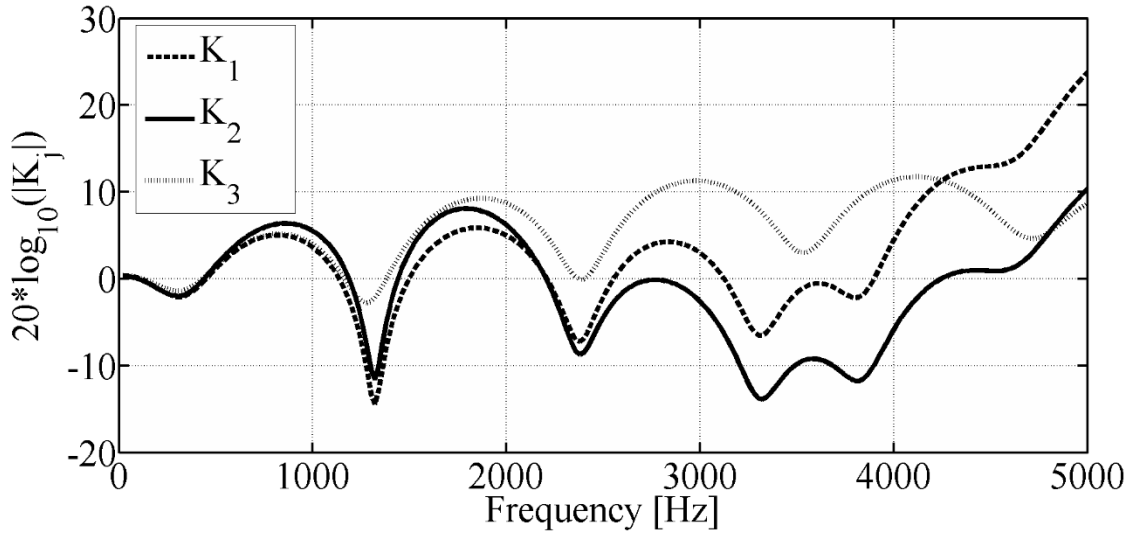

Figure 3.19 Error amplification functions for the two sensor waveguide

In Figure 3.20, the frequency where each transfer function has the minimum modulus is reported. For each frequency, the configuration chosen to calculate the pressure at the measurement section is that leading to the smallest error amplification. On this basis, it is possible to estimate $\delta p_0 = K_j \delta p$ in the range of frequency of interest (0 – 5 kHz).

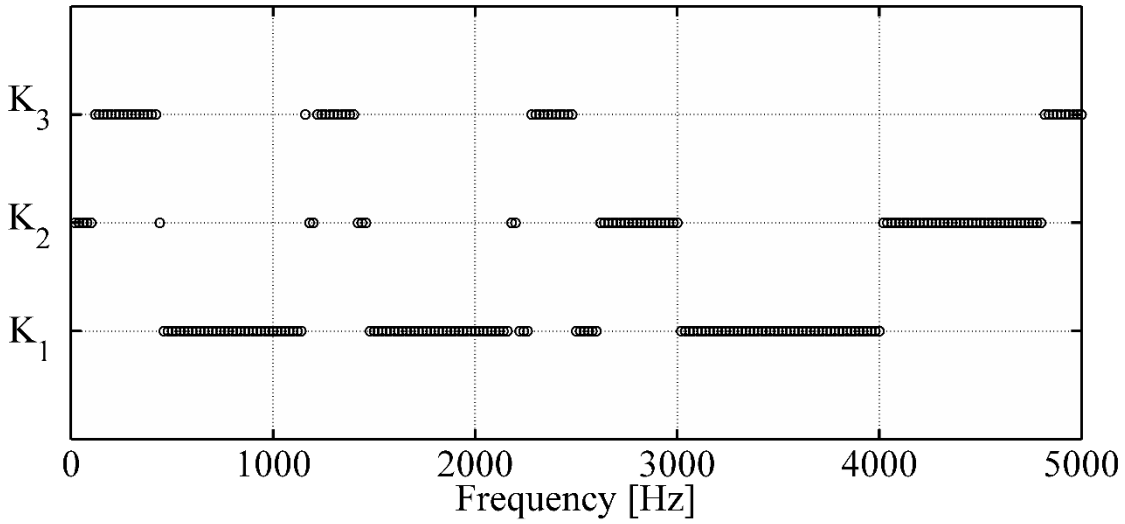

Figure 3.20 Configuration chosen to calculate the pressure at the measurement section as a function of frequency

In addition, for a given p_0, it is also possible to estimate the absolute error in terms of modulus (E_m) and phase (E_φ). For the sake of simplicity, since both E_m and E_φ depend on the modulus and phase of p_0, the pressure at section 0 was assumed as a sinusoidal wave with amplitude (1, 2, 3 psi – 7, 14, 21 kPa) and phase of 0 deg. The results are reported Figure 3.21 and Figure 3.22.

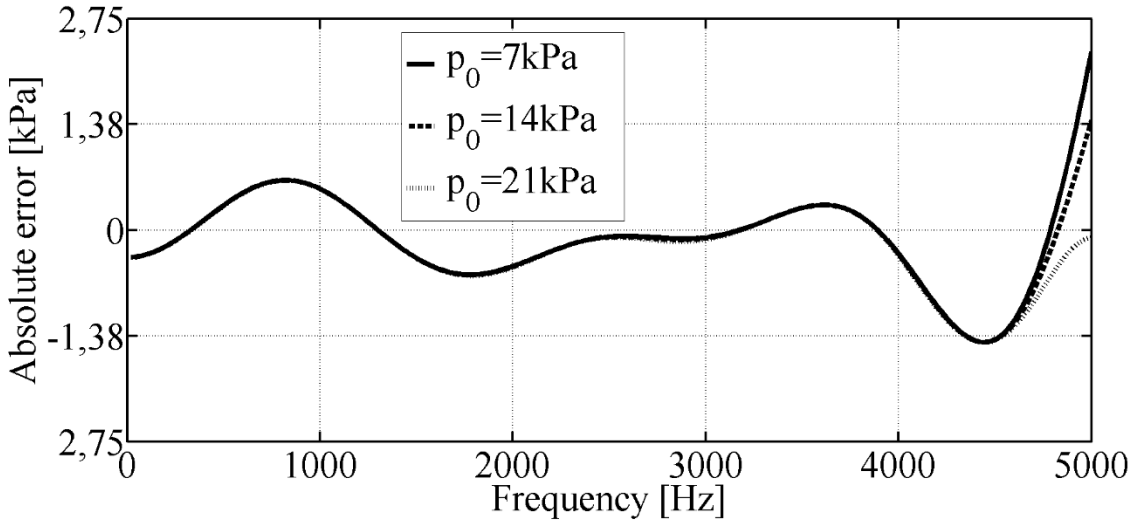

Figure 3.21 Absolute error modulus estimation for different pressure oscillation amplitude at measurement section

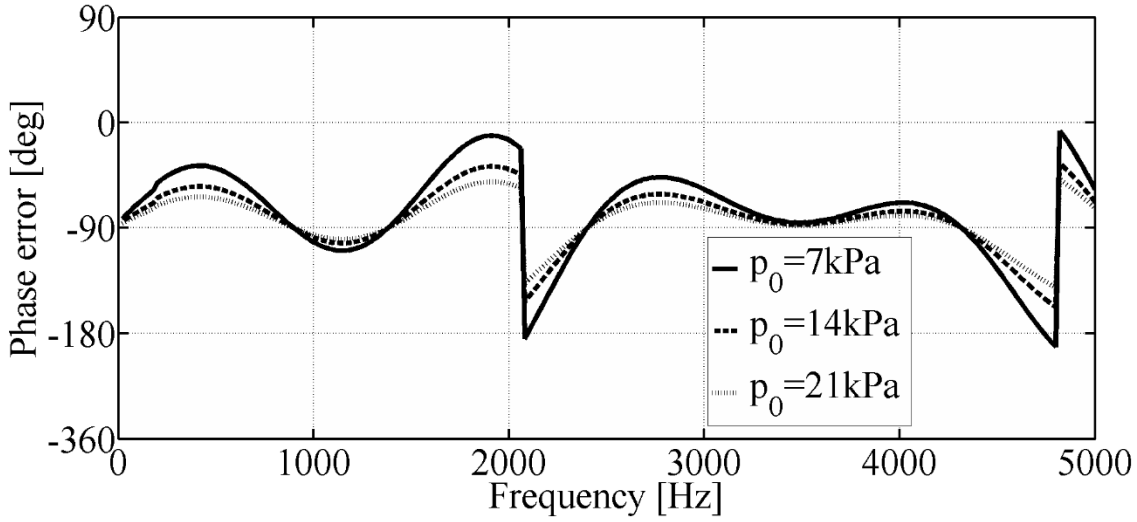

Figure 3.22 Absolute error phase estimation for different pressure oscillation amplitude at measurement section

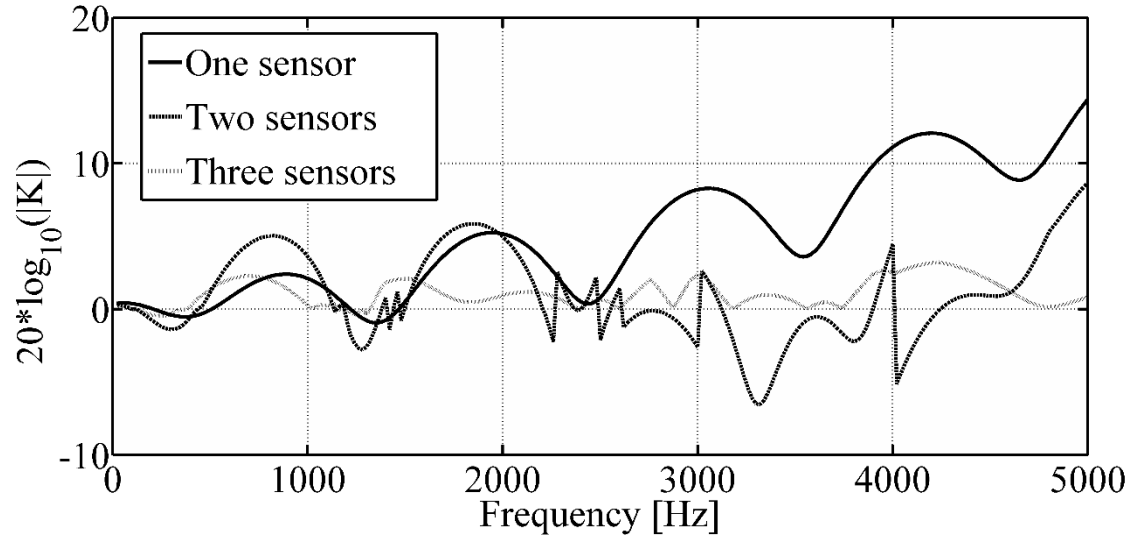

Figure 3.23 Comparison between probes with different number of sensors in terms of error amplification modulus

In general terms by increasing the number of sensors the number of equations that can be used to express p_0 increases exponentially. In case of a three sensor probe, the number of transfer functions among which it is possible to choose becomes eleven. If one decides not to neglect the termination impedance for the signal reconstruction, the equations are seven: *K1(p1), K2(p2), K3(p3), K4(p1, p2), K5(p2, p3), K6(p1, p3),* and *K7(p1, p2, p3).* In Figure 3.23, the error amplification K_j for a probe with one, two and three sensors is reported in the range of 0 – 5 kHz. The three probes have been considered

with the same transmitting duct length and sensor housing geometry. In the three sensor probe, the additional sensor was placed at 8 mm downstream the second sensor. It is evident that by increasing the number of sensors, the amplification of the measurement error becomes smaller for a greater frequency range. In Table 3.2, the average values and the standard deviations of the amplification factor for the three probes are reported.

Table 3.2 Average and standard deviation of the amplification factor in the range of 0 – 5 kHz for a probe with one, two, or three sensors

Quantity	1 sensor	2 sensor	3 sensor
Average	2.01	0.506	0.580
Standard deviation	1.74	1.978	1.718

3.3.2 Multisensor waveguide design

In the previous sub-paragraph, the advantages of using a multisensor probe were highlighted. The present study was limited to the development of a three sensor probe, since this configuration is a valid compromise between the complexity, cost, and accuracy of the probe. The first step of a three sensor waveguide probe design is the determination of the sensors spacing. For this purpose, a simplified model of the waveguide was developed by using the previously described approach and considering an infinite duct as termination. The probe design parameters were: a transmitting duct diameter of 2 mm, a length of 125 mm, and a sensor housing geometry as that reported in Figure 3.6 (L_C an d_N = 2 mm, L_N = 1, d_s = 7 mm). By utilizing the method outlined in the previous paragraph, the model was used to estimate the influence of different sensor spacing on the error propagation in the waveguide (Figure 3.24). To perform this calculation, the authors proposed to use three dynamic pressure sensors with a pressure range of 0 – 5 psi (0 – 35 kPa), a 0.1% error on full scale output, and an error on the phase estimation of 2deg. Referring to the maps in Figure 3.24, it was possible to define the optimal spacing between each sensor that minimizes the error in the estimation of p_0 in terms of average error and standards deviation over the range 0 – 4 kHz. The minimization of the error and probe dimensions was considered as probe constraints to select the proper spacing. Consequently, a spacing between sensor 1 and 2 of 18 mm and of 8 mm between sensor

2 and 3 were chosen. It is important to notice that while the absolute error depends on the sensor error, the error amplification coefficient K_j is only a function of the probe geometry, independent of the sensors fullscale measurement error. For this reason, the optimal spacing that minimizes the error propagation is only related to the geometries of the probe and sensor housings and not to the sensor measurement errors. In other terms, the optimal spacing is not related to the measurement characteristics of the sensor but only to its geometry.

The probe was manufactured taking into account these dimensions (Figure 3.25 and Figure 3.26) and was equipped with three ¼ in pressure microphone type 46BD by G.R.A.S. ® with a measurement range of 44 – 168dB (0.003 – 3169Pa) and an error of 1 dB for frequencies between 10 Hz and 25 kHz. The waveguide prototype needs an experimental characterization to estimate the impedances of each component, since the theoretical model could not take into account possible imperfections or the actual geometrical features due to the probe manufacturing. This experimental calibration procedure was performed on a test rig purposely developed for waveguide probe calibrations (Figure 3.4), the same descripted in paragraph 3.1.3.

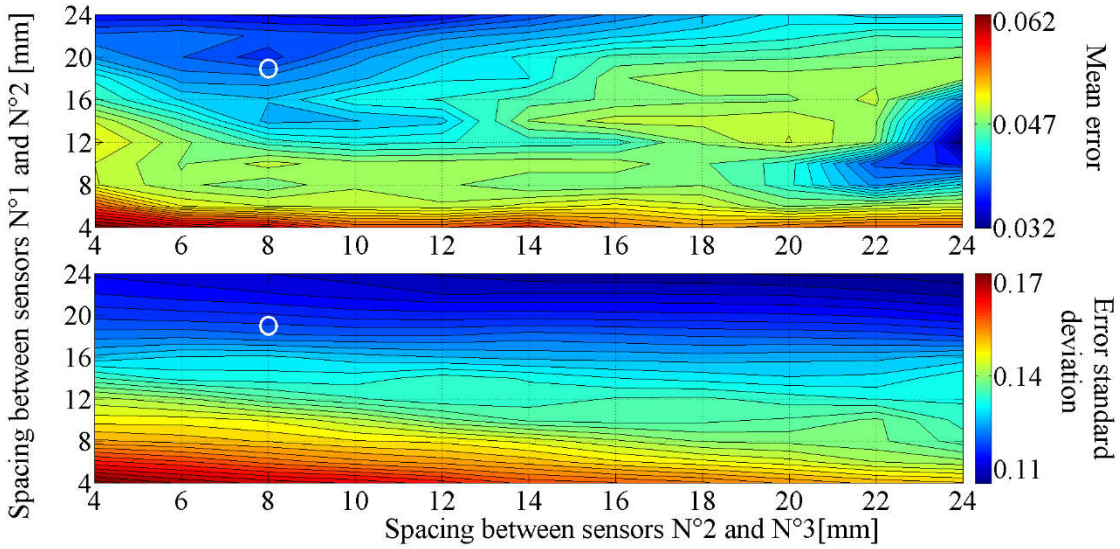

Figure 3.24 Effect of the spacing of the sensors on the modulus of the absolute error (δp_0) with a three sensor probe in terms of average error and standards deviation over the range of 0 – 4 kHz

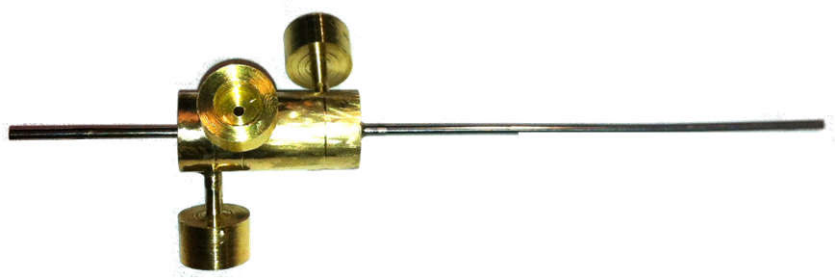

Figure 3.25 Picture of the three sensor probe

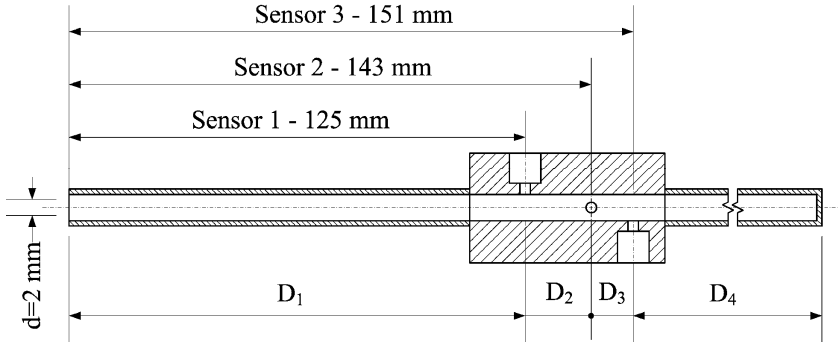

Figure 3.26 Design of probe with infinite duct as damping termination

Because of the complex geometry of the multisensor waveguide, a specific procedure was developed to determine the impedance of the three sensor housings and the two ducts D_2 and D_3 (Figure 3.26). The characterization of the single sensor housing (including the effect of a non-rigid sensor head) was performed by closing the other two housings with a rigid plug. The plugs were designed to restore the shape of the transmitting duct. In this manner, the probe becomes very similar to a single sensor waveguide with an infinite duct as damping termination.

By expressing Eq. 3.1 with the transfer matrix of the transmitting duct Eq. 3.3 (with L_1 instead of L_3), it is possible express the sensor housing impedance including the effects due to a non-rigid sensor head

$$Z_{Sj} = \left[\frac{p_0 - D_1^{(11)} \times p_j}{D_1^{(12)}} - \frac{p_j}{Y} \right]^{-1} \times p_j \qquad 3.20$$

where p_0 is the reference pressure and p_j is the pressure measured by the sensor. The second step was the characterization of the ducts D_2. By referring to Figure 3.26, if one closes the third housing, the waveguide becomes a two sensor waveguide. By

measuring the two pressures p_1 and p_2 and using Eq.3.10, the element of impedance matrix of the duct D_2 can be expressed as:

$$Z_{D2} = \left(\frac{p_1}{p_2} - 1 \right) \times \left(\frac{1}{Z_{S2}} + \frac{1}{Y} \right) \qquad 3.21$$

where Z_{S2} is the impedance of sensor housing estimated at the previous calibration step, and Y is the impedance of the damping duct. Equation derives from the previous theoretical analysis of a two sensor probe. The next step was the characterization of the duct D_3. The first sensor housing was closed and the transfer matrix of D_3 was estimated by using the pressure signals measured by p_2 and p_3

$$Z_{D2} = \left(\frac{p_2}{p_3} - 1 \right) \times \left(\frac{1}{Z_{S3}} + \frac{1}{Y} \right) \qquad 3.22$$

The calibration procedure highlighted some differences between the theoretical and real impedances of the sensor housings and ducts. These differences lead to a deviation of the performance of the real waveguide from the theoretical one. In order to improve the behavior of the developed waveguide, the damping duct was replaced by a muffler.

In theory, for a configuration with three sensors, seven different mufflers would be necessary, each one optimized for a particular configuration. A preliminary study similar to that outlined in the previous paragraph pointed out that the best results in terms of error amplification are achieved when using a three sensor expression of the amplification factor (K_7). For the sake of simplicity, only the muffler optimized for this probe configuration was designed.

By using the impedances obtained with the experimental calibration, the optimal impedance of an ideal muffler that compensates for the error due to the probe manufacturing was estimated. This impedance was used as the goal function of the muffler design process. This process, based on a trial and error approach, can be very time consuming but a full match between the ideal and real impedance curves is not necessary. A result such as that reported in Figure 3.27 is sufficient to guarantee a good compensation of the performance deviation due to manufacturing. The muffler was installed on the waveguide (Figure 3.28) and the whole system was tested on the calibration test rig to estimate the error amplification coefficients. Consequently it was

possible to choose which was the best K_j to use for each frequency (Figure 3.29). Upon examination of Figure 3.29, one can notice that the configuration which uses the combinations of the signals of the three sensors at the same time is the one with the lowest error modulus for the wider range of frequencies.

Once decided which K_j should be used for each frequency, the absolute error in terms of modulus and phase in the estimation of the pressure p_0 can be plotted (Figure 3.30 and Figure 3.31). For this estimation an error of 1.25 Pa and a phase shift of 0.5° were considered. These values come from an analysis of the error given by the sensor producer and the measurement chain. The calculation was carried out by considering a pressure signal at the measurement section of 1, 2 and 8 Pa in the range of 0 - 4 kHz. These pressures were chosen to highlight the error effects; the greater is the pressure, the lower are the errors.

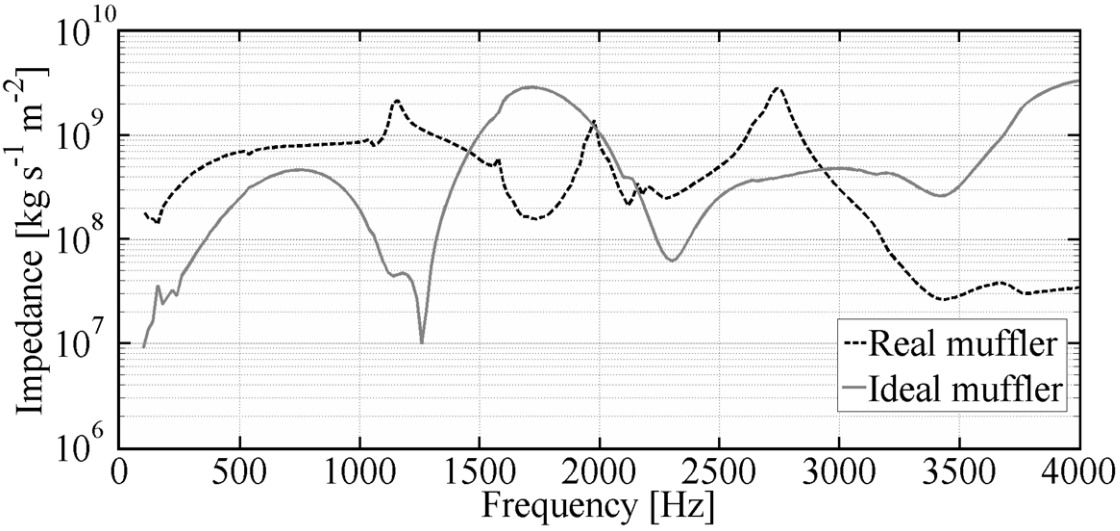

Figure 3.27 Comparison between the ideal muffler an the real one

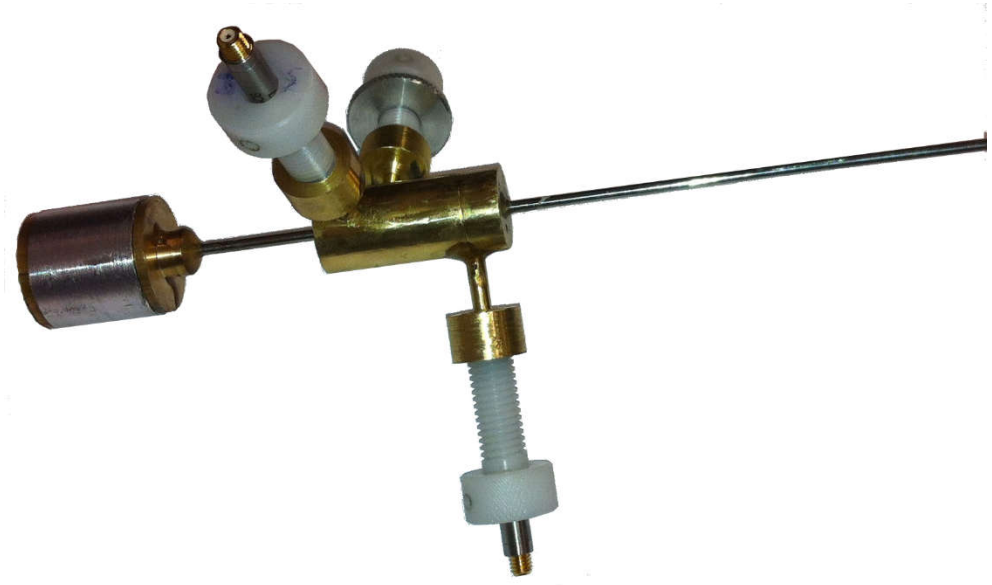

Figure 3.28 Picture of the waveguide equipped with the muffler

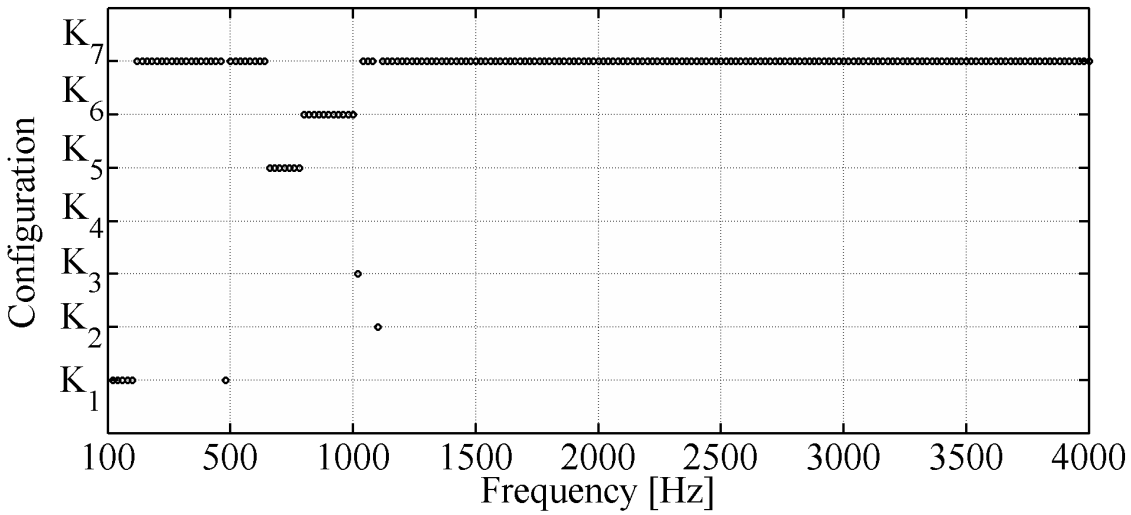

Figure 3.29 Plot of the configuration used as a function of the frequency

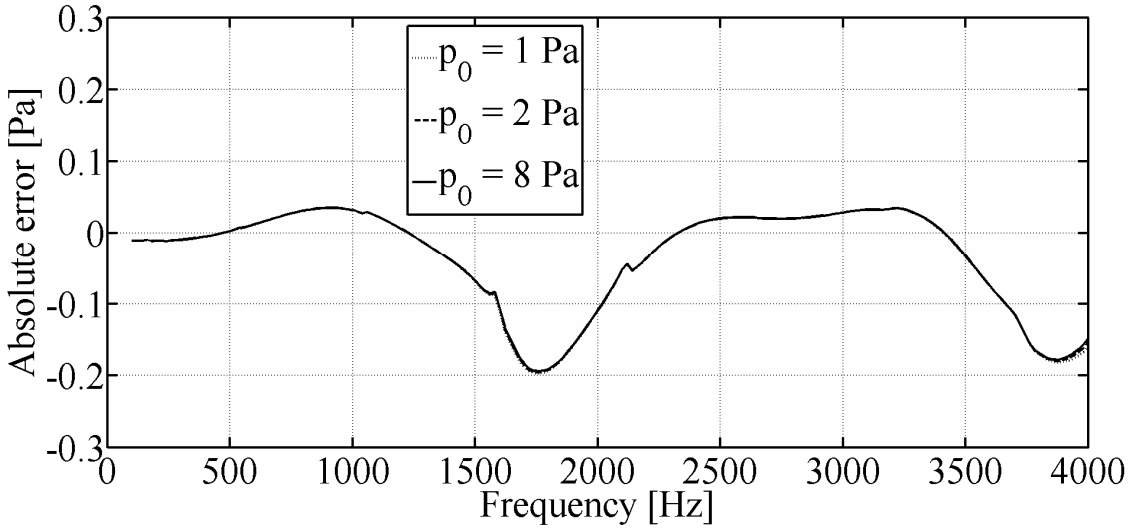

Figure 3.30 Absolute error modulus estimation for different pressure oscillation amplitudes at measurement section

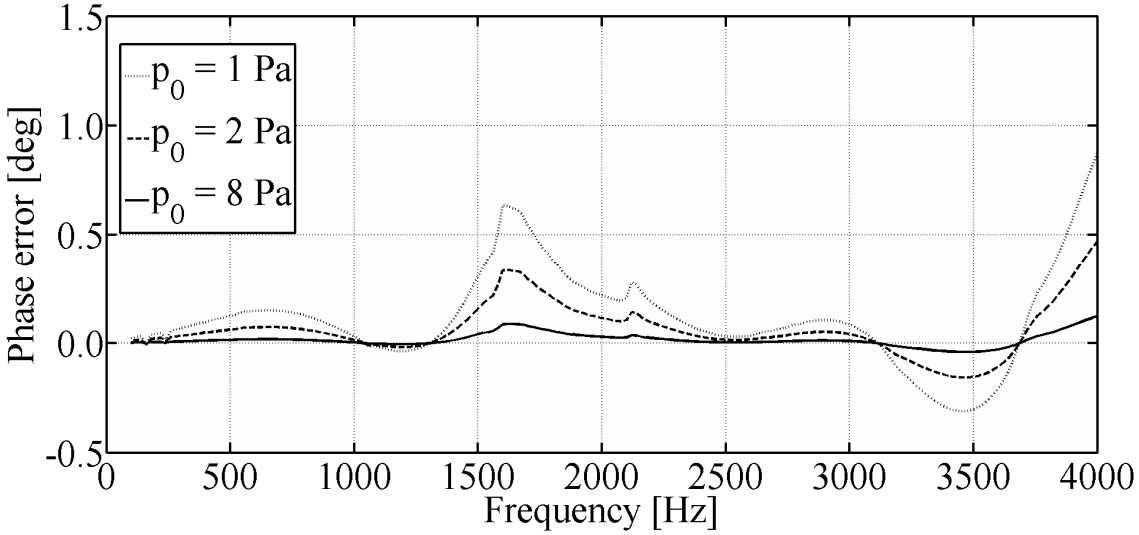

Figure 3.31 Absolute error phase estimation for different pressure oscillation amplitudes at measurement section

3.4 Design of an aerodynamic probe based on waveguide approach

In this section it will presented the design and development process which has been following to realize a waveguide probe with a total pressure tap used to measure static and total pressure, velocity and yaw angle of a flow in unsteady periodic condition. The aim is investigate the possibility to use a waveguide probe in place of a fast response aerodynamic pressure probe (FRAPP). Up to now the FRAPPs and waveguide probes have been always considered as two separated instrumentations with different field of applications, pros and cons. In this study an effort to combine the two base concepts and exploit the benefits of both was performed. In particular, a waveguide probe featured to act as a virtual 3 hole probe FRAPP was conceived, developed and tested to assess its capability to estimate a complex flow field.

3.4.1 Design of the modified waveguide probe

A waveguide probe is made up of three elements: the transmitting duct that connects the measurement section with the sensor section, the sensor housing and the damping duct which has the function of attenuate the reflected waves from the closed end of the duct. A cylindrical shape was chosen for the transmitting duct as this is the best compromise between manufacturing simplicity and range of application [27]. A transmitting duct of 203 mm with an outer diameter of 3.5 mm and inner diameter of 3 mm was chosen. The damping duct was realized by connecting the duct extending of 84 mm from the sensor housing with a reel of duct about 30 m long with the same inner diameter of the probe The probe head was realized by closing the transmitting duct and drilling a hole of 0.6 mm of diameter at 3 mm from the probe end.

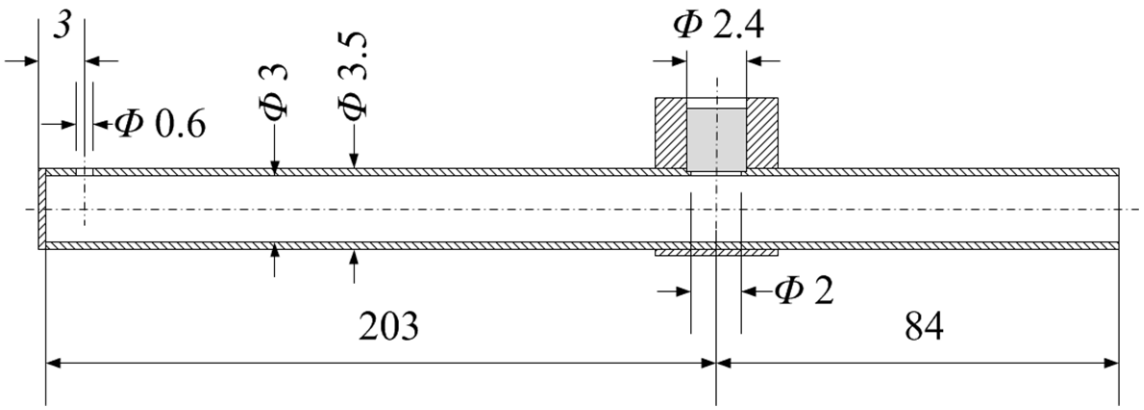

Figure 3.32 Sketch of the modified waveguide probe (dimensions in millimeters)

The sensor housing was realized according to author experience [24] to minimize the effects of the duct discontinuity due to the sensor presence (Figure 3.33). A piezo-resistive sensor model XCQ-093 by the Kulite Semiconductor ® with a diameter of 2.4 mm, a maximum pressure of 2 bar and a sensitivity of 42.865mV/bar was chosen (Table 3.3). This transducer is suited for both dynamic and static pressure measurements.

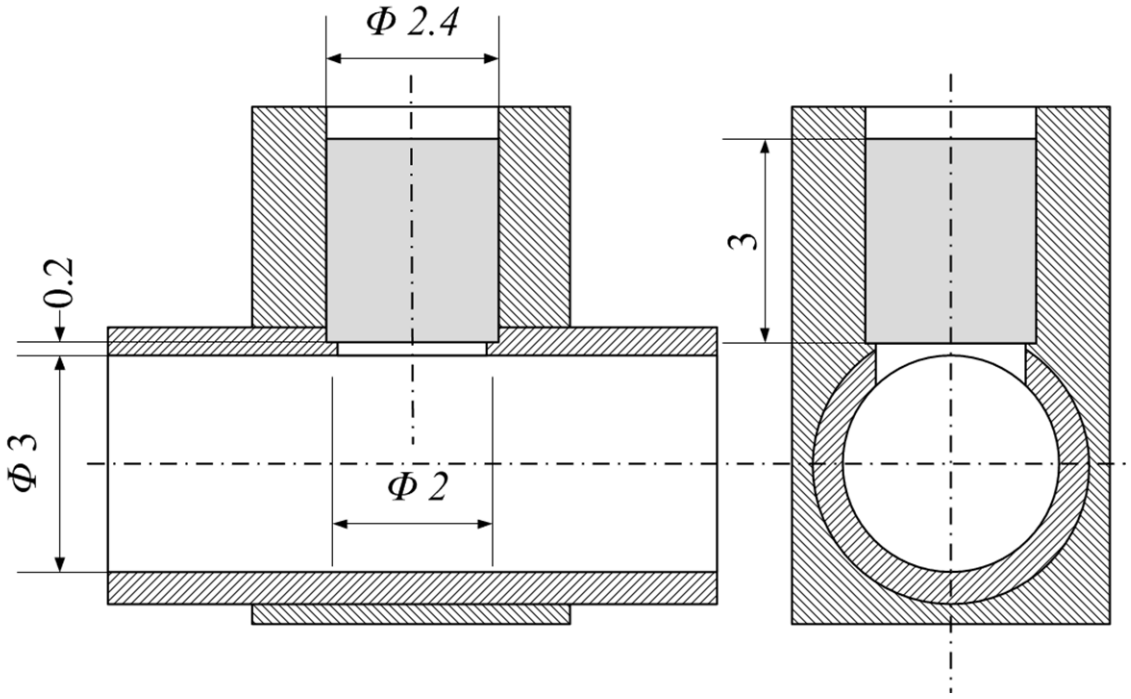

Figure 3.33 Sketch of the sensor housing (dimensions in millimeters)

Table 3.3 Data sheet of the piezo-resistive pressure sensor XCQ-093 by the Kulite Semiconductor ®

	Value
Maximum pressure	2 bar
Type	Absolute
VDC Excitation	10 V
Sensitivity	42.865 mV/bar
Input impedance	1154 Ohm
Output impedance	586 Ohm
Full Scale Output FSO	100 mV
Eigen frequency	>150kHz
Temperature range	-55°C – 120°C
Compensated temp. range	25°C – 80 °C
Weight	0.4 g

The flush mounted position of the sensor was guaranteed by realizing a hole of 2 mm on the transmitting duct and leaving a 0.2 mm of material as a stop. In Figure 3.34, Figure 3.35 and Figure 3.36 the detail of the probe tip, the sensor housing and a picture of the whole probe are reported respectively.

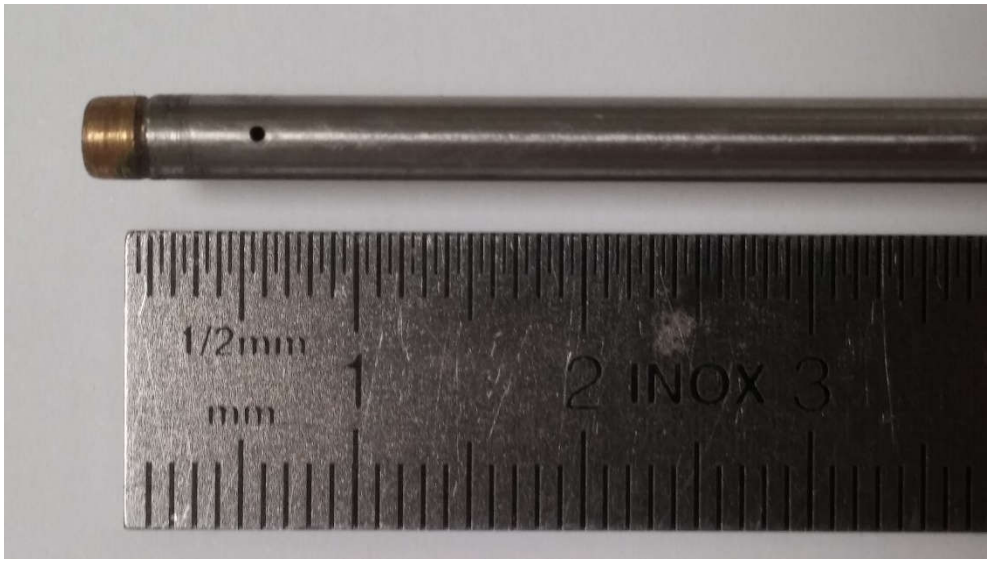

Figure 3.34 Picture of the probe head

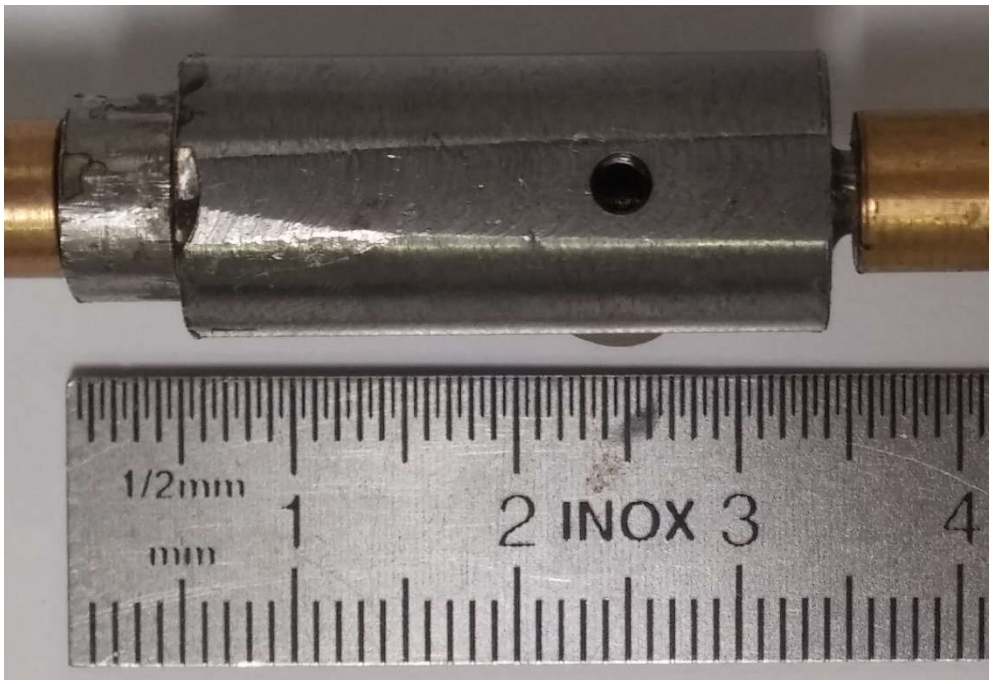

Figure 3.35 Detail of sensor housing

Figure 3.36 Full view of the modified waveguide probe

3.4.2 Theoretical model of the modified waveguide probe

Once the geometric characteristics of the probe have been defined, a numerical model was developed to investigate its performance and to have a reference for the experimental campaign. In particular, there was much interest in analysing the effects of the probe head on the waveguide behaviour. For this reason two models of the same probe but with different head geometry (a standard and a modified one) were realized by using the electroacoustic approach (as showed in Ref. [19], [9] and [41]).

The electroacoustic approach based on the transfer matrix method is the same presented in section 3.3.1 and here is applied to the modified waveguide probe. As stated before, this modelling approach was applied to two probe configurations one with a

standard head and the other with a modified head, as reported in Figure 3.37 and Figure 3.38 respectively. In particular, the modified head was considered as a 3 mm extension of the transmitting duct with a closed end and having a lateral hole with a diameter of 0.6 mm.

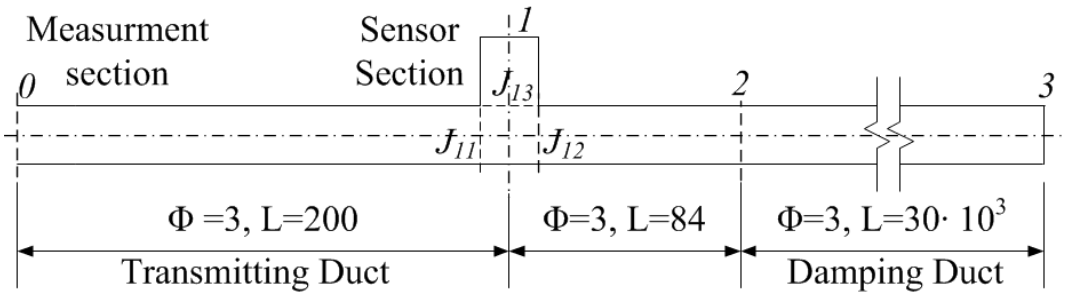

Figure 3.37 Scheme of the waveguide probe with the standard head (WGP-S, simplified waveguide probe)

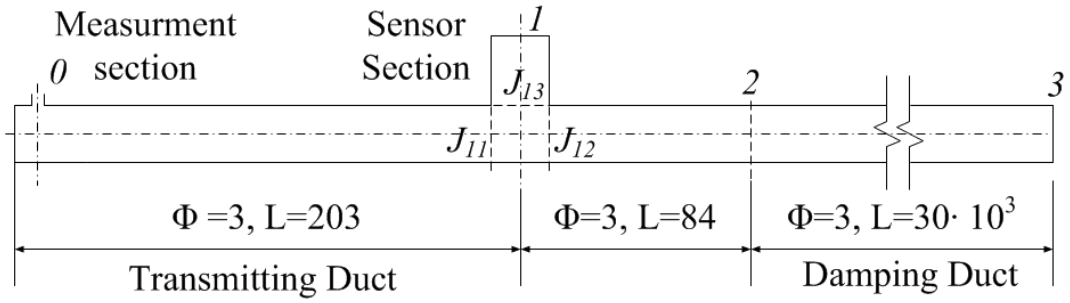

Figure 3.38 Scheme of the waveguide probe with the modified head (WGP-M, modified waveguide probe)

The modelling of the transmitting and the damping duct is the same because they are simple circular straight ducts, the differences on modelling process are focused on the sensor housing and probe head with total pressure tap. As depicted in Figure 3.33 the sensor is quasi-flush mounted on the main duct, only a short duct detaches it from the line, the transfer matrix of this short duct can be modelled as,

$$\begin{Bmatrix} p_{J13} \\ u_{J13} \end{Bmatrix} = \begin{bmatrix} 1 & Z_C \Gamma L_H \\ \frac{1}{Z_C} \Gamma L_H & 1 \end{bmatrix} \begin{Bmatrix} p_1 \\ u_1 \end{Bmatrix} \qquad 3.23$$

where the subscripts *J13* and *1* are related to the picture above, in particular the section 1 correspond to the sensor surface, Z_C is the distributed acoustic impedance of

mono-dimensional line and it is expressed in Eq. 3.4, Γ is the complex propagation constant (Eq. 2.2) and L_H is the length of sensor housing.

The hole has been modelled as an orifice following the studies of Durrieu et al. [42] and Seong et al. [43]. These authors investigated the wave propagation through an orifice in a duct in presence of a steady flow and by taking into account the viscous-thermal dissipation due to the real fluid and the small dimensions of the passage. According to their theory, the transfer matrix of an orifice can be indirectly estimated by means of its scattering matrix, Eq. 3.24. In place of the state variables (pressure and velocity oscillations) of a transfer matrix, a scattering matrix correlates the incident and reflected waves of the element. In more detail, the elements of the matrix are the reflection (r^+ and r^-) and transmission (t^+ and t^-) coefficients between the two ports (Eq. 3.24).

$$\begin{Bmatrix} p^+{}_0 \\ p^-{}_0 \end{Bmatrix} = \begin{bmatrix} t^+ & r^- \\ r^+ & t^- \end{bmatrix} \begin{Bmatrix} p^+{}_A \\ p^-{}_A \end{Bmatrix} \qquad 3.24$$

where the p^+ and p^- are the incident and reflect waves respectively at the inlet (O) and outlet (A) of the orifice.

By following the approach of Durrieu et al. [42] under the hypothesis of no steady flow through the orifice it was possible to estimate the transfer matrix of the head orifice and include it in the probe model.

By combing the matrixes of all the elements it is possible to express the pressure at the measurement section as a complex function of the pressure measured at the sensor section (FRF–frequency response function of the probe, Eq. 3.25):

$$p_0 = FRF(f)\, p_1 \qquad 3.25$$

The FRF is a complex function as the line modifies the pressure signal both in term of amplitude and phase. Usually, the FRF is plotted in terms of Loss coefficient (Eq.3.26) which expresses the attenuation of the pressure signal due to the probe for each frequency.

$$Loss = 20 \log_{10} \left| \frac{p_1}{p_0} \right| [dB] \qquad 3.26$$

In Figure 3.39 Attenuation predicted by the numerical model for standard (WGP-S) and modified (WGP-M) waveguide probe the comparison in term of Loss coefficient

between the waveguide probes with standard and modified head is depicted. As a general comment it is apparent as the orifice produces an increase of the Loss coefficient in all the range of frequencies. Apart from this, the two trends are quite similar, a small difference can be noticed at low frequencies probably due to the closed end of the transmitting duct.

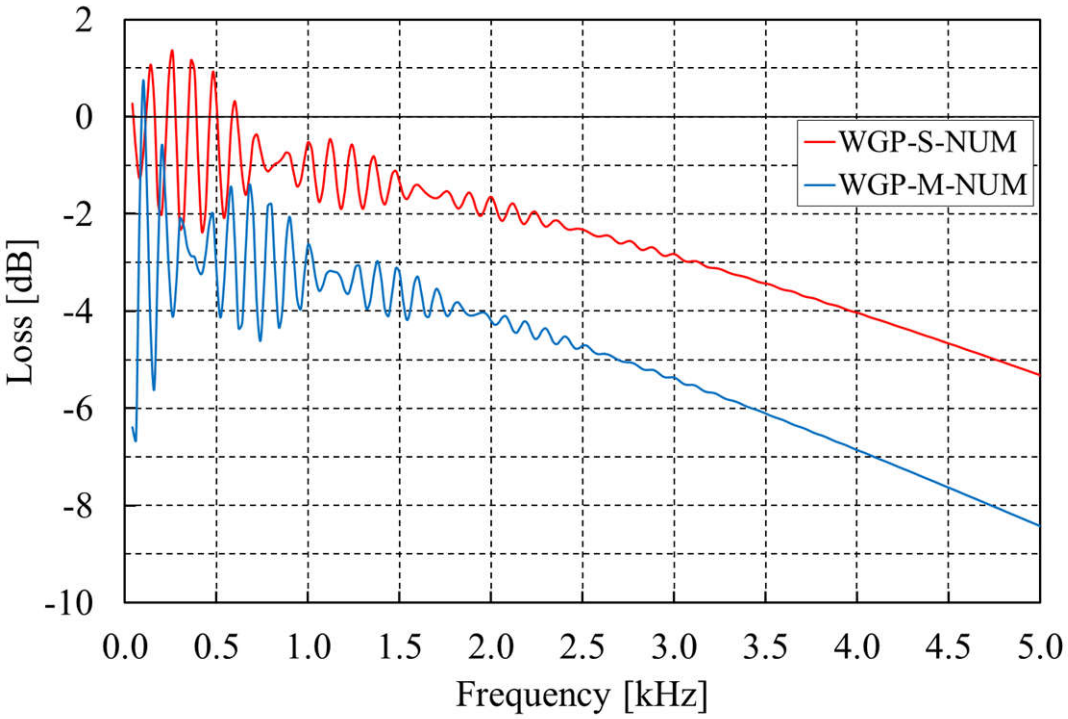

Figure 3.39 Attenuation predicted by the numerical model for standard (WGP-S) and modified (WGP-M) waveguide probe

3.4.3 Dynamic calibration

The dynamic calibration of the probes was performed on the acoustic test rig described in section 3.1.3, which has allowed to calibrate the two device in the frequency range 0 – 5kHz with a planar field of 120 dB (20 Pa). In Figure 3.40 the comparison between the loss coefficient obtained from the dynamic calibration and that estimated with the transfer matrix model is reported for the standard waveguide probe. A good agreement between the two results was achieved up to 2 kHz. The oscillations at low and medium frequencies are due to the waves reflected by the manufacturing discontinuities inside the probe, the most significant of these is the junction between the damping duct and the probe end. Over 2 kHz, a frequency oscillation every 380 Hz is notice. This is

probably due to the discontinuity created by the sensor housing. In addition, an attenuation lower than that predicted by the model is found experimentally. Probably the damping coefficient adopted in the model is too restrictive for that range of frequency for this kind of probe.

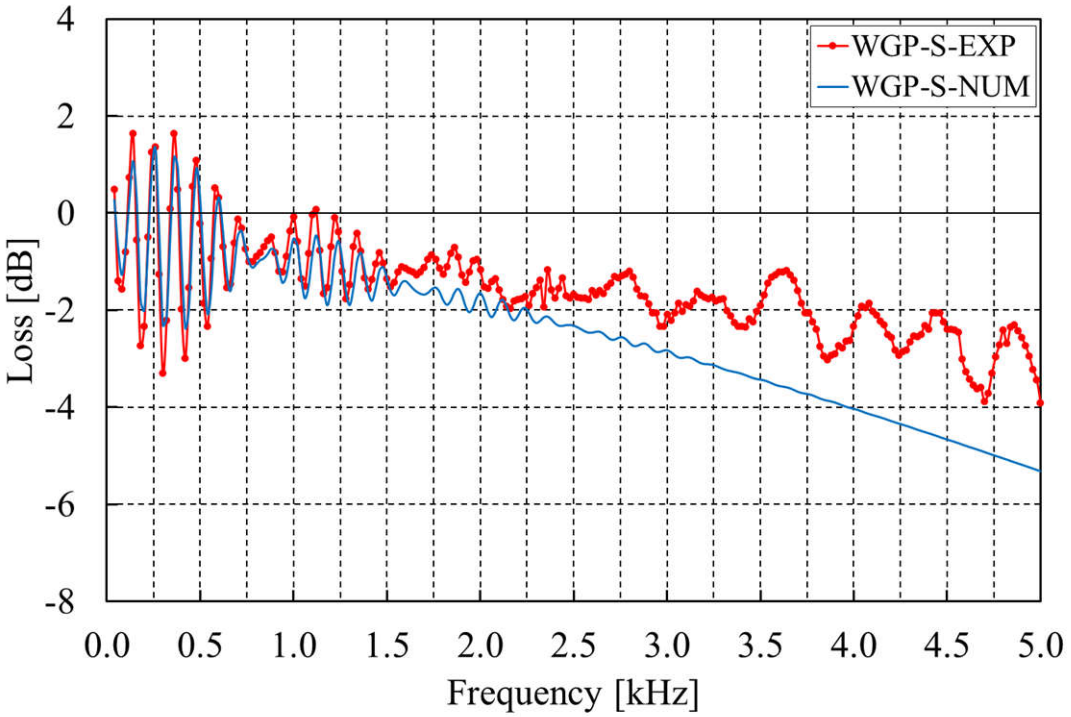

Figure 3.40 Experimental and numerical attenuation for the standard waveguide probe (WGP-S)

In Figure 3.41 the effect of the orifice on the frequency response of the probe is shown. The results confirm the general trend already predicted by the numerical model: a general increase of the losses due to the presence of the orifice and a similar loss coefficient trend. By comparing the experimental characterization of the modified probe with the results from the model, a lower loss coefficient variations at low frequencies but a more oscillating trend at higher frequencies is apparent (Figure 3.42). This results are quite similar to those obtained for the standard waveguide probe and are related to the discontinuities due to the manufacturing that have not been considered in the model.

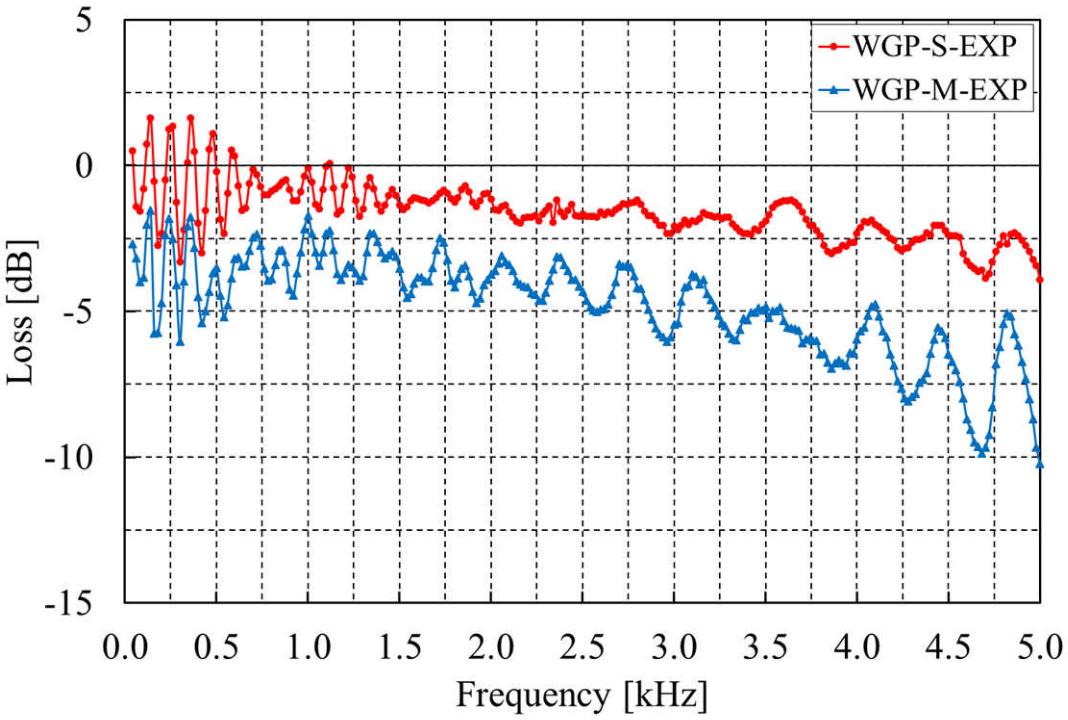

Figure 3.41 Experimental attenuation for standard (WGP-S) and modified (WGP-M) waveguide probe

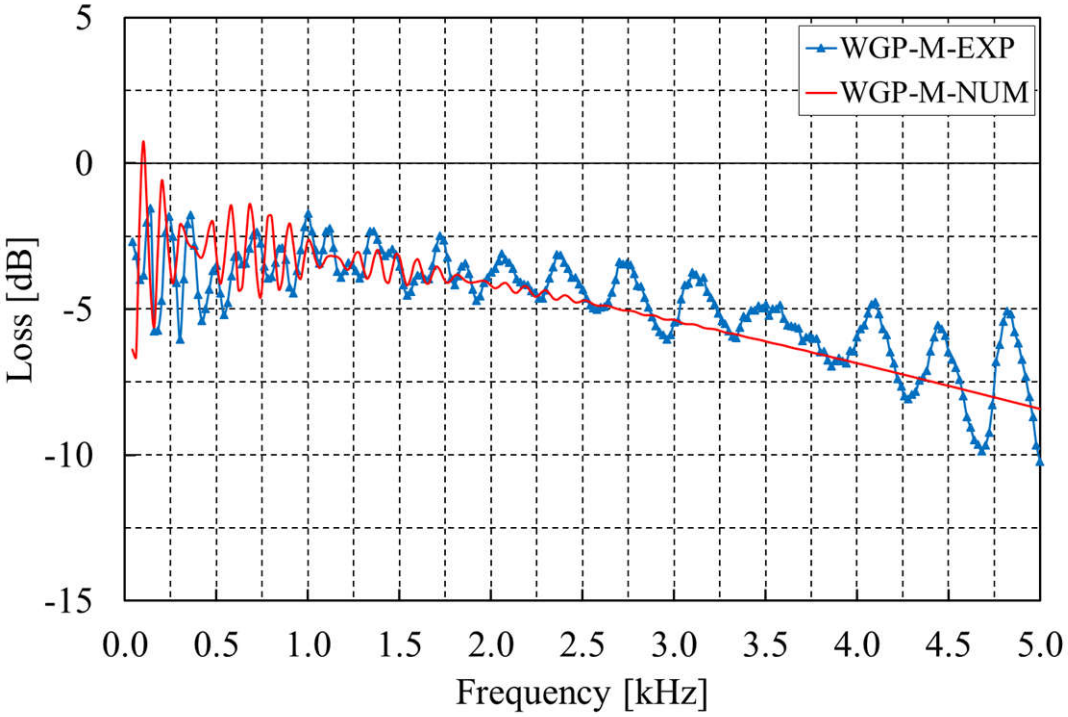

Figure 3.42 Experimental and numerical attenuation for modified waveguide probe (WGP-M)

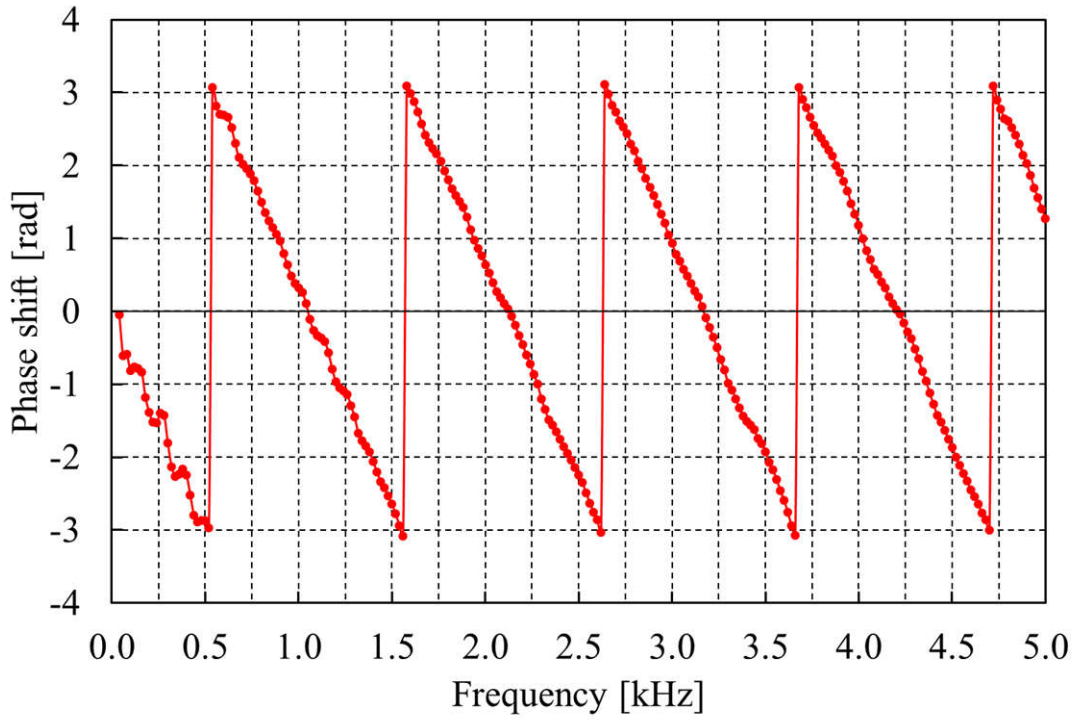

Figure 3.43 Phase shift between the calibration signal and that measured at the sensor section

As a last remark it has to be noticed that the transfer function of a waveguide probe (Eq. 3.25) is a complex function that affects both the signal amplitude and phase (Figure 3.43). Due to the distance between the measurement point and the sensor housing, a time shift depending on the frequency is introduced between the measured signal and the generating one. This phase shift has to be taken into account during the signal reconstruction to obtain a consistent result.

3.4.4 Steady aerodynamic calibration

The modified waveguide probe with lateral pressure tap can work in the same way of a FRAPP probe but to do it a steady aerodynamic calibration is necessary. The probe was calibrated as a virtual 3 hole probe to estimate the aerodynamic coefficients necessary for the calculation of the flow quantities in the future experimental campaigns. The method adopted in the present study has been extensively used in the literature for the aerodynamic calibration of a virtual 3 hole probe. A brief description will be provided here but a more detailed explanation of the technique can be found in Ref. [33] and [44].

The probe was calibrated in a wind tunnel facility made up of a 2950 mm long pipe with a diameter of 150 mm and a bell mouth at the inlet. A centrifugal blower of 15 kW guarantees a maximum flow speed inside the duct corresponding to a Mach number of 0.3 (Figure 3.45). The probe was installed on an automatic traversing system with two degrees of freedom (Figure 3.45), the longitudinal motion (along the Z axis) and yaw rotation (γ rotation around Z axis) at 750 mm from the tunnel inlet. The automatic traverse system has a resolution of 0.1 mm in the axial direction and 0.1° as angular rotation. The probe was placed as to have the probe hole at the center of the measurement section and the tests were performed at a Mach number of 0.2.

From the aligned position, the probe was rotated of ± 56° with steps of 2° and the pressures measured by the waveguide sensor was acquired and processed in terms of the pressure coefficient C_p (Eq. 12):

$$C_P = \frac{p - p_s}{p_t - p_s} \qquad 3.27$$

where p is the measured pressure, p_s is the wall static pressure at the test section and p_t is the total pressure measured with a reference Kiel probe at the probe position. The trend of the pressure coefficient C_P can be seen in Figure 3.47: a slight shift of the 0° position can be observed.

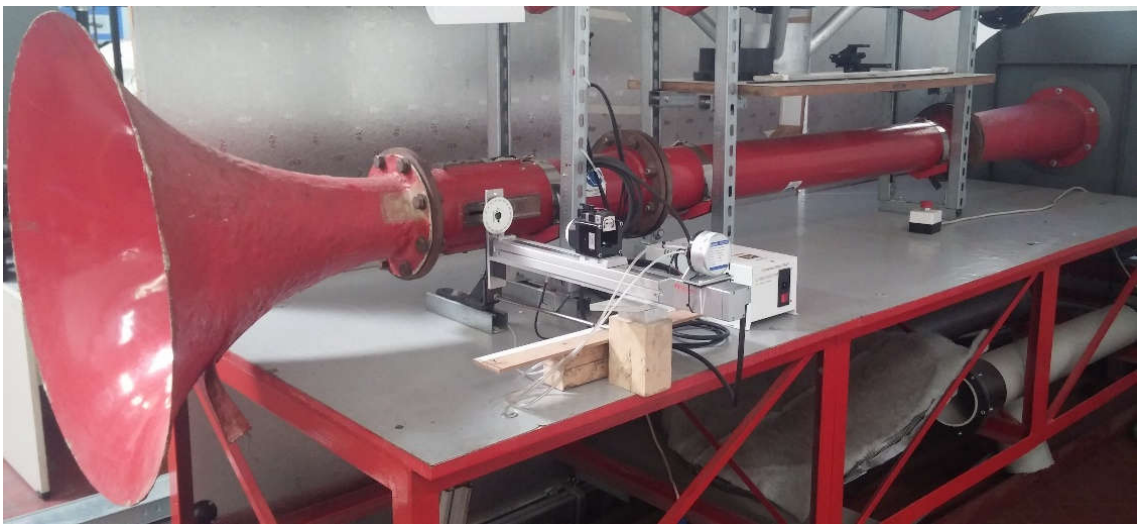

Figure 3.44 Wind tunnel facility, from the left: the air inlet with bell shape, the probe access with the automatic traversing system, the main duct and the blower's case

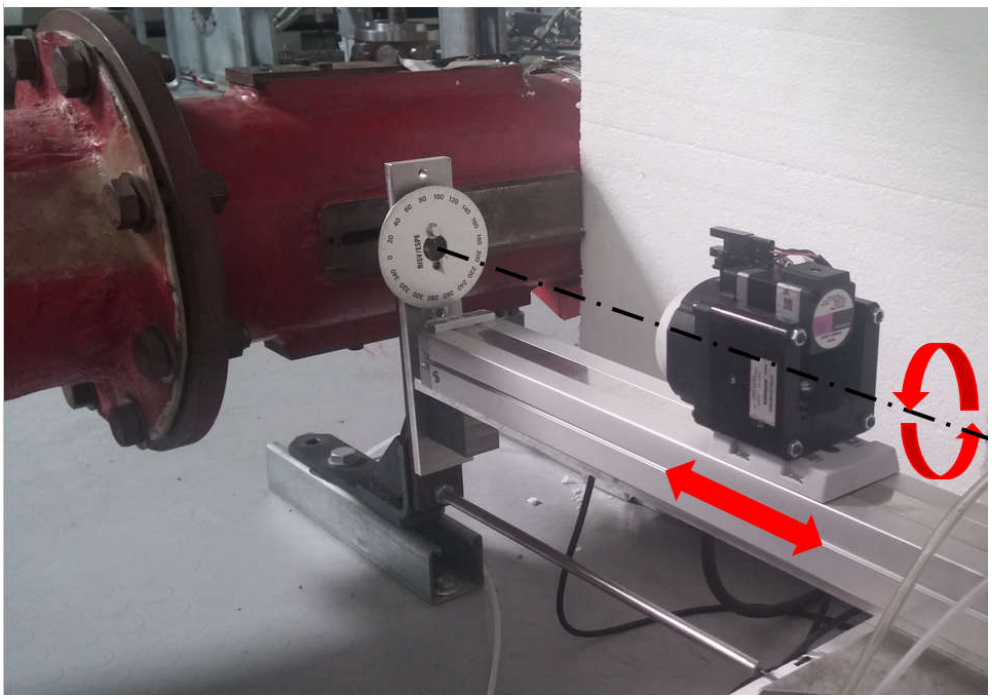

Figure 3.45 Detail of probe access to wind tunnel facility, automatic traversing system, a stepper motor checks the longitudinal position a second stepper motor set the rotation around the longitudinal axis

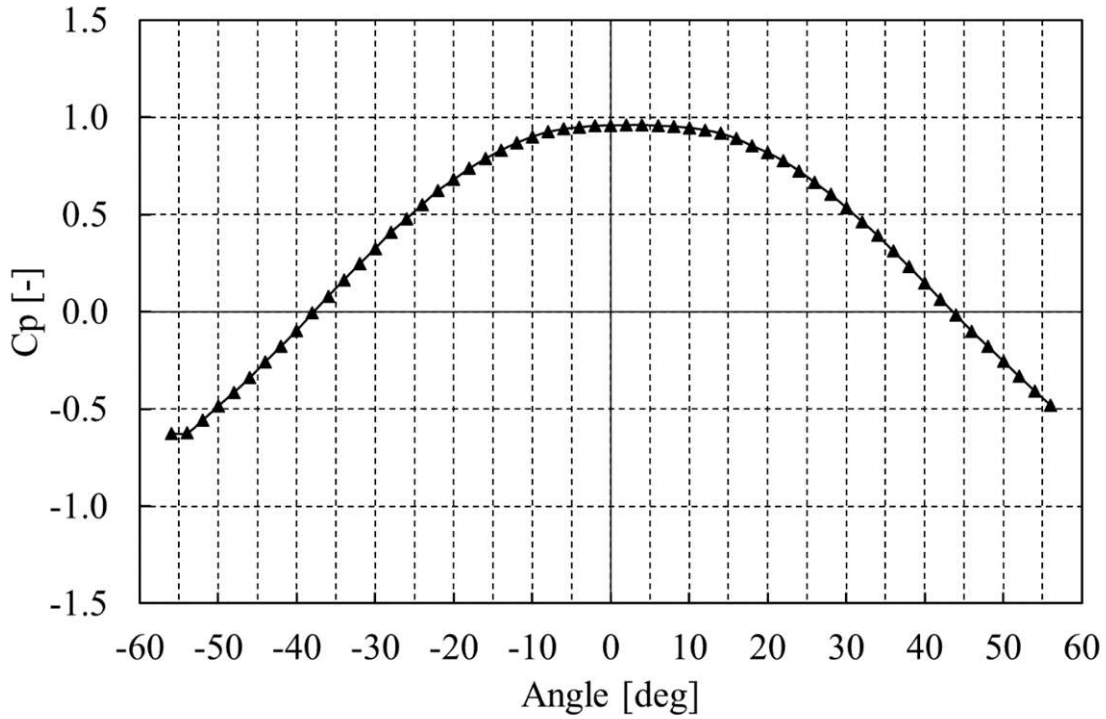

Figure 3.46 Trend of the C_p coefficient for the tested probe as function of the yaw angle

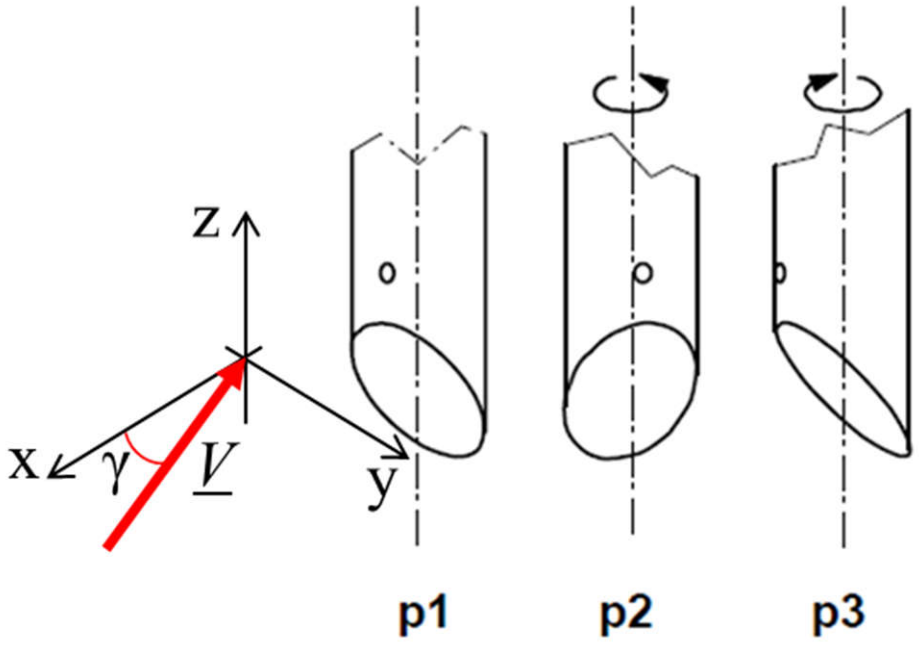

Figure 3.47 Probe position to acquire the three pressure signal

In order to operate the device as a virtual 3 hole probe, three pressure measurements at different yaw angles are necessary (Figure 3.47): the first in a central position (p_1) and two others performed after a rotation of the probe around its stem (at known angles) to simulate the presence of the lateral ports of a 3 hole probe (pressure p_2 and p_3). In this study a rotation of ±30° has been chosen (e.g. p_1 at 26°, p_2 at +56°, p_3 at -16°). These angles were chosen to guarantee the maximum sensitivity, as according to the literature [32], as long as the pressure coefficient C_P is still greater than 0, the wider the angular variation the more sensitive is the probe. Once the set of angles used to operate the probe has been defined, it was possible to estimate the three aerodynamic coefficients K_γ, K_s and K_t that will be used to post process the pressure measurement and calculate the yaw angle, the static pressure and the total pressure respectively. These coefficients depend on the three pressures p_1, p_2 and p_3, and the total (p_T) and static pressure (p_S) measured during the calibration as reported in Eq. 3.28, 3.29 and 3.30.

$$K_\gamma = \frac{p_2 - p_3}{p_1 - \frac{p_2 + p_3}{2}} \qquad 3.28$$

$$K_S = \frac{p_1 - p_S}{p_1 - \frac{p_2 + p_3}{2}} \quad 3.29$$

$$K_T = \frac{p_T - p_1}{p_1 - \frac{p_2 + p_3}{2}} \quad 3.30$$

The trend of $K\gamma$ is reported in Figure 3.48 for different yaw angles (γ) which corresponds to the position of the central measurement. As a results $K\gamma$ is defined in a range of yaw angles form ±26°. Analogously, the coefficients K_S and K_T in function of γ are reported in Figure 3.49 and Figure 3.50 respectively. During the tests the pressure at three probe angles (p_1, p_2 and p_3) will be acquired, the K_γ coefficient calculated and then the flow angle γ estimated from the curve of Figure 3.48. To make this process quicker, the function of Figure 3.48 was inverted and the angle γ was expressed as a fourth-order polynomial function of the K_γ (Eq. 3.31). The polynomial interpolation has a determination coefficient R^2=0.99.

$$\gamma = \sum_{j=0}^{m} k_j K_\gamma{}^j \quad 3.31$$

Once γ is known, the coefficients K_S and K_T can be easily estimated from Figure 3.49 and Figure 3.50 respectively and the total and static pressure calculated. Also in this case, to speed the process, a polynomial interpolation of the sixth order was adopted to express the coefficients K_S and K_T as a function of γ (Eq. 3.32 and Eq. 3.33). The determination coefficient was R^2=0.99 for both the functions.

$$K_S = \sum_{j=0}^{m} k_j \gamma^j \quad 3.32$$

$$K_T = \sum_{j=0}^{m} k_j \gamma^j \quad 3.33$$

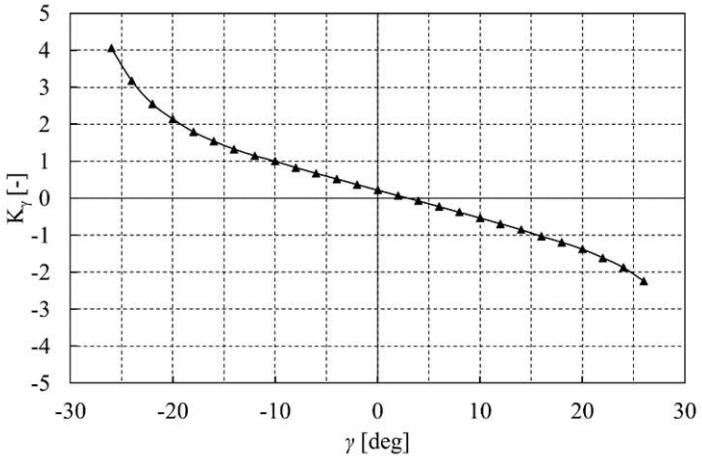

Figure 3.48 Trend of the *Kγ* coefficient as function of the *yaw* angle

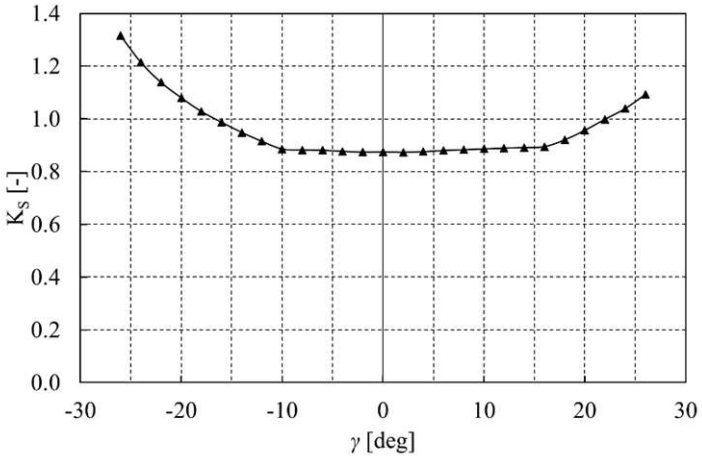

Figure 3.49 Trend of the *Ks* coefficient as function of the *yaw* angle

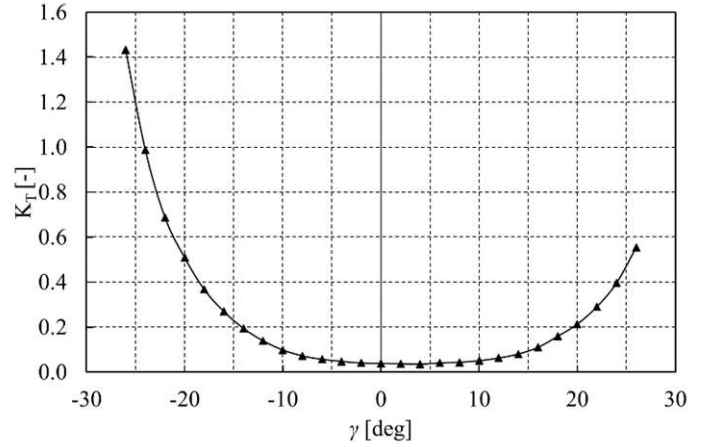

Figure 3.50 Trend of the *Kτ* coefficient as function of the *yaw* angle

4 Results and discussions

In this chapter are described the experimental tests that are used to characterize and demonstrate the improvements in term of measurement capabilities achieved with the probes which were conceived in this work and presented in the previous sections.

The first type of probe presented, the single sensor waveguide probe with miniaturized muffler, was tested in two experimental tests. In the first one the probe was used to measure the 3D acoustic field in a large circular duct where the air column was excited by an acoustic source. The aim is that to define a measurement procedure using the probe thanks to which is possible to reconstruct the acoustic mode that are propagating in an generic volume under known boundary conditions. In the second test a rotating source made up by a couple of rotor-stator is inserted in an annular circular duct, the pressure field generated by the source is measured in proximity of the rotor by inserting the probe at different circumferential and radial positions. The aim is that to obtain a complete map of the acoustic field generated by this type of source.

The multisensor waveguide probe, presented as an upgrade of the single sensor probe, was tested in term of capability to reconstruct a pressure signal by reducing the error estimation in term of amplitude and phase shift respect to the original one. The new probe was used to measure the time pressure signal at the outlet of centrifugal blower, the results were compared to the measurements carried out with a single sensor probe placed at the same position and that of a flush mounted sensor. The intent is that to demonstrate the higher accuracy of the new probe to reconstruct the time pressure signal, reducing the estimation error.

Finally, the last probe developed was an aerodynamic waveguide probe which was tested by measuring the 3D flow at the outlet of the impeller of a centrifugal blower. By means of this test the new probe has to show the capability to measure an unsteady periodic pressure signal and capturing the characteristic frequency of the phenomena which is function of the spinning velocity and the number of blades of the impeller. The intent is that to demonstrate that it may be possible to combine the pro and con of a waveguide probe with that of an aerodynamic pressure probe trying to overtake the thermal limit and miniaturized requirement of the dynamic pressure transducer.

4.1 Single sensor waveguide probe: experimental tests

In this first section of chapter 4 it is shown the measurements capabilities of the single sensor waveguide probe with muffler as damping device. The probe was used in two different test cases. In the first one it was employed to measure the 3D acoustic pressure fields in a circular duct where an acoustic source was used to excite the complex modes of the air column inside. In the second test case the single sensor waveguide probe is used to measure the 3D modes generated by a rotor stator interaction in an annular duct. The theory of the acoustic modes that can propagate inside circular duct and that generated by a rotating source in an annular duct have been already subject of many studies and their theory is well noted, for sake of brevity the reference theory is reported in the Appendix.

4.1.1 Methodology for the measurement of the acoustic wave field

Before to use the probe and acquire the pressure signals measured with the probe itself it is necessary to define a specific measurement methodology for the two test cases described above. The aim of the measurement methodology is the estimation of the global acoustic field and the measurement of the single components which compose it. The global wave field is obtained by the measurement of the local acoustic pressure in a section of the duct. The experimental map is compared with that from a theoretical model developed for this specific purpose. This theoretical model needs the acoustic impedance

of the end of the duct to estimate the reflected acoustic wave, which brings to the making of a standing acoustic wave inside the duct. The reflection coefficient of simple duct end it has been studied in many works, there are specific formulation for simple cases as presented by Morse et al. in their book Ref. [45].

From an experimental point of view the reflection coefficient estimation is commonly performed with the two microphone technique (TMT) implemented by Ross and Seybert in their work Ref. [46], this technique has been widely applied in the acoustic of ducts, mufflers and pipe systems. Unfortunately, this measurement technique has some limits in the post-process procedure highlighted by Bodén and Abom in Ref.[47]. In fact, the results are reliable only in a range of frequencies that depends on the distance between the two microphones. This problem can be overcome by adopting an extension of the TMT: the multi microphone technique (MMT) finalized by Jang and Hi in their research to develop a method for measuring in-duct acoustic properties in the presence of a mean flow Ref. [48]. The above-mentioned measurement techniques are generally used for the analysis of a planar wave field but can also be applied in a 3D approach by adopting the 3D wave equations as suggested by Shultz et all. In Ref. [49]. In this paper, the approach proposed by Shultz is applied to a MMT both to overcome the post process errors and to extend the range of analysis to a 3D acoustic field. The acoustic impedance of the duct termination is estimated with this approach thereby allowing the identification of the reflected modes. This data is used in the theoretical model to reconstruct the global acoustic field in each section of the test rigs, in order to compare the numerical and experimental results.

4.1.2 Global wave field measurement

Defined an acoustic domain, a circular or annular duct is the same, when considering a frequency the acoustic pressure distribution in a cross section is the result of two or more waves which are moving in opposite directions. In each measurement point the pressure field is characterized by an amplitude and a phase; the two parameters depending on the geometrical setup of the test rig (distance from the acoustic source, source sound pressure level and duct termination).

A correct description of the acoustic field in a duct section needs several measurement points. In this study the pressure distribution is measured by twelve measurement points in a tangential direction and nine along each radius. Consequently, the wave field reconstruction involves twelve measurement sessions, where both the tangential distribution and the one along the radius are acquired, Figure 4.1. The twelve measurement sessions are clocked and scaled by considering a reference signal p_{ref} in Eq. 4.1 whose nature is different for the test case in circular duct and for the test case in annular duct with rotor-stator interaction.

$$p_{map}(r,\theta) = \frac{|p_{r\theta}|}{|p_{ref}|} cos\left(\varphi_{r\theta}|_{ref}\right) \qquad 4.1$$

In Eq. 4.1 p_{map} is the pressure of wave field function of r and θ coordinates, p_{ref} is the reference signal and φ_{ref} is the relative phase between the measured signal $p_{r\theta}$ and the reference signal p_{ref}.

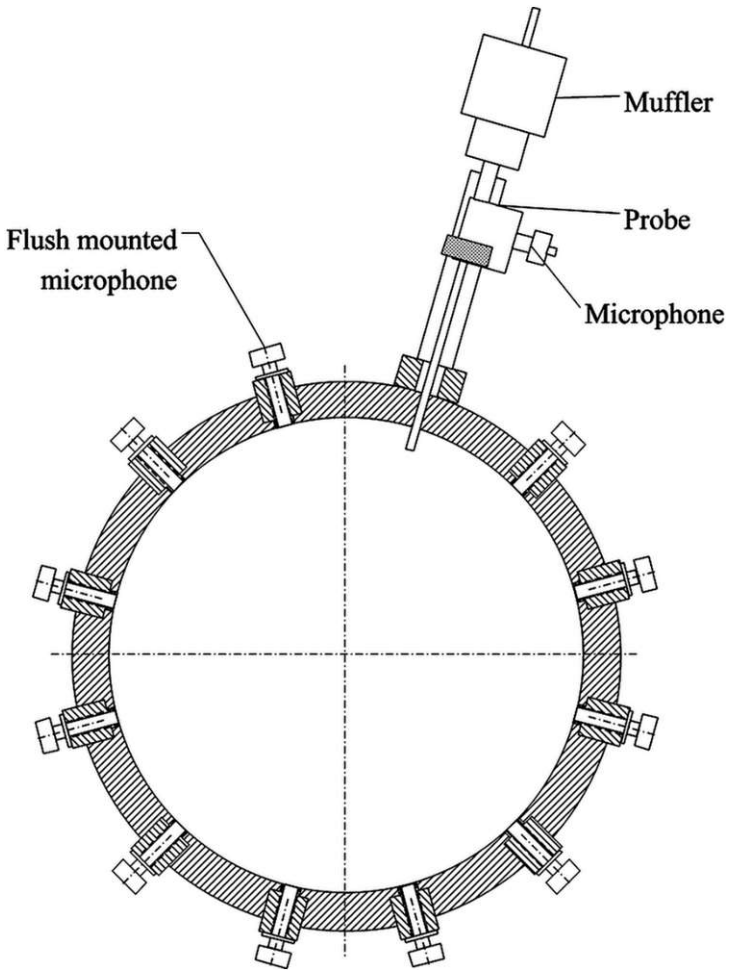

Figure 4.1 Mapping measurement section for circular and annular duct

4.1.3 Clocking for the acoustic source

In the first experimental campaign the wave field propagating inside the circular duct depends only on the source frequency and duct geometry. The acoustic source is driven by a waveform generator, so there are no fluctuations of the amplitude of the generated acoustic wave: the acoustic field should be considered stable. Consequently, a microphone flush mounted on the duct wall (Figure 4.1) can be used as reference signal. The phase difference between the reference signal and that measured by the probe can be estimated by a cross correlation function.

4.1.4 Clocking for the rotating source

In the second experimental campaign, on the acoustic field generated by a rotor stator interaction inside an annular duct, the wave field generated depends on the rotor spinning frequency and the number of vanes and blades (note the Eq. 7.11 and 7.12 in the Appendix) but only the planar mode can propagate. The acoustic field generated by the rotor decays in a few diameters to a planar wave. An optical encoder is mounted on the rotor shaft and the once-per-round signal was used to trigger the probe acquisition. In this way, each acquisition is started with the rotor in the same angular position. The reference pressure amplitude is estimated with a flush mounted microphone mounted 8 mm downstream the rotor section.

4.1.5 Acoustic boundary condition measurement

The solution of wave equation (Eq. 7.8) shows that the global wave field in a duct is the sum of the incident and the reflected acoustic fields. These fields are made up of one or more acoustic modes depending on the *cut-off* frequencies. The solution of wave equation at *i-th* point along the duct axis z is expressed by means of Eq. 4.2. This equation can be write for other random z positions along the duct, writing a system of equations. The incident (p_{mn+}) and the reflected (p_{mn-}) acoustic waves inside the duct are calculated by solving the linear system made up of the dissipative equation (Eq. 4.2) estimated in each measurement point z_i.

$$p_i(r,\theta,z_i) = \sum_{m=0}^{\infty}\sum_{n=0}^{\infty} J_m(k_{rmn}r)\, e^{im\theta}(p_{mn+}e^{-ik_{zmn}z_i} + p^{-}{}_{mn-}e^{+ik_{zmn}z_i}) \qquad 4.2$$

The wave number k_{zmn} , Eq. 4.3, considers also the longitudinal decay effects included in the Γ coefficient.

$$k_{z,m,n} = \sqrt{\Gamma^2 \quad k_{r,m,n}{}^2} \qquad 4.3$$

As highlighted in Ref. [48] the error on the solution of the above mentioned inverse problem depends on the spatial positioning of the measurement points. In this work, an exponential law distribution on each coordinate is chosen (Figure 4.2). This distribution guarantees a singularity factor SF [48] close to one in a frequency range between 0.05 – 5 kHz. This parameter describes how the linear system is close to a singular matrix. This value is a good compromise between the number of microphones and the reliability of the solution. In detail, 4 microphones are flush mounted on duct wall and two probes are placed inside the duct.

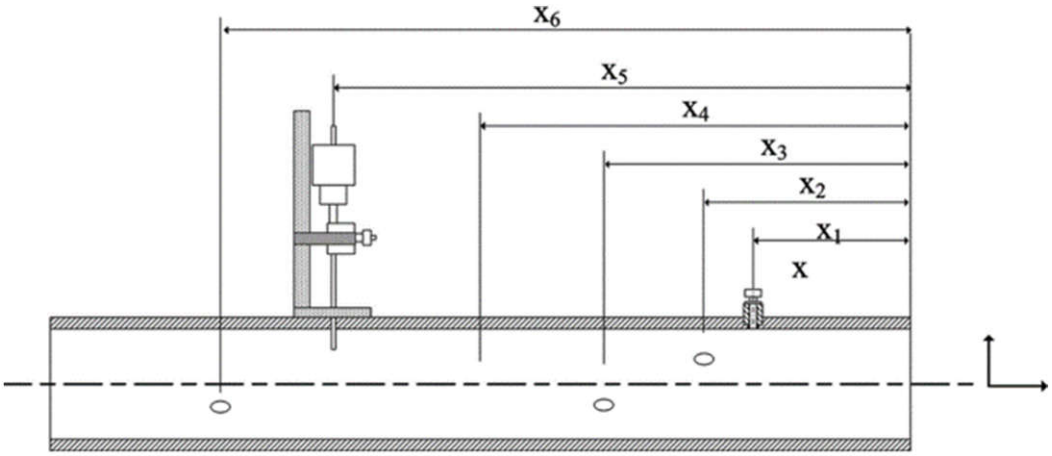

Figure 4.2 Measurement points distribution for boundaries condition evaluation in circular duct

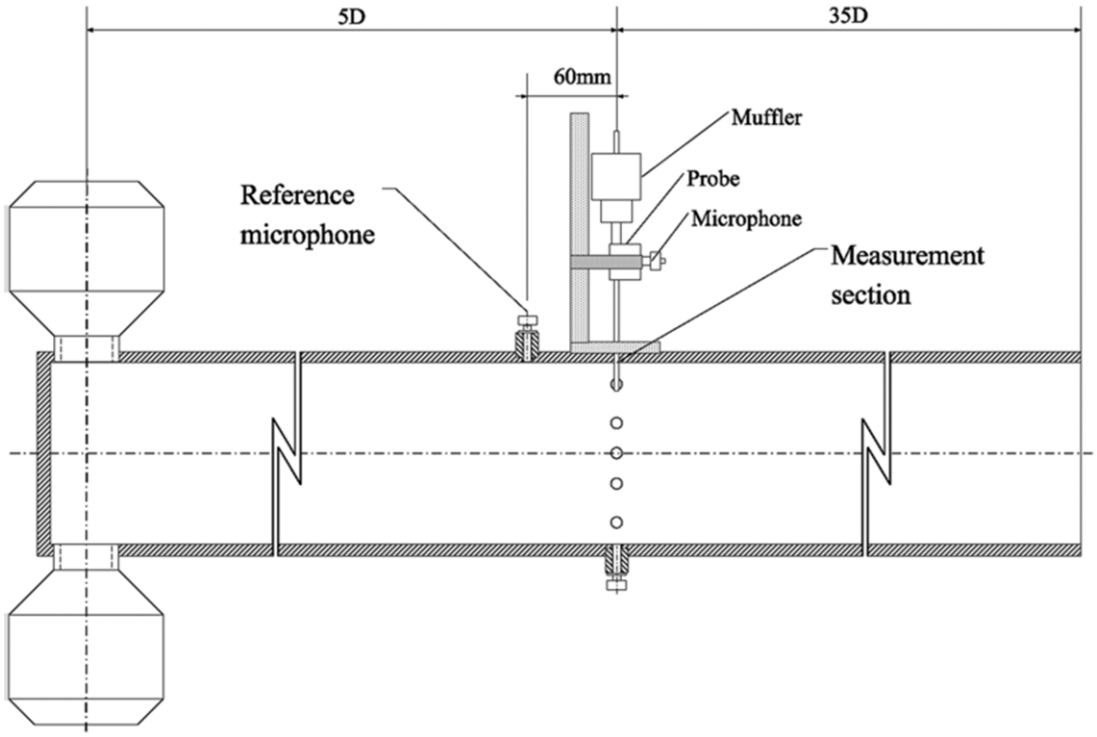

Figure 4.3 Test rig for the measure of 3D acoustic mode inside a duct, on the left side the compression drivers on the right side the open duct end

4.2 Wave field in circular duct by pure acoustic source

4.2.1 Experimental setup

The test rig for acoustic field mapping is a straight duct 4m long with a diameter of 150 mm. The acoustic source is located at one end of the duct whereas the other is open to the air (Figure 4.3). The measurement section is at five diameters from the source; a reference microphone is flush mounted 60 mm upstream. The source is made up of four compression drivers Monacor® KU616T circumferentially mounted.

The probe is mounted on a slide allowing the measurement in both radial and circumferential direction maintaining the geometrical alignment. The microphones used in the test are G.R.A.S® ¼" (pressure type). Their signals are acquired with a National Instrument C-DAQ system and an acquisition module NI 9234 with a maximum sample rate per channel of 51.2 kS/s, this hardware devices are controlled by an ad hoc developed

software in Labview. The speakers are driven by a waveform generator Agilent® 33220A and amplified by means of a sound amplifier Monacor® PA-940.

4.2.2 Results

Speakers are driven at 4.2 kHz, to have a fully 3D wave front shape propagating in the duct. The resulting wave field in the measurement section is the sum of six fields: three generated by the speakers (Figure 7.3) and three reflected by the open end. The theoretical reconstruction of the acoustic field by means of the 3D wave equation requires the determination of the open duct end global acoustic impedance (Eq. 4.4) in terms of reflection coefficient and the energy distribution of the acoustic field modes (GR). The first can be expressed as indicated in Eq. 4.4, where R is the reflection coefficient of open duct end.

$$Z_{open\ duct\ end} = Y_0 \frac{1+R}{1\quad R} \tag{4.4}$$

The energy distribution parameter can be determined by considering the solution of wave equation in circular duct (Eq. 7.8). The amplitudes scaled that of mode (m=4, n=0) together with the reflection coefficients for each mode propagating in the duct are shown in Table 4.1.

In the literature, no correlations are present for the determination of the reflection coefficient for a 3D mode, indeed they are limited only to the planar wave field. The accuracy of the estimation can be confirmed by the comparison between the numerical and experimental results shown further in this chapter.

Table 4.1 Boundary condition of the test rig for the theoretical model

	m=4, n=1		**m=0, n=1**		**m=1, n=1**	
	Modulus	**Phase**	**Modulus**	**Phase**	**Modulus**	**Phase**
R	0.61	-36.96	0.47	-120.09	0.25	5.45
GR	1.00		1.12		0.87	

The above mentioned reflection coefficients refer to an open end duct geometry disregarding the length of the duct. For this reason, once properly scaled with the Helmholtz number (He), they can be used for any lengths as long as the end geometry and outlet conditions are the same. The theoretical acoustic field in the measurement section can be reconstructed starting from the characteristics of the modes generated by the acoustic source (amplitude and phase) and the reflection coefficients of the open duct end. Among these parameters, the only ones missing are the source mode phases. Since the generation source is made up of a pure acoustic source [45], the modes can be considered in phase. The comparison between the experimental and the theoretical distributions is shown in Figure 4.4 and Figure 4.5; the pressure amplitude is normalized with respect to a reference pressure (Eq. 4.1). The comparison between Fig 16 and Fig. 17 highlights the same clocking on the geometrical plane of the theoretical and experimental maps. This result confirms that the estimated duct boundary conditions and the mode separation are reliable. The pressure distribution of the two maps is also similar: in both of the two figures the positive pressure peak is placed in the second quadrant of the map and the four valleys on the circumference. The differences are probably related to the finite number of measurement points and to the simplifications in the theoretical description (3D wave equation in the explicit form).

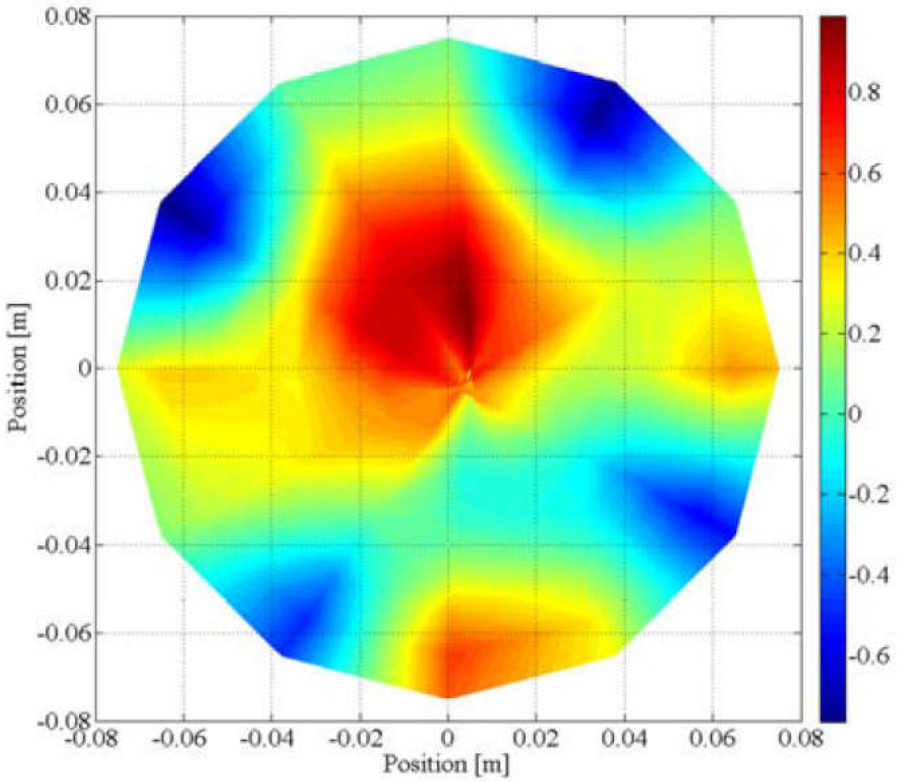

Figure 4.4 Experimental pressure map of the wave field at 4.2kHz

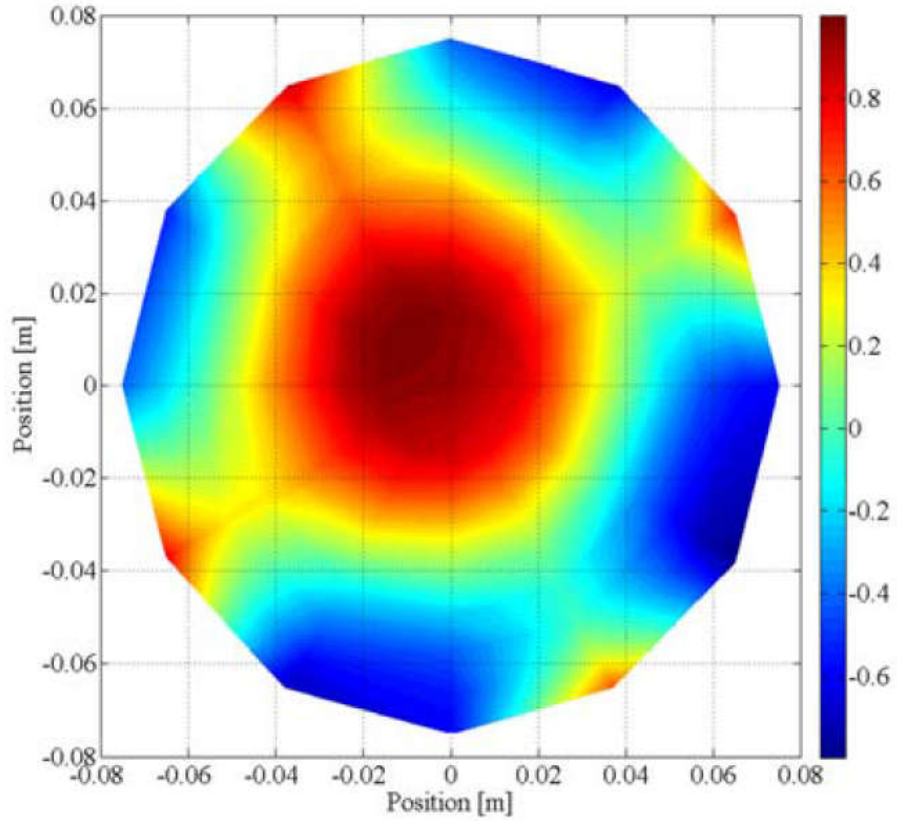

Figure 4.5 Theoretical pressure map of the wave field at 4.2kHz

4.3 Wave field in annular duct by rotating source

4.3.1 Experimental setup

The tests with the rotating source are performed in a test rig with an annular section (external diameter of 150 mm and internal diameter of 60 mm). The source is made up of a 5 blade fan and 3 static rods supporting the rotor. The variable speed electric motor of the rotor is placed inside the inner duct, an encoder gives the signal to measure the spinning rate and blade positions (Figure 4.6). The test has been carried out with a rotor spinning velocity of 76Hz. For these particular test conditions the complex acoustic modes and their cut-off frequency can be found in section 7.1.2. The measurement section is 20 mm upstream the rotor, 450 mm far from the duct inlet and 225 mm from the duct outlet. The probe is mounted on a slide for radial measurements. A flush mounted microphone is placed at 8 mm upstream the rotor, this sensor gives the reference signal for the probe. The signals of the microphones and the encoder are acquired with a National Instrument C-DAQ® system driven by an ad-hoc developed Labview® software.

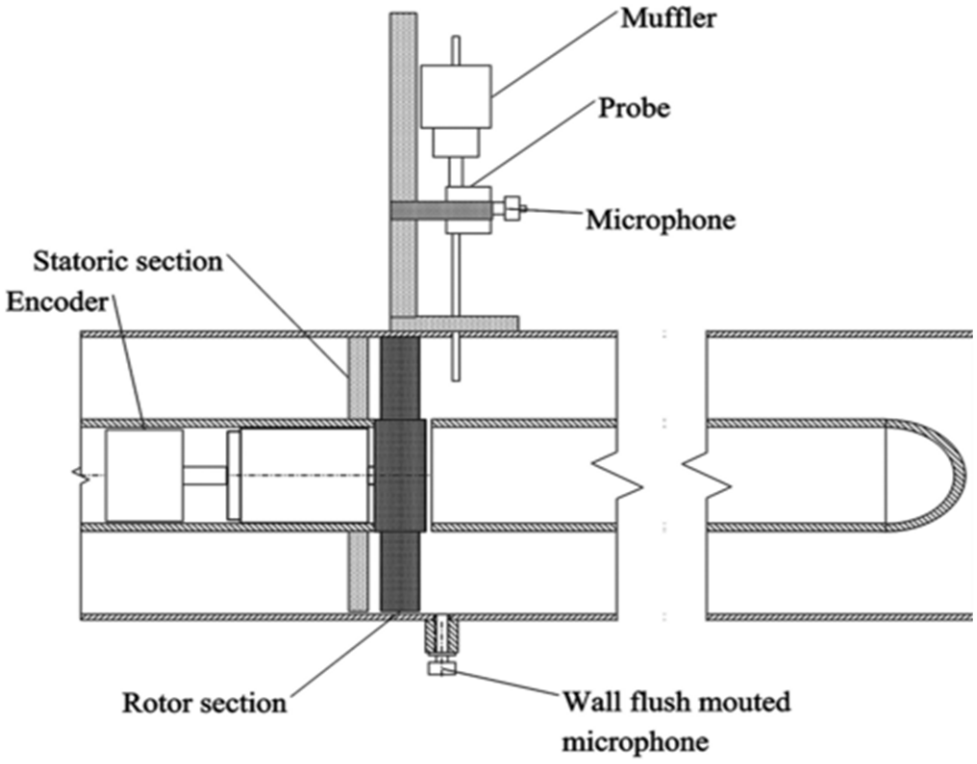

Figure 4.6 Scheme of the annular duct section with rotor and stator element

The acoustic source emits both to upstream and downstream direction. In the first case, the acoustic waves have the opposite direction of the air flow and in the other case they have the same direction of flow. If the flow velocity is lower than Mach=0.01, the convective contribution on the decay coefficient is negligible. The ends of the annular duct needs an experimental estimation of acoustic behaviour in terms of the reflection coefficient. The procedure adopted has been described previously in section 4.1.5.

Even though the acoustic source generates 3D acoustic waves, only the planar wave can propagate in the annular duct the other modes decay with an exponential law (see section 7.1.2). This behaviour is due to the fact that the *cut-off* frequencies of this modes are lower than the first *cut-off* frequency of annular duct. In Figure 4.7 the theoretical decay law of the mode m=1, n=1 respect to the axial position in the annular duct is shown.

Only the planar wave reaches the open end and as consequence the reflected wave is planar as well. The reflection coefficient in the planar field is shown in Fig. 20, and is represented in function of the Helmholtz number calculated by considering the span of the annular section. Since the geometry of the duct ends is the same, they have the same reflection coefficient. In general terms, the acoustic field in a section of the duct is the sum of the incident and reflected waves from both the upstream and downstream sections of the duct. In this study, since the source amplitude is low and the distance from the upstream end of the duct is great, the contribution of the wave that crosses the source after being reflected by the upstream end is neglected.

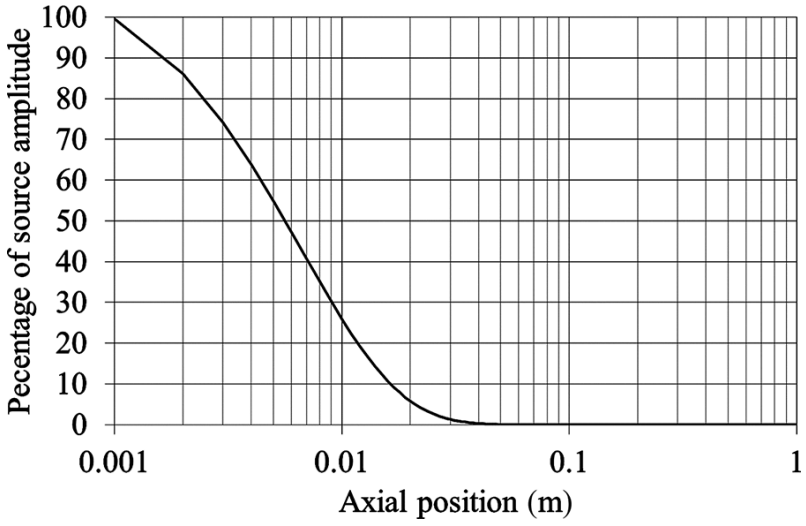

Figure 4.7 Percentage axial decrease of mode (m=1,n=1) in the planar range of propagation for annular duct

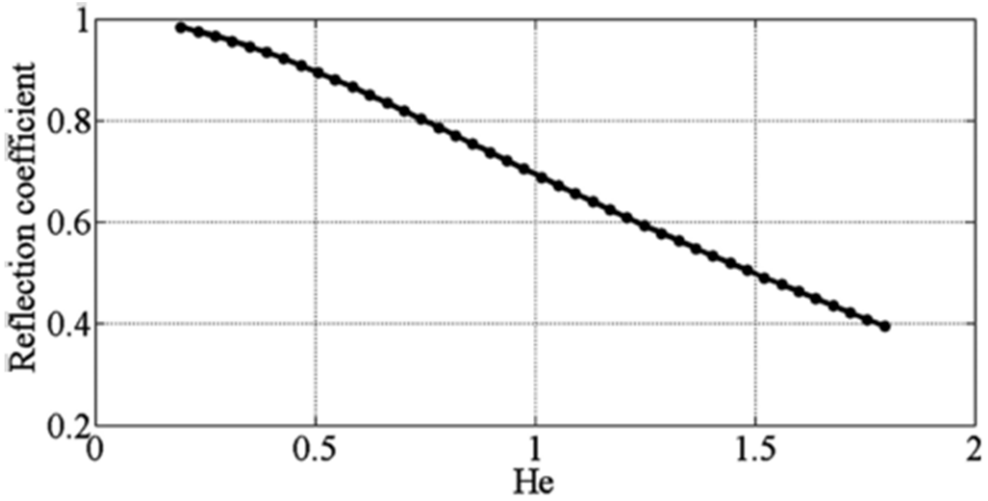

Figure 4.8 Reflection coefficient of the end of annular test rig

4.3.2 Rotating source data analysis

As shown in the theoretical analysis of the acoustic generation of the rotor-stator interaction (Table 7.2 and Table 7.3), since the frequency of the rotor shaft is 76 Hz, the maximum frequency of the source emission is 380 Hz. The first *cut-off* frequency of the annular duct is at 1082Hz this mean that the rotating acoustic source generates only in the planar range of the duct. In other words the 3D modes decrease in a short axial distance from the source.

Referring to the work of Tyler and Sofrin [39] the rotor-stator interaction can generate specific acoustic modes (reported in Table 7.2), each mode is generated at a fixed frequency ω_m (see Table 7.3) related to the shaft angular velocity ω.

The pressure signal near the source is so a superimposing of several modes, each one with its characteristic spinning frequency. In Figure 4.9 the FFT of the signal of reference microphone is shown in terms of blade passing frequency (*BPF*). The acoustic field mode with the highest amplitude is at the fifth harmonic *BPF=5* (380Hz) which corresponds to the first tangential and radial mode (m=1, n=1). At *BPF=1* (76Hz), the three radial harmonics of the fifth tangential mode can be detected (m=5, n=1). The acoustic wave field at *BPF=2.5* (190Hz) is the sum of the modes m=2, n=1, m=4, n=2 and m=6, n=3.

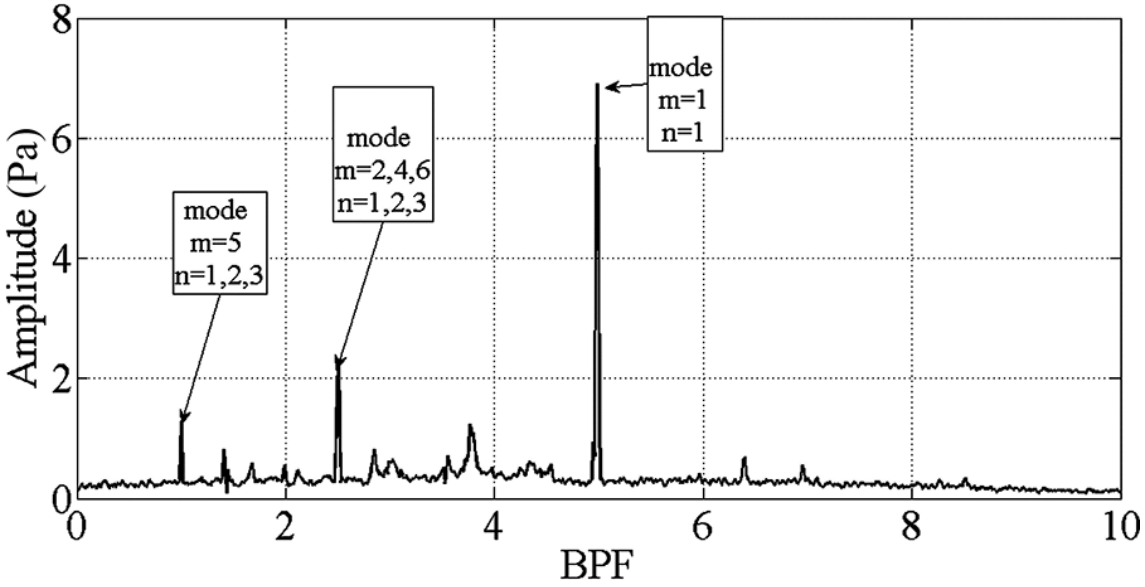

Figure 4.9 Spectrum of the flush mounted microphone

Each mode corresponds to a pressure distribution and the pressure field in the measurement section is the sum of each distribution considering their frequencies and phases. For the sake of simplicity, in the present study, only the first tangential and radial mode (m=1, n=1) was investigated. For this reason the measurements were clocked on the blade passing frequency and the resulting acoustic map is shown in Figure 4.10. The map has an offset due to the superimposing of the reflected planar mode that shifts only the mean value without changing the shape and the clocking.

In Figure 4.11 the theoretical map is shown. This is calculated with the same generation condition and duct end reflection coefficient of the experimental test case. The comparison of the two maps shows a notable agreement in terms of positioning on the geometrical plane. The overall pressure trend of the two maps is the same, and the differences could be related to the vibration of the rotor during its revolution.

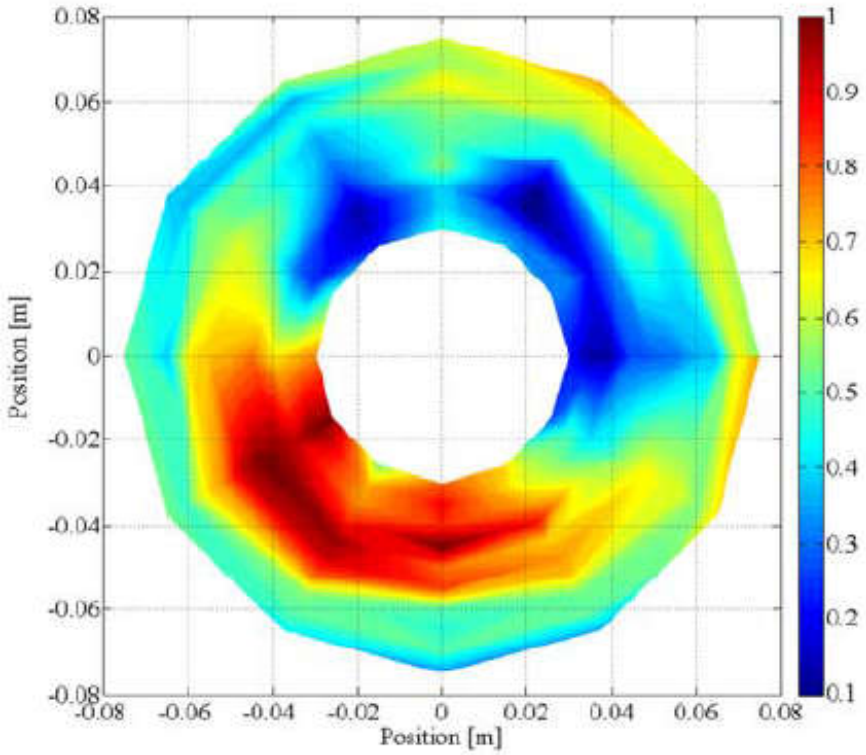

Figure 4.10 Experimental map of the acoustic mode in rotor stator interaction at 380Hz

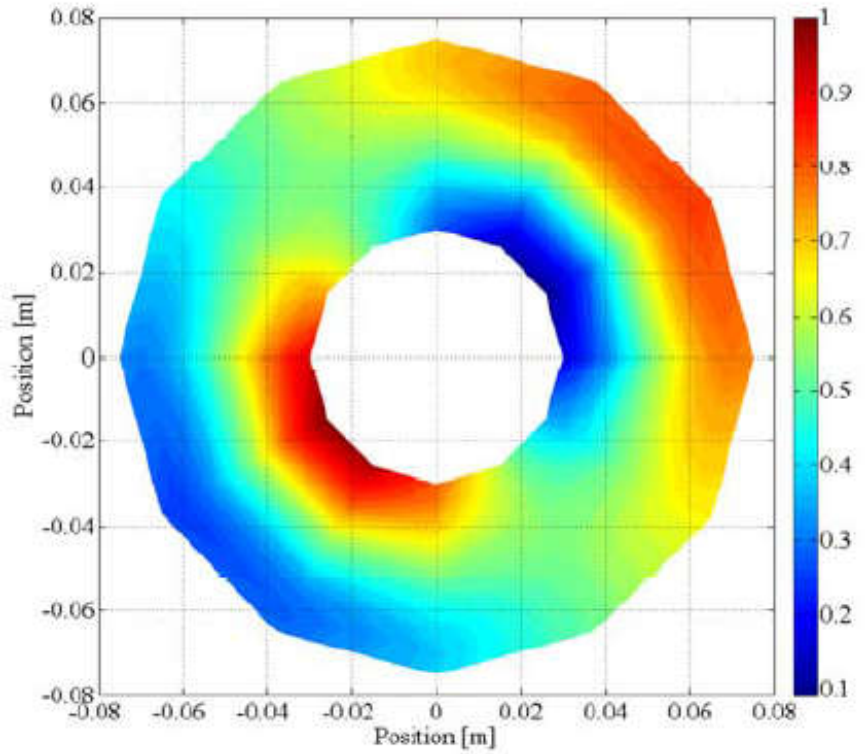

Figure 4.11 Theoretical map of the acoustic mode in rotor stator interaction at 380Hz

4.4 Multisensor waveguide probe experimental test

4.4.1 Centrifugal blower test

In order to test and assess the capability of the probe to estimate a pressure oscillation with slight error in terms of modulus and phase (this aspect especially important for a proper signal reconstruction in time domain) some tests on a centrifugal blower were performed. In particular, the probe was installed near the impeller outlet of a centrifugal blower and the pressure oscillations measured during a revolution. A reference microphone such as those on the probe (¼'' by G.R.A.S. ®) was flush mounted near to the probe tip. In order to compare the performance of the developed probe with that of a standard probe, a single sensor waveguide with an infinite long damping duct was also developed and tested in the same conditions.

The standard probe had the same geometry of the three sensor probe except that the second and third housings were closed and the muffler was replaced by an infinite long dumping duct. This probe was equipped with a microphone such as those on the multi-sensor probe and calibrated. The resulting attenuation factor and phase correction are depicted in Figure 4.12.

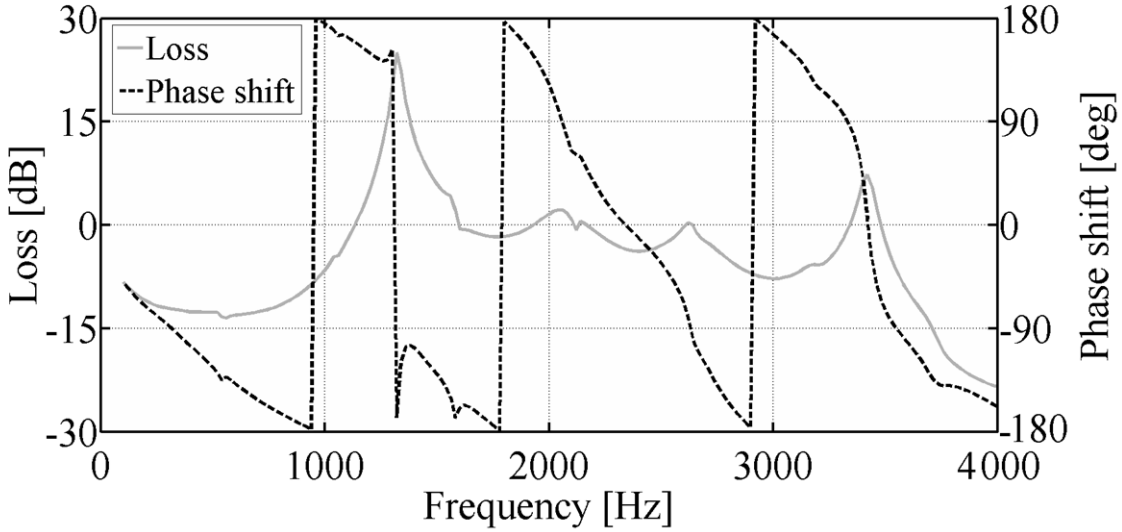

Figure 4.12 FRF and phase shift of a single sensor waveguide with infinite long damping duc

All signals are acquired by a Compact DAQ 9178 by National Instrument® equipped with NI 9234 acquisition modules (resolution of 24 bit; maximum acquisition frequency: 51.2 kS/s/channel; overall pressure measurement resolution of 0.2 mPa). The acquisition is triggered by the passing blade signal coming from a Hall effect sensor mounted on the blower's shaft (Figure 4.13). The impeller has 12 blades and its rotation frequency was 35 Hz thus resulting in a blade passing frequency of 420 Hz.

In Figure 4.14 and Figure 4.15 the pressure measured by the reference sensor and that estimated by the two probes are depicted in the time domain. A particularly good agreement can be observed between the reference signal and that measured by the multi-sensor waveguide, both in terms of amplitude and phase. A significant signal distortion can be noticed when a single sensor waveguide is adopted.

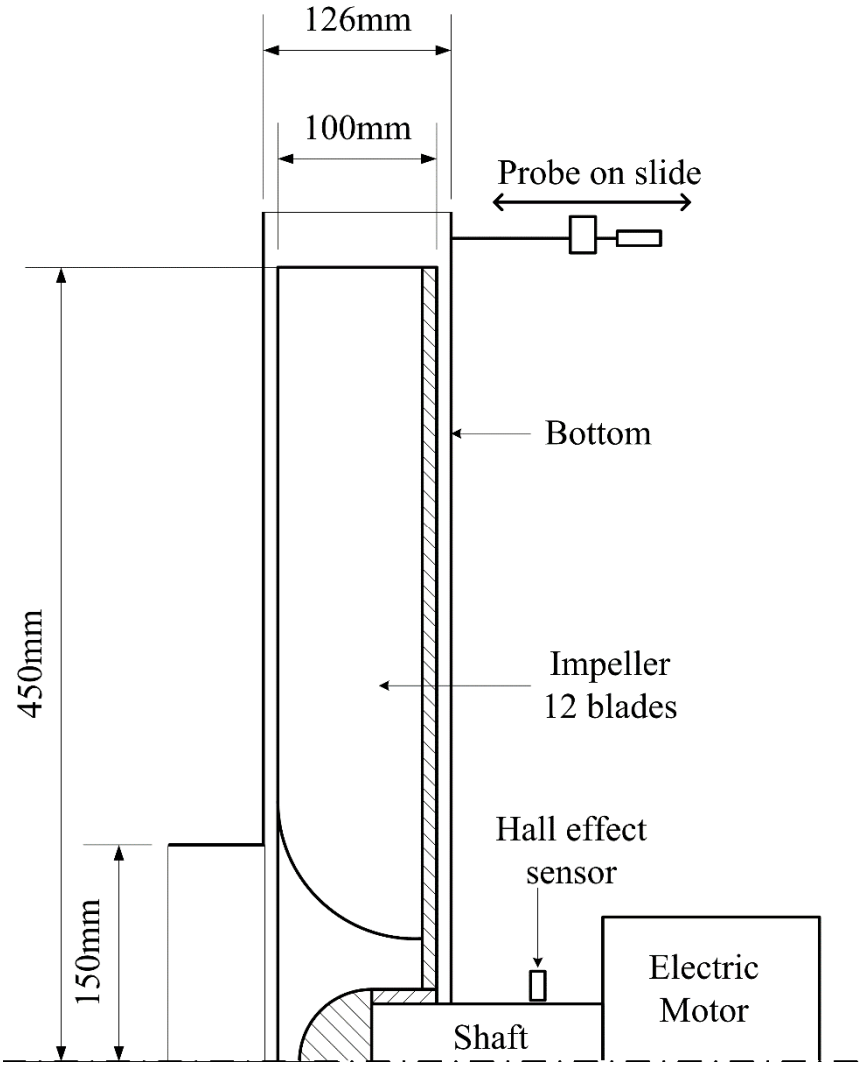

Figure 4.13 Schematic of the blower and probe positioning

To quantify the differences between the signals of the two probes and the reference sensor, the coefficient of determination R^2 was used. This coefficient indicates how well data points fit a line or curve: the closer is its value is to 1, the better is the correspondence. While for the single sensor waveguide the coefficient has the value of 0.68 for the three sensors waveguide it assumes the value of 0.95.

A similar comparison is depicted in Figure 4.16 and Figure 4.17, where the pressure measured by the reference sensor and those estimated by the probes are analyzed in the frequency domain. The three sensor waveguide has a good match with the reference sensor signal up to 4kHz: the probe shows a good frequency response function over the whole frequency range of interest without any undesired amplification or filtering. To highlight the different performance of the two probes, the difference between the FFTs of the signals estimated by the waveguides and the corresponding reference signals are depicted in Figure 4.18. The capabilities of the multi-sensor probe in comparison to those of a single sensor probe are clear.

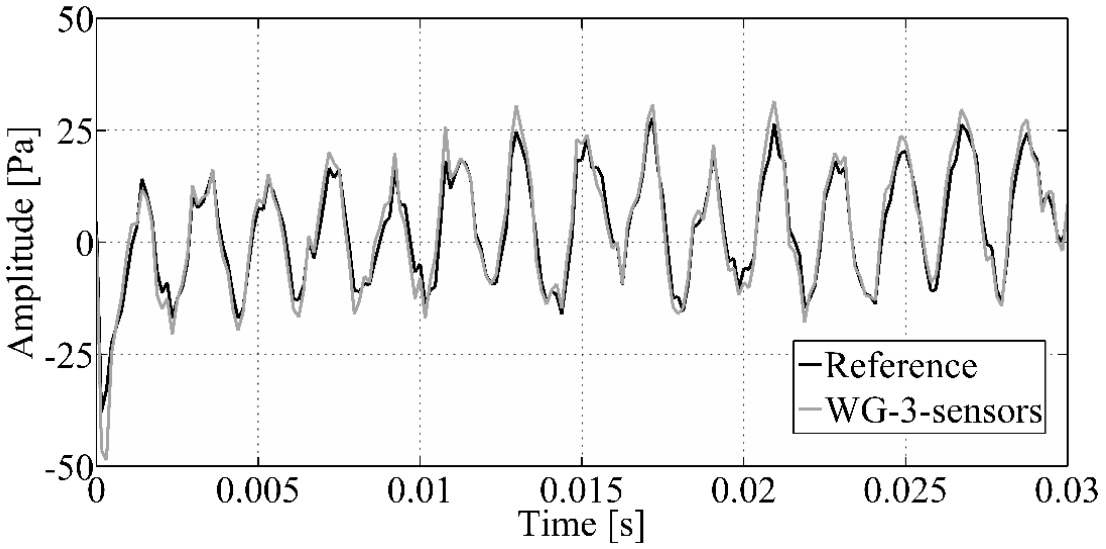

Figure 4.14 Pressure oscillations measured by the reference sensor and estimated by the multisensor waveguide

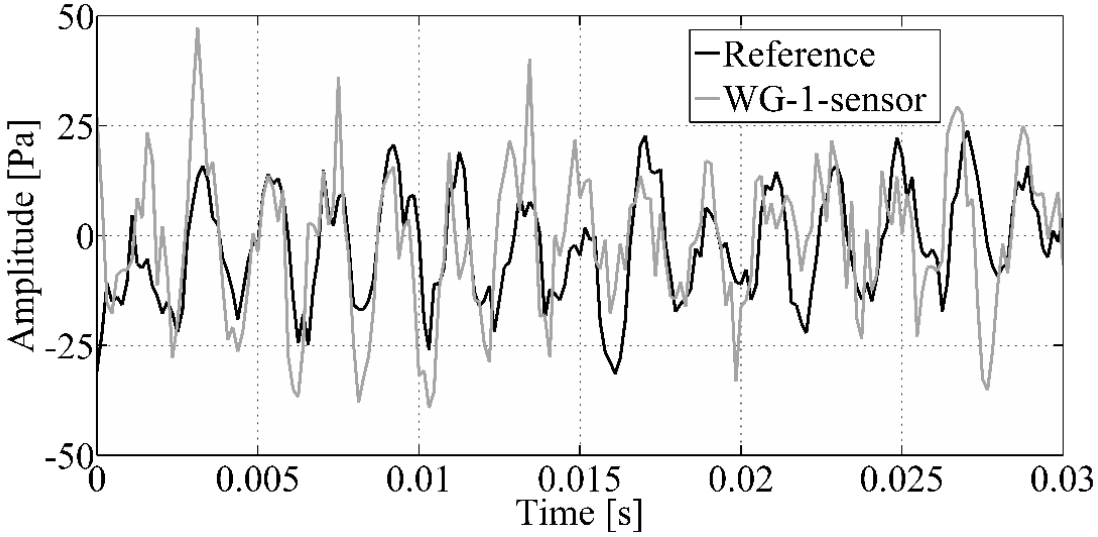

Figure 4.15 Pressure oscillations measured by the reference sensor and estimated by the single sensor waveguide

Thanks to the probe's capabilities to correctly estimate the pressure oscillations in terms of phase and amplitude, the measurement of the pressure oscillations across the blower blades was performed as a further demonstration of potential probe applications. The three sensor probe was installed on a slide which allows one to move the probe from the flush mounted position to the mid-span section. By using the slide it was possible to move the probe inside the channel at a step of 7 mm along the span up to mid channel height and measure the oscillations of static pressure. Each measurement was triggered by a pick-up sensor mounted on the rotor shaft. Thanks to the great accuracy in reconstructing the pressure signal in the time domain, a 2D map of the pressure oscillations between the blower blades can be built by moving the probe along the slide (Figure 4.19). It can be noticed how the vane passage effect becomes stronger moving from the hub to the mid-span. This is just an example of the capabilities of the probe and of the possible applications in the turbomachinery and aerodynamic fields.

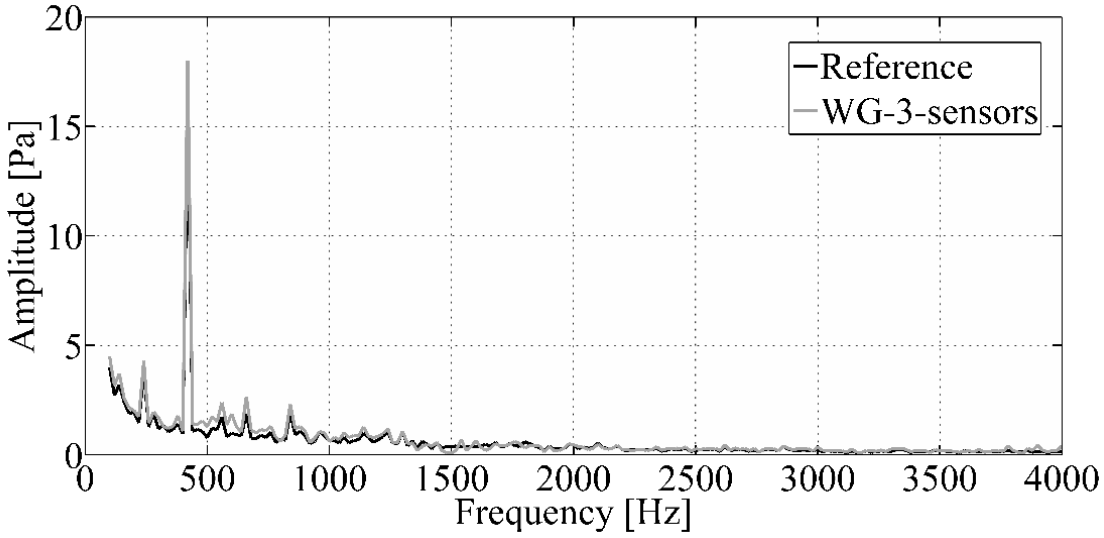

Figure 4.16 FFT of the pressure oscillation measured by the reference sensor and estimated by the multisensor waveguide

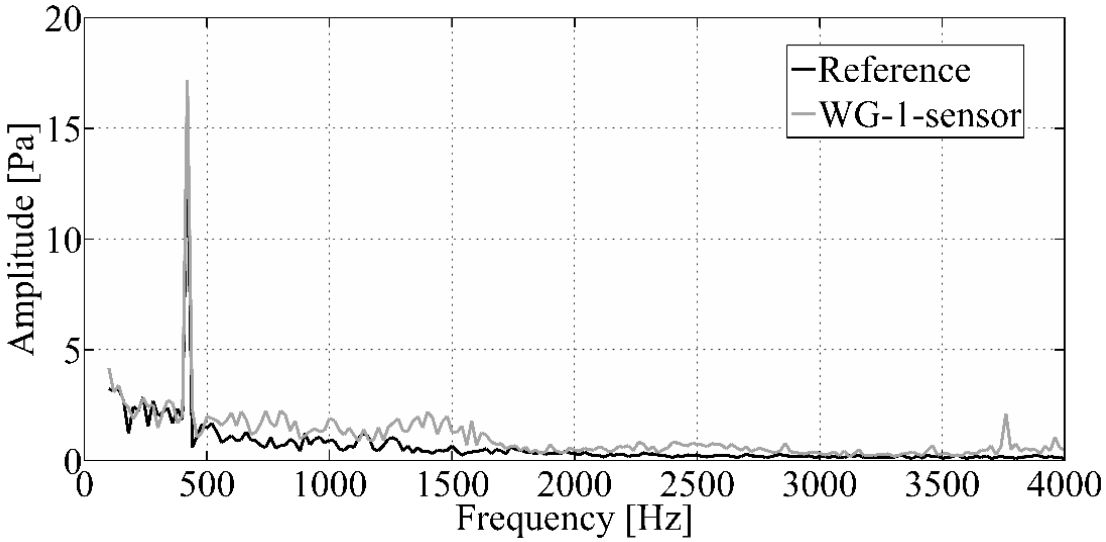

Figure 4.17 FFT of the pressure oscillations measured by the reference sensor and estimated by the single sensor waveguide

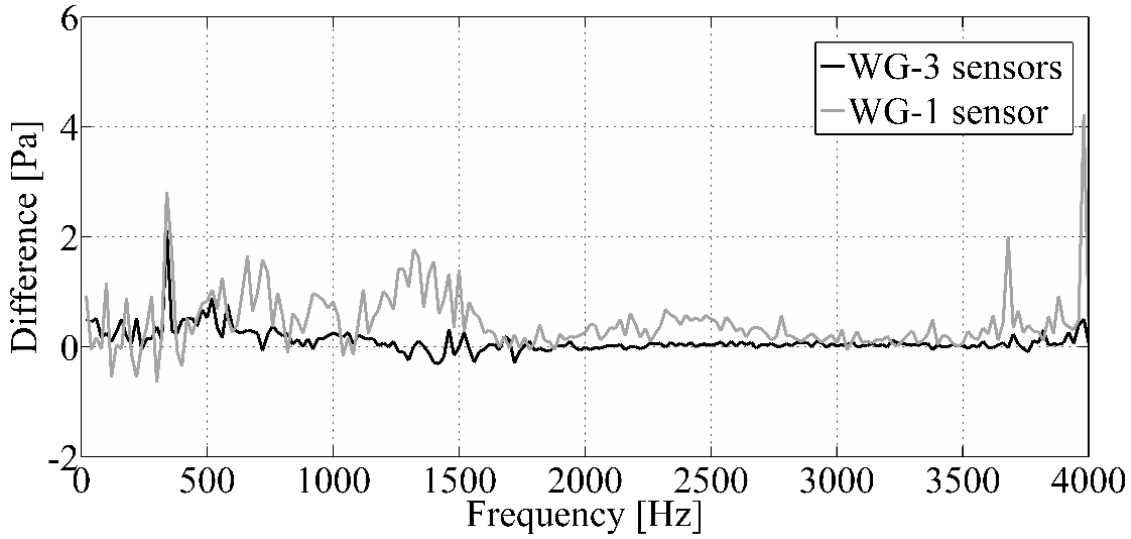

Figure 4.18 Differences between the FFT of the reference sensor and those estimated by the two probes

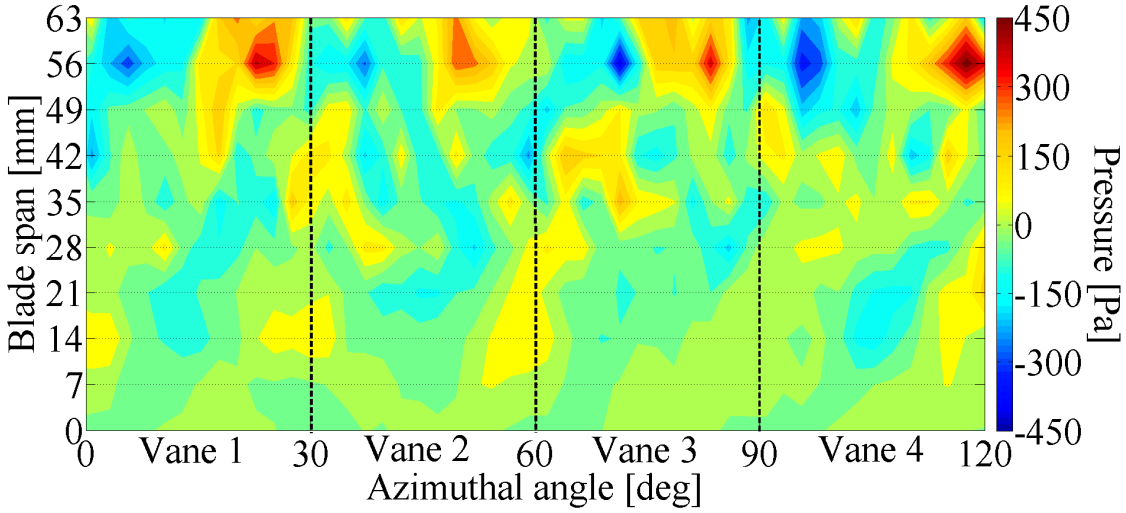

Figure 4.19 Map of the static pressure oscillation at the outlet of three blower blades

4.5 Test on centrifugal blower with waveguide probe modified

To assess the capabilities of the last waveguide probe which was designed and presented in chapter 3, considering that it has been conceived to measure a 3D flow, the probe was adopted to reconstruct the flow field at the outlet of a centrifugal blower. The

test case is the same used in the previously section. The blower had 12 blades, an outer diameter of 450 mm and was operated at a rotation speed of 1000 rpm by means of an electric motor. The probe was mounted on a traversing system at 10 mm from the impeller blades end, as depicted in Figure 4.20 and Figure 4.21. Six different positions equally spaced of 5 mm along the span were investigated. For each span position the pressure measured by the sensor was acquired at a first angular position (p_1) that was taken as a reference and two others at ±30° (p_2 and p_3). This is a simplified application but it is a good test case to assess easily the capabilities of the probe.

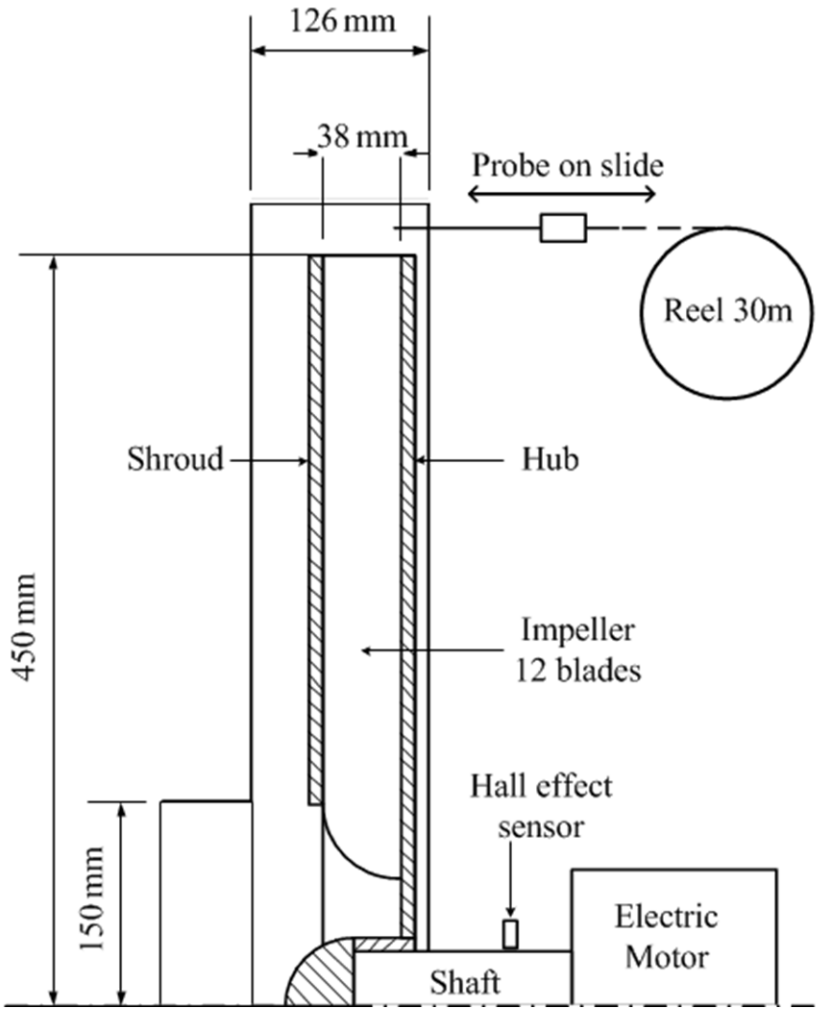

Figure 4.20 Centrifugal blower facility and probe (WGP-M) measurement position, the slice sets the position of probe

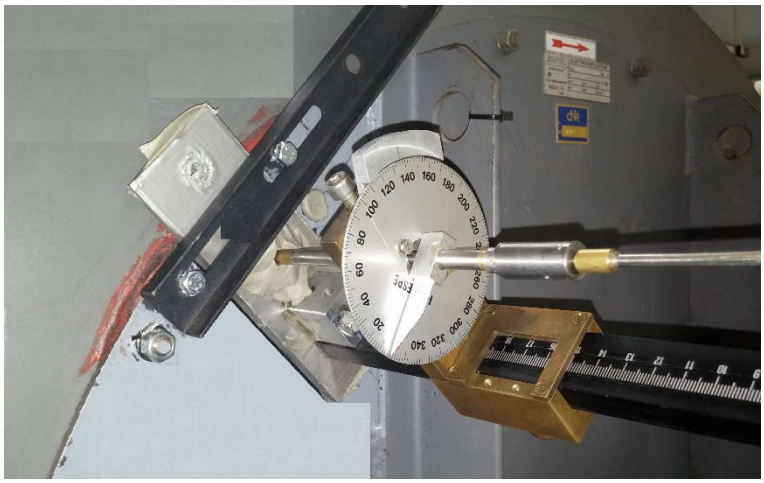

Figure 4.21 Probe (WGP-M) placed on the manual slide used to set the position on the blade span of the centrifugal blower, the angular marker sets the orientation of pressure tap respect to the main flow

The pressure signals were acquired by a Compact DAQ 9178 by National Instruments, equipped with NI 9215 acquisition module (resolution of 24 bit, maximum acquisition frequency 100 kS/s/channel). The acquisition was triggered by a Hall effect sensor mounted on the blower's shaft (Figure 4.20). A sampling frequency of 45 kHz was adopted in order to have at least 240 point per vane. For each probe position, about 75 rotations of the impeller were acquired. For each pressure measurement, the signal post-process was the following:

1. An ensemble average was applied to reduce the noise effects. A bin dimension of 1° was used.
2. The time signal for each pressure measurement was converted in a frequency signal by applying a FFT.
3. The FRF of the probe was applied both in terms of amplitude and phase (Eq. 3.25). This operation allows one to consider the attenuation and phase shift produced by the waveguide configuration.
4. The modified frequency spectrum was converted to a time signal by an Inverse FFT.

It is of interest to compare the signals before and after the application of the probe FRF. In Figure 4.22, an example for the pressure measured at mid span is reported (p_1). The time shift due to the presence of the damping duct and the amplitude variations are

apparent. On the other hand, it is readily noticeable that the signal is not strongly altered by the probe and its main characteristic are still visible before and after the application of the FRF.

Once the corrected pressure trends (p_1, p_2 and p_3) were obtained for each span position it was possible to calculate the K_γ coefficient (Eq. 3.28) and the yaw angle (Eq. 3.31). By using the yaw angle and the polynomial expression of Eq. 3.32 and 3.33 it was possible to calculate the K_S and K_T coefficients and then the total and static pressures from Eq. 3.29 and 3.30. In Figure 4.23, the flow angle (referenced to the radial direction), the static and the total pressures are reported during a revolution at the mid span position.

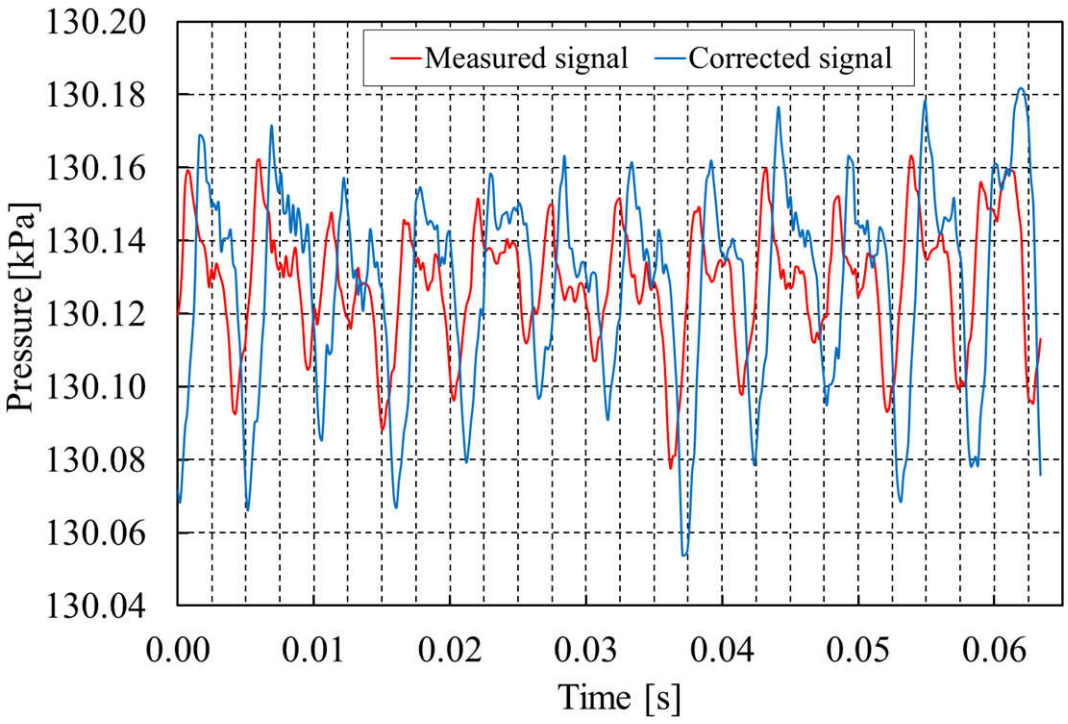

Figure 4.22 Measured and corrected signals at position p_1 (at mid span)

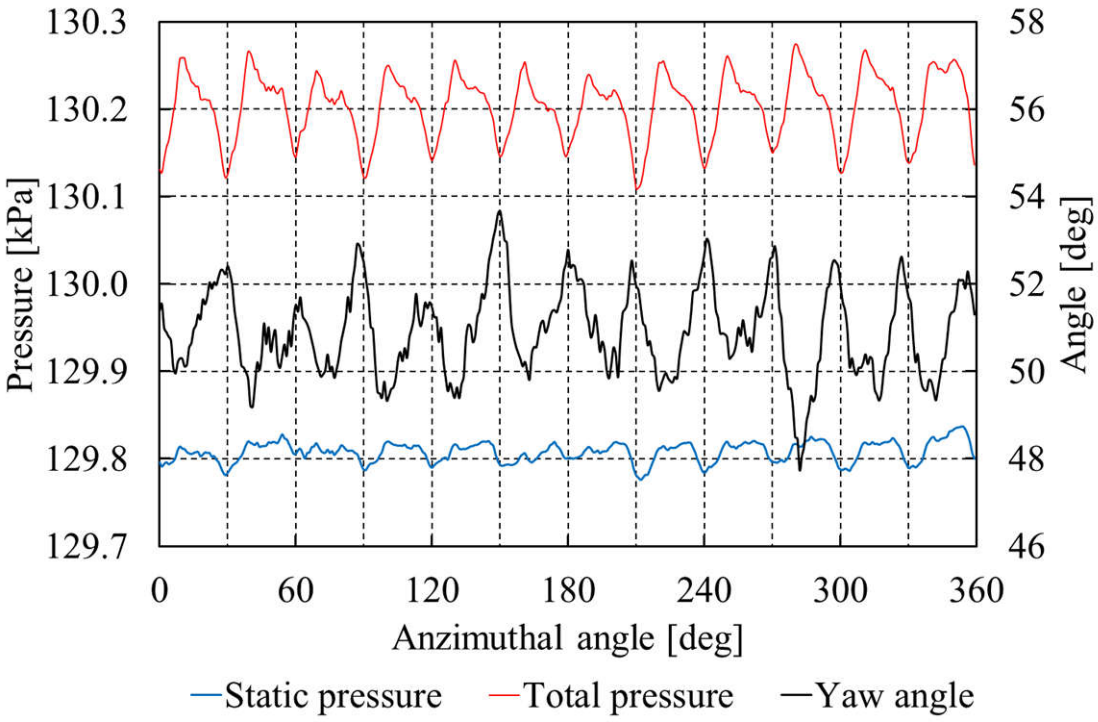

Figure 4.23 *Yaw* angle, total and static pressures at mid span

By extending this procedure to all the measurement points along the span, it was possible to estimate the flow angle, total pressure, static pressure and velocity distribution at the impeller exit. The obtained contour maps of these quantities are reported in Figure 4.24 Yaw angle referenced to radial direction over a revolution, Figure 4.25, Figure 4.26 and Figure 4.27 respectively. In particular, the static and total pressures were reported as a percentage value (the Eq. 4.5) to make more evident the pressure variations.

$$p^* = \frac{p - p_{\min}}{p_{\max} - p_{\min}} \qquad 4.5$$

As it possible to notice, once the effects of the transmitting duct are taken into account in terms of amplitude and phase, the probe turned out to be capable to reconstruct the complex flow field at the impeller exit.

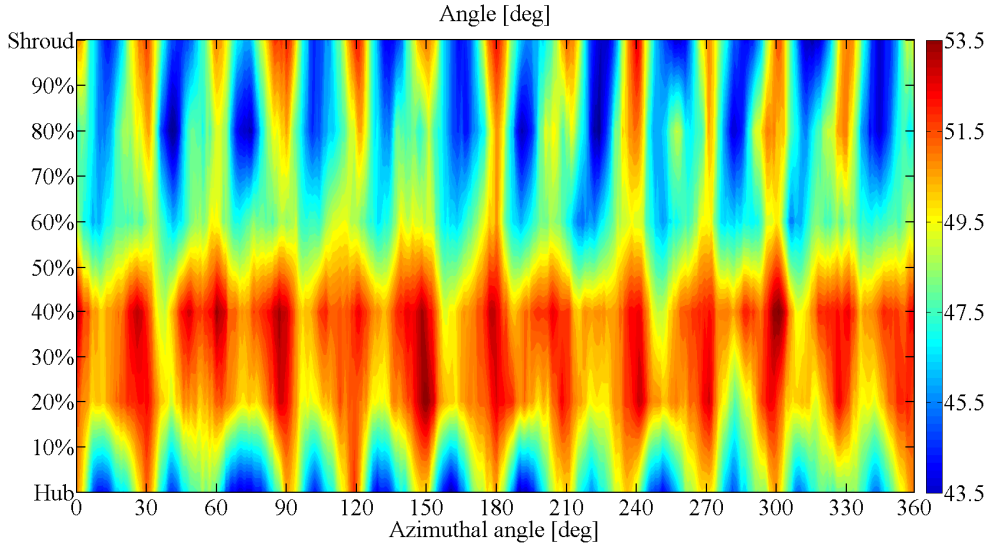

Figure 4.24 Yaw angle referenced to radial direction over a revolution

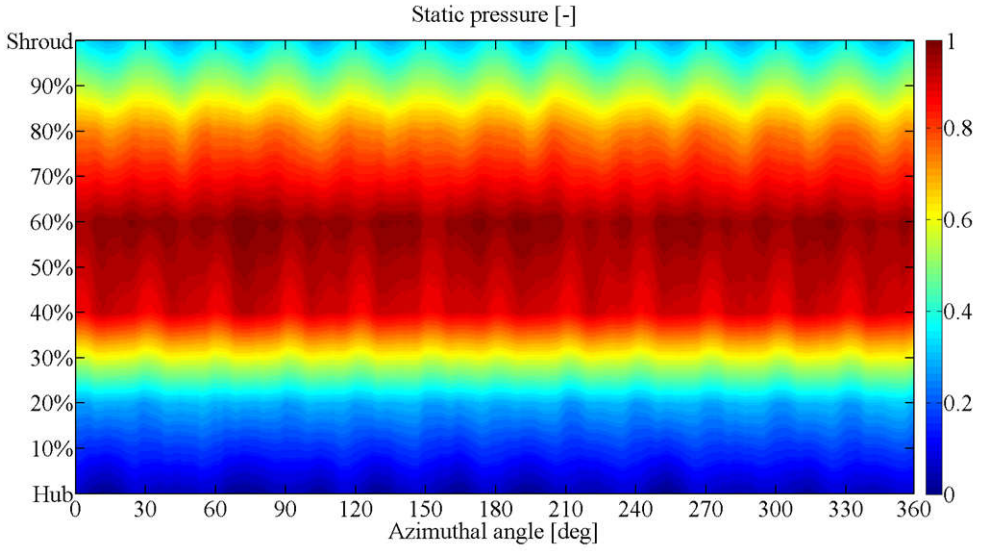

Figure 4.25 Normalized static pressure over a revolution

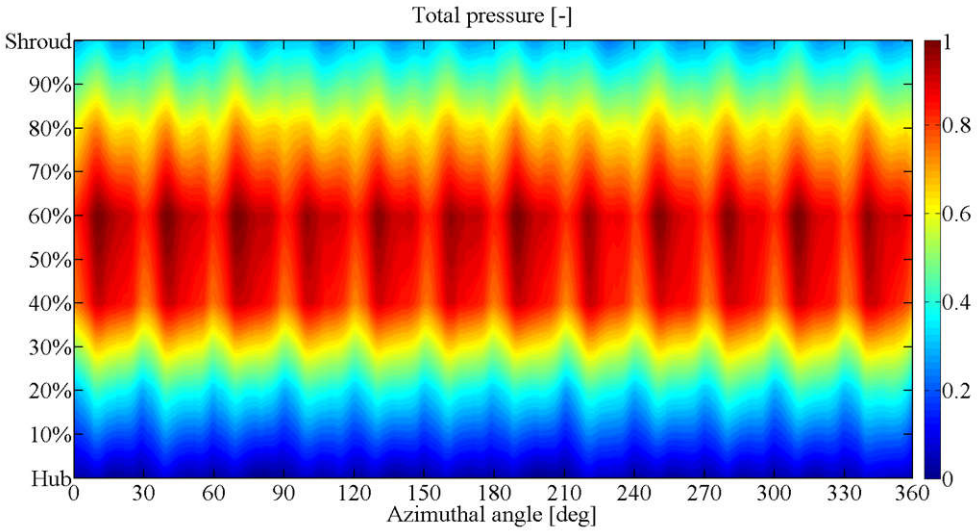

Figure 4.26 Normalized total pressure over a revolution

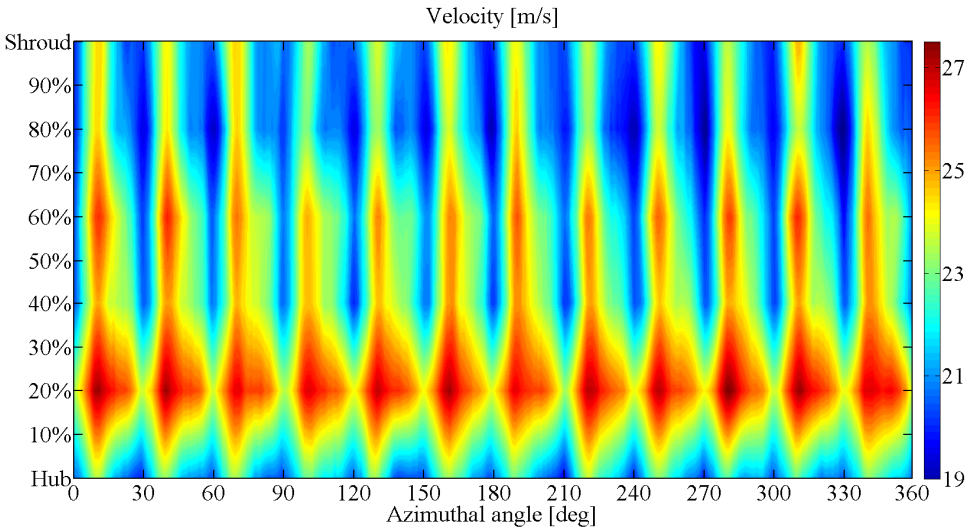

Figure 4.27 Absolute velocity over a revolution

5 Conclusions

In the turbomachinery field, when a pressure sensor cannot be used because of the harsh environment (high temperatures) which can damage the transducer or when the measurement point is scarcely accessible, the waveguide probes can represent a valid alternative.

A waveguide probe is made up of a transmitting duct which connects the measurement point to the sensor section, this duct makes the wave path, and a long damping duct attenuates the waves reflected by the duct end. These probes are defined by a complex transfer function which express how the signal is attenuated in amplitude and modified in phase during the transmission path. Usually, the transfer function of a waveguide probe has a monotone decreasing trend in frequency, the higher is the frequency the higher is the attenuation. The maximum frequency order of the phenomena under study is limited by the maximum attenuation permitted on the signal amplitude. Furthermore, in literature these probe are commonly used to measure the unsteady static pressure with a flush mounted location on statoric blade or case walls.

In the present work three different types of waveguide probes with improvement measurement capabilities have been presented. All this three types of probe have been conceived, designed and developed during this three years of research.

5.1 Single sensor waveguide probe

In the first study has been presents a new-concept of waveguide probe which uses an *ad-hoc* damping termination in place of the long damping termination. The narrow

transmitting duct is connected to a sensor housing where is placed a pressure transducer with higher surface synonymous of high sensitivity, an accurate design of damping termination allows to compensate the discontinuities introduced by the changing in size and to use in advantages the reflected waves to make flat the transfer function of probe.

This first type of probe developed has been used to carry out the measurement of a 3D acoustic field propagating in a circular duct and in an annular duct. An analytical procedure has also been developed to distinguish the contribution of incident and reflected wave. This two test case would represent in part the possible applications of this probe. The acoustic pressure field is commonly performed with rakes of dynamic pressure probes, however, the size of rake support could influence the acoustic field. In addition, the measured acoustic pressure field is generally the sum of an incident and a reflected wave, with the two contributions not being distinguished.

The first new concept of waveguide probe is developed according to the waveguide layout with a transmitting duct, a transducer on a side branch, and a damping device. A transmitting duct with an outer diameter of 2.5mm (2mm inner diameter) is chosen in order not to influence the acoustic pressure field. As a transducer, a 1/4" pressure microphone is adopted to ensure a sensitivity high enough to measure the acoustic pressures. Several geometries of the interface between the microphone and the transmitting duct have been tested and the solution with a side branch of 2mm diameter turns out to be the one that performs best. The influence of the damping device has also been investigated in detail because it has a strong influence on the frequency response of the probe. A single solution that is completely suitable for all of the frequency range of interest is not available. The solution is the replacement of the commonly used damping duct (30m long duct) with a set of specifically designed mufflers. In particular, three mufflers are designed to cover the frequency range from 50 Hz to 4200 Hz.

These probes are adopted to measure the 3D acoustic pressure fields in two case studies: the propagation of a multimodes acoustic field in a circular duct and downstream a rotating source in an annular duct. The first could be representative of an acoustic field in a combustion chamber and the latter of that generated by a rotor stator interaction. In order to compare the experimental results with the expected ones it is necessary to reconstruct the theoretical field in the measurement section. This is the sum of the incident

wave (which can be estimated easily) and that reflected by the duct end whose behaviour needs to be characterized. The characterization of the duct acoustic reflection coefficient is performed by extending the multimicrophone technique from the planar to the 3D wave field. The procedure was specifically developed in this work based on previous studies.

In the first case study the acoustic field is generated by four speakers driven at the frequency of 4.2 kHz at one end of a 150mm circular duct. The corresponding acoustic wave field has a strong 3D distribution and is made up of three acoustic modes (m=4, n=0; m=0, n=1; m=1, n=1). The acoustic pressure map was measured on a planar grid with 108 points with a proper synchronizing technique. The result is compared with the distribution from the theoretical analysis. The two maps show notable agreement in terms of amplitude distribution and clocking.

A similar mapping procedure was adopted in the second case study. Among the acoustic fields generated by the rotor-stator interaction, that with the highest amplitude was chosen for the mapping procedure (380 Hz). At this frequency, the source generates a contra-rotating field corresponding to the mode m=1, n=1. The acoustic pressure distribution was measured and compared to that from the theoretical analysis and also in this case the agreement between the two reconstructions was good both in terms of pressure distribution and clocking.

5.2 Multisensor waveguide probe

Starting from the typical limitations of a standard waveguide probe a further improvement has been reached with the conceived of multisensor waveguide probe. As already said, the waveguide probes are affected by errors on the pressure estimation (both in terms of modulus on phase) due to transfer functions with trends typically strongly frequency dependent. In addition, the transfer function values generally become higher with frequency, leading to an increase of the absolute error on pressure estimations due to the error propagation. The reason for this behaviour is usually due to a real probe geometry that is far from that expected by the theoretical approach. As a consequence, the use of waveguides is limited to the analysis of low frequency pressure fluctuations in

the frequency domain. The time domain signal reconstruction is generally deemed to be not accurate.

The second type of waveguide probe was developed starting from the intent to reduce the absolute error on pressure estimation on a wide range of frequency. The new concept of probe was based on the use of three sensors placed at a proper distance from each other at the end of the transmitting duct. Instead of using the transfer function, the probe is based on the innovative concept of using, for each frequency, the combination of the signals measured by the sensors that leads to the smallest error amplification. In addition, the probe is equipped with a muffler that substitutes the infinite long damping duct. As seen before, this innovative feature not only reduces the probe size and encumbrance but also allows one to compensate for the difference between the real and expected behaviour of the probe. Moreover, the muffler allows one to have a small error amplification over a wide range of frequency.

The design of the probe was performed following a rigorous procedure. A theoretical model of the probe is realized based on the electro acoustic analogy. As a damping device, an infinite duct is considered, allowing one to ignore the presence of reflected waves. The sensor surfaces are considered as rigid walls. By using the theoretical model, the influence of the spacing between the sensors on the error propagation is investigated. The best configuration is that with the lower error amplification. A probe with a sensor housing disposition in agreement with the optimized one is realized and equipped with an infinite duct as termination. This preliminary probe is calibrated by providing a known pressure input by means of acoustic speakers and recording the pressure measured by the sensors. All the internal impedances of the probe (sensor housings—including the sensor head impedance, internals duct, and possible junction imperfections) are described by lumped and distributed transfer matrix models based on the pressure measurements. A muffler with a proper impendence is designed to compensate the distortions due to the sensor housing and other manufacturing imperfections. The muffler is manufactured and its acoustic behaviour assessed. The probe with the muffler as a damping device is assembled and the new combinations table which gives the smallest error for each frequency is determined by means of the theoretical model which uses the impedances measured during the calibration. During the

measurement, the pressures measured by the sensors are combined according to the combination table for each frequency.

The probe capability was assessed by measuring the pressure oscillation at the outlet of a centrifugal blower and comparing it to that measured by two other devices: a standard single sensor probe with an infinite long damping duct located in the same position and a reference sensor placed near the probe tip. Unlike the results obtained with the single sensor probe, the measurements performed with the three sensor probe showed a remarkably good agreement with the pressure measured directly at impeller outlet both in the time and frequency domains (a R^2=0.68 for a standard probe versus a R^2=0.95 for the multisensor probe). This result confirms the great accuracy of this innovative probe and emphasizes its capability to operate with small estimation errors in a wider range of frequencies in comparison to a standard single sensor probe with the same geometry. The range of frequencies investigated in this study was only limited by the adopted calibration device and can be easily extended once a different calibration system is used. The procedure demonstrated in this paper can be easily replicated for other probe geometries, ranges of frequencies, and sensor types without affecting the expected results.

5.3 Aerodynamic pressure probe based on a waveguide approach

Up to now the FRAPPs and waveguide probes have been always considered as two separated instrumentations with different field of applications, pros and cons. As last step of this study an effort to combine the two base concepts and exploit the benefits of both was performed. The basic idea was to develop a waveguide probe with a modified tip to act as a virtual 3 hole probe. The probe was mainly made up of a cylindrical head with a 0.6 mm lateral hole, a transmitting duct, a sensor housing and a damping duct. This arrangement can combine the benefits of having a sensor placed far from the measurement environment (e.g. no temperature restriction on the sensor) to the spatial resolution of a virtual 3 hole probe. Obviously, the adoption of waveguide probe leads to some drawbacks (as a limit to the frequency range and a frequency response function which is not flat) but a proper design and calibration of the probe can strongly reduce them.

As a proof of concept, a probe featured as described above was conceived, developed and tested on a centrifugal blower to assess its capability to estimate a complex flow field. The attention was focused on the general performance of the probe and then the waveguide probe was designed to be as simple as possible (infinite long damping duct and single sensor probe). Before its use, the probe underwent to two calibrations:

1. A dynamic calibration to estimate the frequency response function in terms of attenuation and phase shift. This calibration was performed in the acoustic test bench up to 5 kHz, this bandwidth being limited by the calibration facility.
2. A steady aerodynamic calibration to estimate the $K\gamma$, K_S and K_T coefficients to be used in the angle, static and total pressure estimation. This calibration was performed in a wind tunnel by performing three measurements: one at a reference angle and two by rotating the probe of ±30°.

Once the effects of the transmitting duct are taken into account in terms of amplitude and phase, the probe turned out to be capable to reconstruct the complex flow field at the impeller exit.

5.4 Summary

In summary, the new concept of single sensor waveguide probe presented together an advanced decomposition method for the measurement of a 3D acoustic field represent an improvement in the field of use of this devices. The probe is designed to have a flat response in a wide range of frequency and is able to measure also inside the pressure field. The experimental tests have shown that the probe is able to perform excellent measurements both with time-independent and time-dependent acoustic source. The definitive agreement between the measured acoustic maps and the theoretical ones confirms the reliability of the measures and the negligible obtrusiveness of the probe on the pressure field.

The second concept of waveguide probe presented uses the combination of signals measured by two or more sensor placed along the transmitting duct. The concept of a

waveguide probe with a flat frequency response has been reviewed. With this new probe it is of interest to find the function that leads to the minimum error amplification on the pressure estimated. Furthermore, this probe has been equipped with a muffler as termination using the know-how acquired in the previous study. The experimental comparison on a centrifugal blower test case between the multisensor waveguide probe and the traditional single sensor one showed the capability of the first one to operate with a smaller estimation error on pressure that is reflected in the higher accuracy of the signal time domain reconstruction.

Finally, it was performed an effort to combine the concepts of a waveguide probe with those of a fast response aerodynamic pressure probe. The intent was that to combine their benefits without limiting the applications. The experimental measurements of the complex flow at the outlet of the centrifugal blower test case have shown the applicability of this concept. Even though this solution is not intended to be extended to all the applications due to its probable maximum frequency limitations, this can represent an interesting improvement in all those situations where the unsteady periodic phenomenon under investigation has not a very high frequency but the operating temperatures could represent a limit for the transducer.

6 References

[1] Fischer, J., 1971,"Fluctuating Pressure Measurements From DC to Over 100kHz in Jet Engine Testing", Proceedings of the 17th International ISA Aerospace Instrumentation Symposium, May 10–12, Instrument Society of America, Research Triangle Park, NC, Vol. 17, pp. 117–123.

[2] Wegner, M., Nance, D., and Ahuja, K., 2007, "Characterization of Short and Infinite-Line Pressure Probes for In-Duct Acoustic Measurements Under Hostile Environment," Proceedings of the 13th AIAA/CEAS Aeroacoustics Conference (28th AIAA Aeroacoustics Conference).

[3] Johnson, C. E., Neumeier, Y., Lubarsky, E., Lee, J. Y., Neumaier, M., and Zinn, B. T., 2000, "Suppression of Combustion Instabilities in a Liquid Fuel Combustor Using a Fast Adaptive Control Algorithm," Proceedings of the 38th Aerospace Sciences Meeting and Exhibit

[4] Christensen, D., Cantin, P., Gutz, D., Szucs, P. N., Wadia, A. R., Armor, J., Dhingra, M., Neumeier, Y., and Prasad, J. V. R., 2006, "Development and Demonstration of a Stability Management System for Gas Turbine Engines," ASME Conference Proceedings, 2006 4241X , pp. 165–174.

[5] Fischer, A., Sauvage, E., and Röhle, I., 2008, "Acoustic PIV: Measurements of the acoustic particle velocity using synchronized PIV-technique" in 14th Int Symp on Applications of Laser Techniques to Fluid Mechanics, Lisbon.

[6] Souchon, G., Gazengel, B., Richoux, O., and Duff, A., L., 2004, "Characterization of a dipole radiation by Laser Doppler Velocimetry", Conference paper at 7th Acoustic Congress France.

[7] Blackshear, P., Rayle, W., and Tower, L., 1955, "Study of Screeching Combustion in 6-Inch Simulated Afterburner," National Advisory

Committee for Aeronautics, Washington, DC, Report No. NACA-TN-3567, p. 58.

[8] Zinn, H., and Habermann, M., 2007, "Developments and Experiences with Pulsation Measurements for Heavy-Duty Gas Turbine," ASME Paper No. GT2007-27475.

[9] White, M. A., Dhingra, M., and Prasad, J. V. R., 2010, "Experimental Analysis of a Wave Guide Pressure Measuring System," ASME J. Eng. Gas Turbines Power, 132(4), p. 041603.

[10] Tijdeman, H., 1977, "Investigations of the Transonic Flow Around Oscillating Airfoils," National Aerospace Laboratory, Amsterdam, The Netherlands, Report No. NLR TR 77090 U.

[11] Kupferschmied, P., Koppel, P., Gizzi, W., Roduner, C., and Gyarmathy, G., 2000. "Time-resolved flow measurements with fast-response aerodynamic probes in turbomachines". Meas. Sci. Technol., 11, pp.1036-1054.

[12] Sieverding, C., H., Arts, T., Dénos, R., and Brouckaert, J., F., 2000 "Measurments Tecniques for unsteady flows in turbomachines", Exp. Fluids, 28, No 4.

[13] Palmer, M. E., Davis, M. A., Engelbrecht, G. P., Fielder, R. S., Ng, W., Song, B., and Ringshia, A., 2006, "Un-Cooled Fiber-Optic Pressure Sensor for Gas Turbine Engines, Operation to 1922DGF and 500psig," 44th AIAA Aerospace Sciences Meeting and Exhibit, pp. 9–12.

[14] Matlis, E. H., Corke, T. C., Cameron, J., Morris, S. C., and Fay, P., 2008, "High-Bandwidth Plasma Sensor Suite for High-Speed High-Enthalpy Measurements," 46th AIAA Aerospace Sciences Meeting and Exhibit

[15] Iberall, A., 1950, "Attenuation of Oscillatory Pressures in Instrument Lines," J. Res. Natl. Bureau Standards., 45, pp. 85–108.

[16] Bergh, H., and Tijdeman, H., 1965, "Theoretical and Experimental Results for the Dynamic Response of Pressure Measuring Systems," National Aero and Astronautical Research Institute, Amsterdam, Netherlands, Technical Report No. NLR-TR F.238.

[17] Tijdeman, H., 1975, "On the Propagation of Sound Waves in Cylindrical Tubes," J. Sound Vib., 39(1), pp. 1–33.

[18] Nyland, T. W., Englund, D. R., and Anderson, R. C., 1971, "On the Dynamics of Short Pressure Probes: Some Design Factors Affecting Frequency Response", National Aeronautics and Space Administration, Lewis Research Center, Cleveland, OH.

[19] Richards, W. B., 1986, "Propagation of Sound Waves in Tube of Noncircular Cross Section," NASA Lewis Research Center, Cleveland, OH, Report No. NASA-TP-2601.

[20] Englund, D., and Richards, W., 1984, "The Infinite Line Pressure Probe," NASA Lewis Research Center, Cleveland, OH, Report No. NASA-TM-83582.

[21] Van de Wyer, N., Brouckaert, J. F., and Miorini, R. L., 2012, "On the Determination of the Transfer Function of Infinite Line Pressure Probes for Turbomachinery Applications," ASME Paper No. GT2012-69563.

[22] Parrott, T. L., and Zorumski, W. E., 1992, "Sound Transmission Through a High-Temperature Acoustic Probe Tube," AIAA J., 30(2), pp. 318–323.

[23] Ferrara, G., Ferrari, L., and Sonni, G., 2005, "Experimental Characterization of a Remoting System for Dynamic Pressure Sensors," ASME Paper No. GT2005-68733.

[24] Ferrara, G., Ferrari, L., and Lenzi, G., 2014, "An Experimental Methodology for the Reconstruction of 3D Acoustic Pressure Fields in Ducts," ASME J. Eng. Gas Turbines Power, 136(1), p. 011505

[25] Munjal, M. L., 1987, Acoustic of Ducts and Mufflers, Wiley, New York.

[26] Brouckaert, J., F., Sievering C., H., and Manna, M., 1998, "Development of a Fast Response 3-Hole Pressure Probe", 14th Symposium on Meas. Tech. For Transonic and Supersonic Flows in Cascades and Turbomachines, Limerick.

[27] Humm, H., J., and Verdegaal, J., 1992, "Aerodynamic design criteria for fast-response probes", 11th Symposium on Measuring Techniques in Transonic and Supersonic Flow in Cascades and Turbomachines, Rhode Saint Genèse.

[28] Humm, H., J., Gizzi, W., P., and Gyarmathy, G., 1994, "Dynamic response of aerodynamic probes in fluctuating 3D flows", 12th Symposium on

Measuring Techniques in Transonic and Supersonic Flow in Cascades and Turbomachines, Prague, CZ.

[29] Mersinligil, M., Brouckaert, J., Courtiade, N., and Ottavy, X., 2011, "A High Temperature High Bandwidth Fast Response Total Pressure Probe For Measurements In A Multistage Axial Compressor," ASME Turbo Expo, Power for Land Sea and Air, Vancouver, Canada.

[30] Persico, G., Gaetani, P., and Guardone, A., 2005, "Design and analysis of new concept fast-response pressure probes", Measurement Science And Technology, UK

[31] Mansour, M., Chokani, N., Kalfas, A., and Abhari, R., 2008, "Time-resolved entropy measurments using a fast response entrophy probe", Measurment Science and technology, 19, 115401, pp. 14

[32] Pfau, A., Schlienger, J., Kalfas, A.,I., and Abhari, R.,S., 2002, "Virtual four sensor fast response aerodynamic probe", 16th Symposium on Measuring Techniques in Transonic and Supersonic Flow in Cascades and Turbomachines, Cambridge, UK.

[33] Lenherr, C., Kalfas, A., I., and Abhari, R., S., 2010, "High Temperature Fast Response Aerodynamic Probe" ASME Turbo Expo 2010: Power for Land, Sea and Air, Glasgow, UK.

[34] Pfau, A., Schlienger, J., Kalfas, A. I., and Abhari, R. S., 2003, "Unsteady, 3-Dimensional Flow Measurement Using a Miniature Virtual 4 Sensor Fast Response Aerodynamic Probe FRAP," ASME Paper No. GT2003-38128.

[35] Pfau, A., Schlienger, J., Rusch, D., Kalfas, A. I., and Abhari, R. S., 2005, "Unsteady flow interactions within the inlet cavity of a turbine rotor tip labyrinth seal", Journal of Turbomachinery, Vol. 127, pp. 679-688.

[36] Schilienger, J., Pfau, A., Kalfas, A., L., and Abhari, R., S., 2002, "Single pressure transducer probe for 3D flow measurements", 16th Symposium on measuring techniques in transonic and supersonic flow in cascades and turbomachines, Cambridge, UK

[37] Kinsler, L., E., and Frey, A., R., 1962, "Fundamental of acoustic", John Willey and sons, New York

[38] Dowling, A., 1995, "The calculation of thermo-acoustic oscillations", Journal of Sound and Vibration, 180(4), pp. 557–581.

[39] Tyler, J., M., and Sofrin, T., G., 1962, "Axial flow compressor noise studies" Transactions of the Society Automotive Engineers, 70, pp. 309-332.

[40] Zwikker, C., and Kosten, C., 1949, Sound Absorbing Materials, Elsevier, Amsterdam, The Netherlands.

[41] Lenzi, G., Fioravanti, A., Ferrara, G., and Ferrari, L., 2015, "Development of an innovative waveguide probe with improvement capabilities", ASME J. Eng. Gas Turbine Power, 137(1), p. 051601

[42] Durrieu, P., Hofmans, G., Ajello, G., Boot, R., Aurégan, Y., Hirschberg, A., and Peters, M., 2001, "Quasisteady aero-acoustic response of orifices", Journal of Acoustic Society of American, Volume 110, N° 4, pp.1859-1872

[43] Seong-Hyun, L., and Jeong-Guon, Ih., 2003, "Empirical model of the acoustic impedance of a circular orifice in grazing mean flow", Journal of Acoustic society of America, Volume 114, N°1, pp.98-113.

[44] Gossweiler, C. R., Kupferschmied, P., and Gyarmathy, G., 1995, "On fast-response probes. Part 1: Technology, calibration, and application to turbomachinery", Journal of Turbomachinery, 117(4), pp. 611-617.

[45] Morse, P., M., and Ingard, K., U., 1968, "Theoretical acoustics", Ed. McGraw-Hill, New York.

[46] Ross, A., F., and Seybert, A., F., 1977, "Experimental determination of acoustic properties using a two-microphone random excitation technique", Journal of Acoustic Society of America, Volume 61, N°5, pp. 1362-1370.

[47] Bodén, H., and Abom, M., 1986, "Influence of errors on the two-microphone method for measuring acoustic properties in ducts", Journal of Acoustic Society of America, Volume 79, N°2, pp.541-549.

[48] Ih, J., G., and Jang, S., H., 1998, "On the multiple microphone method for measuring in-duct acoustic properties in the presence of mean flow", Journal of Acoustic Society of America, Volume 103, N°3, pp. 1520-1526.

[49] Schultz, T., Cattafesta, L., N., and Sheplak, M., 2006, "Modal decomposition method for acoustic impedance testing in square ducts", Journal of Acoustic Society of America, Volume 120, N°6, pp.3750-3758.

[50] Verdon, J., M., Montgomery, M., D., and Kousen, K., A., 1995, "Development of linearized unsteady Euler analysis for turbo machinery blade rows" NASA, East Hartford, Connecticut.

[51] Sutliff, D., L., 2005, "Rotating Rake Turbofan Duct Mode Measurement system", NASA, Cleveland, Ohio.

[52] Holste, F., 1997, "An equivalent source method for calculation of the sound radiated from aircraft engines" Journal of Sound and Vibration, 203(4), pp. 667-695

7 Appendix

7.1.1 Theoretical acoustic wave field in an axially symmetrical duct

The propagation of a sound wave field in an axially symmetrical infinite circular duct is described by the convective wave equation, Kinsler et al. in Ref. [37] and Munjal in Ref. [25], here expressed in cylindrical coordinates Eq.7.1:

$$\left(\frac{\partial^2}{\partial t^2} \quad c^2\nabla^2\right)p(z,\theta,r,t) = 0 \tag{7.1}$$

where z is the axial position, θ is the circumferential one, r is the radial position, t is the time, c is the sound velocity, and ∇^2 is the Laplace operator Eq. 7.2 in cylindrical coordinate system (Figure 7.1) for cylindrical tube.

$$\nabla^2 = \frac{\partial^2}{\partial r^2} + \frac{1}{r}\frac{\partial}{\partial r} + \frac{1}{r^2}\frac{\partial^2}{\partial \theta^2} + \frac{\partial^2}{\partial z^2} \tag{7.2}$$

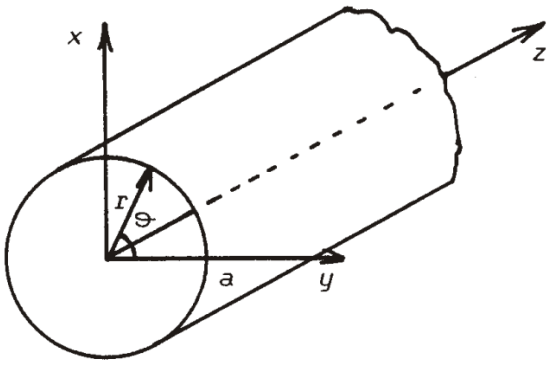

Figure 7.1 A duct with circular cross section

The boundary condition for a tube with rigid walls is:

$$\left.\frac{\partial p(z,\theta,r,t)}{\partial r}\right|_{r=a} = 0 \qquad 7.3$$

making use of the method of separation of variables, and writing the time dependence as $e^{i\omega t}$, the ϑ dependence as $e^{im\vartheta}$ and z dependency as e^{ikz} the hypothesis of solution is:

$$p(r,\theta,z,t) = p_r(r)e^{im\theta}e^{ikz}e^{i\omega t} \qquad 7.4$$

Substituting Eq. 7.4 in the wave equation 1.1 one gets the Bessel equation for $p_r(r)$. Eq. 7.5.

$$\frac{d^2p_r(r)}{dr^2} + \frac{1}{r}\frac{dp_r(r)}{dr} + \left(k_0^2 \quad k_z^2 \quad \frac{m^2}{r^2}\right)p_r(r) = 0 \qquad 7.5$$

Finally, it is possible to introduce the transversal wave number $k_r^2=k^2-k_z^2$. The Bessel's equation has a general solution Eq.7.6 which depends on the Bessel function (J_m) of order m and the Neumann function (N_m) of order m. only the Bessel functions are finite at $r=0$ therefore $G=0$.

$$p_r(r) = FJ_m(k_r r) + GN_m(k_r r) \qquad 7.6$$

while from the boundary condition Eq. 7.3 it follows Eq. 7.7, this last equation can be satisfied only for certain discrete values of k_r.

$$\left.\frac{\partial J_m(k_r r)}{\partial r}\right|_{r=a} = J'_m(k_r a) = 0 \qquad 7.7$$

This equation can be satisfied only for certain discrete value of k_r. Upon denoting the value of k_r corresponding to the *n-th* root of Eq.7.7 as k_{rmn} with n=0,1,2… one gets the harmonic solution Eq. 7.8 to Eq. 7.5.

$$p(r,\theta,z,t) = \sum_{m=0}^{\infty}\sum_{n=0}^{\infty} J_m(k_{rmn}r)\, e^{im\theta}e^{i\omega t}(p_{mn+}e^{-ik_{zmn}z} + p^{-}{}_{mn-}e^{+ik_{zmn}z}) \qquad 7.8$$

Each term in the sum represents a mode and k_{zmn} is expressed as:

$$k_{z,m,n} = \sqrt{{k_0}^2 \quad {k_{r,m,n}}^2} \qquad 7.9$$

The constant p^+ and p^- have to be determined by means of the boundary condition, like source and termination applied at the circular duct. The wave number expressed in Eq. 7.9 describes the propagation of waves in the axial direction of duct. In a inviscid stationary medium the waves are not attenuated and the term k_0 is real and positive, while in a viscous stationary medium like air the waves are attenuated along the axial direction by the visco-thermal effects. In order to consider this latter aspect the constant k_0 is replaced by a complex value Γ that considers this attenuation effects.

The solution of Eq. 7.1 without mean flow gives the acoustic pressure distribution in the duct Eq. 7.8 for given acoustic boundary conditions. As already said the acoustic pressure distribution turns out to be the sum of several acoustic modes (indicated with a *m* and *n* integer index). Index *m* denotes the nodal planes where the sound pressure is zero and *n* denotes the coaxial nodal cylindrical surfaces where the pressure is zero. More in detail, each mode has a *cut-off* frequency that follows from Eq. 7.9 with k_{zmn}=0, Eq. 7.10.

$$f_{m,n} = \frac{\eta_{mn} c}{2\pi a} \qquad 7.10$$

where η corresponding to the *n-th* root of Eq.7.7 and $f_{m,n}$ is the *cut-off* frequency. If a mode is driven with a frequency above its *cut-off* frequency the mode can propagate unattenuated. On the other hand, if the mode is driven with a frequency below its *cut-off* frequency the mode declines exponentially.

For example, if one considers a 150 mm diameter cylindrical duct, the *cut-off* frequencies of the acoustic modes *(m,n)* are reported in Table 7.1 and the corresponding shapes are depicted in Figure 7.2.

Table 7.1 Cut-on and cut-off frequencies of a 150 mm diameter circular duct

***Cut-off* frequencies**						
n\m	**0**	**1**	**2**	**3**	**4**	**5**
0	0	1363	2261	3110	3937	4750
1	2837	3947	4965	5934	6873	7789
2	5194	6320	7381	8400	9390	10356

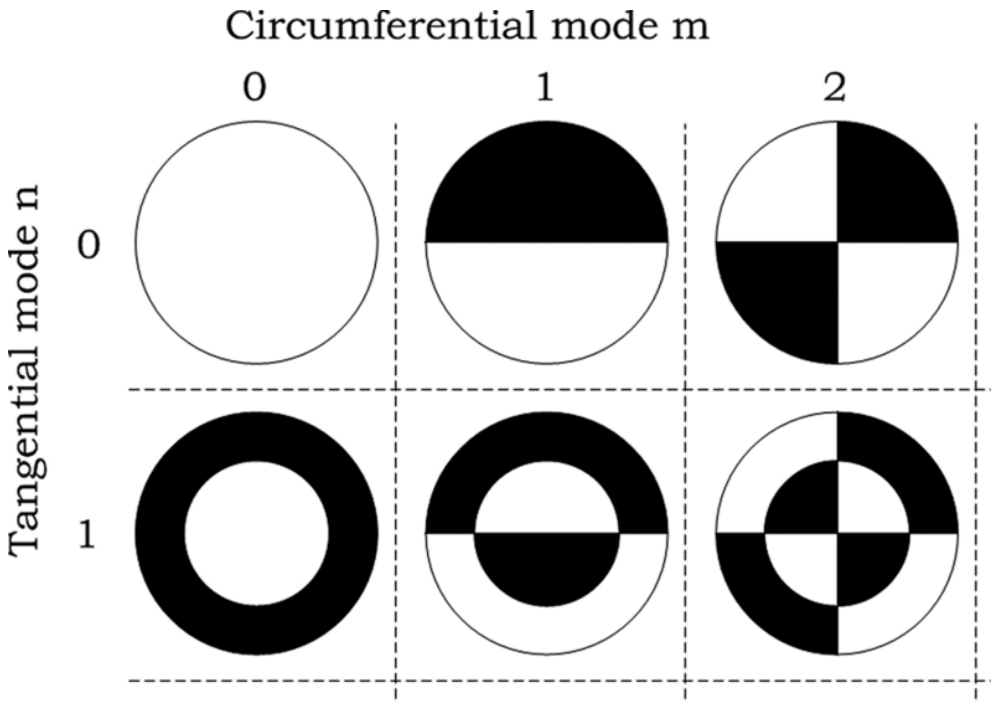

Figure 7.2 Schematic shapes of acoustic modes of a cylindrical duct

The first tangential higher-order mode (0,1) can propagate when the frequency is above to $f_{0,1}$=2837Hz, while the lowest *cut-off* frequency in the duct is the cut-off frequency of the first circumferential mode (1,0), $f_{1,0}$=1363Hz.

The total acoustic wave field can be the superposition of different propagation modes. For example, in a frequency range between 1.39 and 2.28 kHz both the planar wave field (*0,0*) and the first mode (*1,0*) can propagate: the total acoustic field is given by the complex sum of the two modes. When the frequency increases the acoustic wave field becomes more and more complex; if one considers a frequency range between 3.95 and 4.78 kHz, the acoustic pressure field is made up of three modes: the fourth tangential (*m=4, n=0* Fig. 2-a), the zero radial (*m=0, n=1* Fig. 2-b) and the first radial (*m=1, n=1* Fig. 2-c) modes.

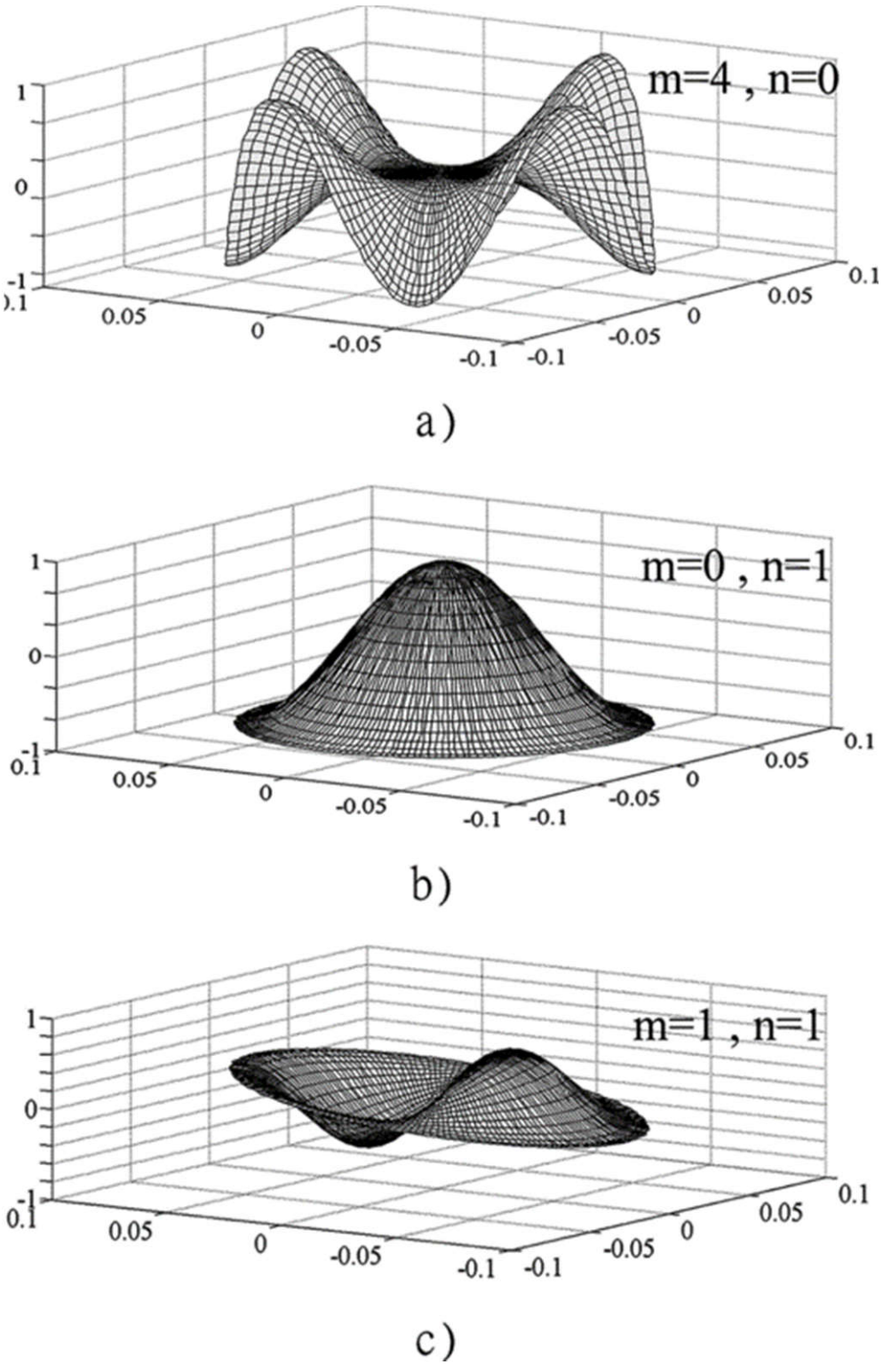

Figure 7.3 Theoretical single modes of a 150mm diameter circular duct at 4.2 kHz

Furthermore, in the case of a semi-infinite duct with an acoustic source at one end, only one travelling wave with the above mentioned characteristics propagates. However,

in the case of a finite length duct or in the presence of discontinuities, the global pressure field is made up of two travelling waves that propagate in opposite directions: the first one coming from the acoustic source (incident wave) and the latter that is reflected by the discontinuity (reflected wave). In a generic section of the duct the acoustic pressure distribution is the combination of the incident and the reflected waves.

7.1.2 Rotor stator interaction

If the acoustic field is the result of the interaction between a rotor and stator, the modes generated do not only depend on the duct geometry but also on the number of blades and vanes (look at Ref. [50][51][52]) The theory behind this generation was presented by Tyler and Sofrin in their work [39] for fan-duct systems. In the case of a rotor with N_B number of blades and a stator of N_V vanes, the modes generated and their spinning frequencies are described by Eq. 7.11 and Eq. 7.12 in which K is an integer with sign. In this case m is a function of blade and vanes numbers.

$$m = nN_B \pm KN_V \tag{7.11}$$

$$\omega_m = \frac{nN_B\omega}{m} \tag{7.12}$$

The modes generated by rotor-stator interaction propagate or decay depending on the characteristic of the duct connected to the source. Considering for example a rotor with five blades $N_B=5$, a shaft spin rate of $\omega=76\ Hz$ and a stator with three rods $N_V=3$. From Eq. 7.11 and Eq. 7.12 the modes generated by the source and their characteristic frequencies are reported in Table 7.2 and Table 7.3. A negative number indicates a counter-rotating mode.

The rotating acoustic source can generate the mode of Table 7.2 each rotating with its own spinning frequency indicated in Table 7.3. The modes that actually propagate in the duct depend on the *cut-off* frequency of the duct itself. If the rotating source generates an acoustic mode field different from those allowed by the duct, it decays in few diameters. Considering the fan stator example above indicated, the spinning frequencies turns out to be very low. If one compares their values with the *cut-off* frequencies of the annular section with an outer and inner diameter of 150 mm and 60 mm respectively,

showed in Table 4.4, deduced from the wave equation solved in an annular domain, only the planar acoustic field could propagate in the duct for frequencies from 0 to 1.08 kHz (m=0, n=0).

For example, by considering a spinning frequency of -380 Hz, the associated acoustic mode is the one corresponding to *m=1, n=1*, Figure 7.4. This mode can only be measured close to the source because it will decay in few diameters

Everywhere, developing and using suitable measurement device which are able to measure this unsteady pressure signal in different and hard environment it could possible analyse this phenomena validating the numerical investigations.

Table 7.2 Tangential mode (m) of rotor stator interaction

	n		
K	**1**	**2**	**3**
-3	-4	1	6
-2	-1	4	9
-1	2	7	12
0	5	10	15
1	8	13	18
2	11	16	21
3	14	19	24

Table 7.3 Spinning frequency of the wave fields

	n		
K	**1**	**2**	**3**
-3	-95	760	190
-2	-380	190	127
-1	190	109	95
0	76	76	76
1	48	58	63
2	35	48	54
3	27	40	48

Table 7.4 Cut-off frequencies for an annular duct with 150mm outer diameter and 60mm inner diameter

Cut-off frequencies			
m	**n**		
	0	**1**	**2**
0	0	3992	4067
1	1082	4190	6817
2	2104	4750	8186
3	3041	5579	8637
4	3911	6554	9255
5	4741	7571	10027

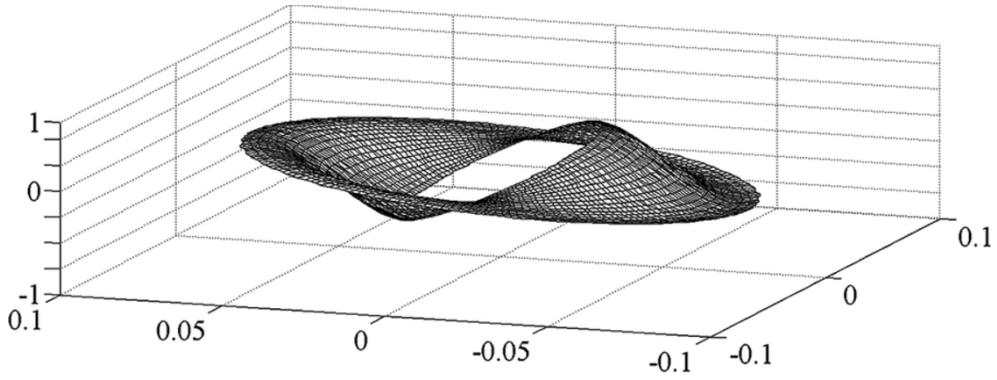

Figure 7.4 First radial and tangential mode in annular duct with 150mm outer diameter and 60mm inner diameter